2011

DC-DC Power Converter Design for a Portable Affordable Welder System (PAWS)

Curt Stephen Zackiewicz
Wright State University

DC-DC Power Converter Design for a Portable Affordable Welder System (PAWS)

A thesis submitted in partial fulfillment

of the requirements for the degree of

Master of Science in Engineering

By

CURT STEPHEN ZACKIEWICZ

B.S., Michigan Technological University, 2002

2011

Wright State University

WRIGHT STATE UNIVERSITY

SCHOOL OF GRADUATE STUDIES

March 11, 2011

I HEREBY RECOMMEND THAT THE THESIS PREPARED UNDER MY SUPERVISION BY Curt Stephen Zackiewicz ENTITLED DC-DC Power Converter Design for a Portable Affordable Welder System BE ACCEPTED IN PARTIAL FULFILLMENT OF THE REQUIREMENTS FOR THE DEGREE OF Master of Science in Engineering

Marian Kazimierczuk, Ph.D.
Thesis Director

Kefu Xue, Ph.D., Chair
Department of Electrical Engineering College of Engineering and Computer Science

Committee on
Final Examination

Saiyu Ren, Ph.D.

Ronald Riechers, Ph.D.

Andrew Hsu

Dean, School of Graduate Studies

ABSTRACT

Zackiewicz, Curt Stephen. M.S.Egr, Department of Electrical Engineering, Wright State University, 2011. DC-DC Power Converter Design for a Portable Affordable Welder System

Arc welding machines are typically large, heavy devices that transform an alternating current (AC) input into a low-voltage, direct current (DC) output. Traditionally these high power devices have required steel and copper transformers that account for their bulky size and weight. While the cost of raw materials in electromagnetic components has been increasing the cost of high-power silicon devices has been decreasing. This disparity creates an opportunity for a cost-effective DC-DC switching welder in the consumer market. While DC-DC power electronics are not new to the welding industry, this study, under the commission of a welding equipment manufacturer, aims to develop and prototype a design specifically for an affordable and portable battery-powered welding machine. By eliminating the need for electromagnetic components for isolation and voltage regulation, and focusing on a DC-DC battery-powered device, a unique opportunity exists to create a high-feature product with a minimalist design. The design is implemented with a high-current voltage chopping circuit as well as an assortment of feedback, control, and safety circuitry necessary to complete the machine. By combining simulation, prototype validation and real-world cost limitations, this project outlines the development of a new product for the welding equipment market.

TABLE OF CONTENTS

Chapter 1 Introduction....9

1.1 Background.... 11

1.2 Motivation.... 15

1.3 Objective.... 18

Chapter 2 Design.... 21

2.1 Power Circuit....21

2.2 Switching Methodology....26

2.3 Switching Components....28

2.4 Output Inductance....34

2.5 Power Circuit Simulations.... 37

Chapter 3 Control Circuit Design.... 39

3.1 Over-Current Protection.... 42

Chapter 4 Additional Design.... 44

4.1 Wire Feed Motor....45

Chapter 5 Simulation and Test Results.... 46

Chapter 6 Summary and Conclusion.... 55

6.1 Recommendations for Future Work....56

6.2 Acknowledgments..... 59

References..... 60

Appendix A Voltage and Current for GMAW Welding, Table..... 62

Appendix B IRFP2907 MOSFET Abridged Data Sheet..... 63

Appendix C STOS40H100CW Diode Abridged Data Sheet..... 65

Appendix D LM2524D PWM Modulator Abridged Data Sheet..... 67

Appendix E HTB 200-P LEM Current Transducer Abridged Data Sheet..... 72

Appendix F LM324 Quad Op Amp Abridged Data Sheet..... 73

Appendix G Switching Waveforms of Prototype Welder..... 77

Appendix H Switching Frequency Tests of Prototype Welder..... 91

Appendix J Saber Sketch Simulation Data of Switching Circuit..... 95

LIST OF FIGURES

1.1 Typical MIG or “Wire Feed” welder.....11

1.2 GMAW (MIG) welding.....12

1.3 Simplified MIG power supply.....13

1.4 GMAW (MIG) current and voltage waveform.....14

1.5 Constant Voltage power supply for MIG welder with multi-tap transformer (T1) and inductive choke.....16

1.6 Diagram of existing, high-feature, battery powered welder.....18

1.7 Diagram of proposed low cost switching battery welder.....19

2.1 (a) Basic switching voltage step down circuit and (b) Switching circuit with energy storage component.....22

2.2 (a) Voltage chopper circuit with inductive load (b) Continuous and discontinuous current mode waveforms.....24

2.3 Common positive rail circuit, adapted from Kazimierczuk, 2004.....26

2.4 Switching circuit, as built and simulated, shown without output choke.....34

2.5 Minimum and Maximum output current at various duty cycles and loads...37

3.1 Analog Voltage Mode PWM Control Circuit as used for DC-DC Converter and Wire Feed Motor Speed Control.....44

5.1 Prototype power and control PCB for PAWS design.....47

5.2 Working prototype of the PAWS design.....48

5.3 Current (bottom, blue) and voltage (top, yellow) output of the PAWS prototype design.....49

5.4 Enhanced zoom of current (bottom, blue) and voltage (top, yellow) output of the PAWS prototype design..... 50

5.5 Simulated welder output, ideal circuit with non-ideal component.....52

5.6 Simulated welder output, non-ideal circuit with non-ideal components.....54

LIST OF TABLES

3.1 Control Loop Action Table.....41

4.1 Additional Circuitry in the PAWS design.....45

Chapter 1 Introduction

DC-DC switching converters are widely used in all industries and switching power supply technology is finding new homes as the prices of silicon components comes down and current density of these devices goes up. The Welding industry has traditionally been dominated by transformer-based designs, particularly for low-cost consumer-level machines. This is because nearly all welders are utility line powered machines and transformers are well suited for stepping down the alternating current (AC) input voltage and rectifiers are simple devices to convert AC to direct current (DC). More over, these designs are well established and because consumers favor low cost products, it has been historically difficult to justify the higher costs associated with advanced technologies.

However, while the cost of raw materials such as copper and steel in electromagnetic components have been increasing, the cost of high-power silicon devices has been decreasing. This disparity creates an opening for a new, low-cost DC-DC switching welder in the consumer market. AC-DC Switching power supplies are not new to the welding industry but there is now a unique opportunity to create an entry-level machine that utilizes a high power DC-DC converter. This new design will be made particularly unique by using two external automotive batteries to power the machine, which combined with the light weight switching circuit, makes for an ideal portable welder. Portability is not a standard feature of welders, both due to weight and power supply issues.

This new opportunity to introduce a portable, affordable welding systems (PAWS) has

been identified by the welding equipment manufacturer that has sponsored this design. During the design, the highest priority was given to keeping the cost low and the design simple, while still creating a high quality welding machine. Ultimately this design will be evaluated for production feasibility based on manufacturing costs and market viability.

The first chapter of the following report gives a brief overview of welding technology, particularly focused on wire-feed welders. Background information is presented about transformer-based welders as well as the state of the industry, including existing usage of switching power supplies in welding machines. The second, third and fourth chapters discuss process of designing a welder power supply, including engineering requirements and constraints. Chapter two addresses the switching circuit first from a theoretical standpoint and then discusses the application there of, including how the switching components were chosen and requirements of the output inductor. Chapter three explains the theory behind the voltage regulated control loop used to regulate the DC-DC converter and then explains the specific challenges faced in the real world implementation. Chapter three is a brief overview of the various additional subsystems that were necessary to round out the complete welding machine.

In Chapter five a short description is given to the process of constructing a prototype of the new welder design. Initial test results are presented that demonstrate the functionality of the new machine. Real world data is compared to software simulations of the DC-DC switching circuit, where the limitations are noted in the software's ability to predict the parasitic loses of real world circuits. Lastly in the chapter 6, the PAWS study is presented as an accomplished and feasible design and comment is made to the remaining engineering work necessary to carry the design into production.

1.1 Background

Welding is a process used across several industries. [1] The most common forms of welding use an electric arc to join pieces of metal, often with the addition of a filler or bonding material with like properties. One process, Gas Metal Arc Welding (GMAW) is a form of arc welding common in all applications. GMAW is often seen in the form of a Metal Inert Gas (MIG) welder. [2] A MIG welder is also often referred to as a *wire feed* welder because of the spooled wire feed mechanism that dominates the mechanics of the machine. Fundamentally, a MIG machine is composed of a welding gun with wire feed unit, a direct current (DC) power supply, and plumbing to deliver shielding gas. The weld gun receives the filler material wire from the wire spool. The gun then delivers the wire, electrical potential and shielding gas to the work material. [1] The shielding gas is needed because moisture as well as other elements present in the atmosphere can negatively influence the molten weld puddle. [3] Wire feed welders are popular also because of they are easy to use, and a diagram of a MIG wire feed welder can be seen in Fig 1.1.

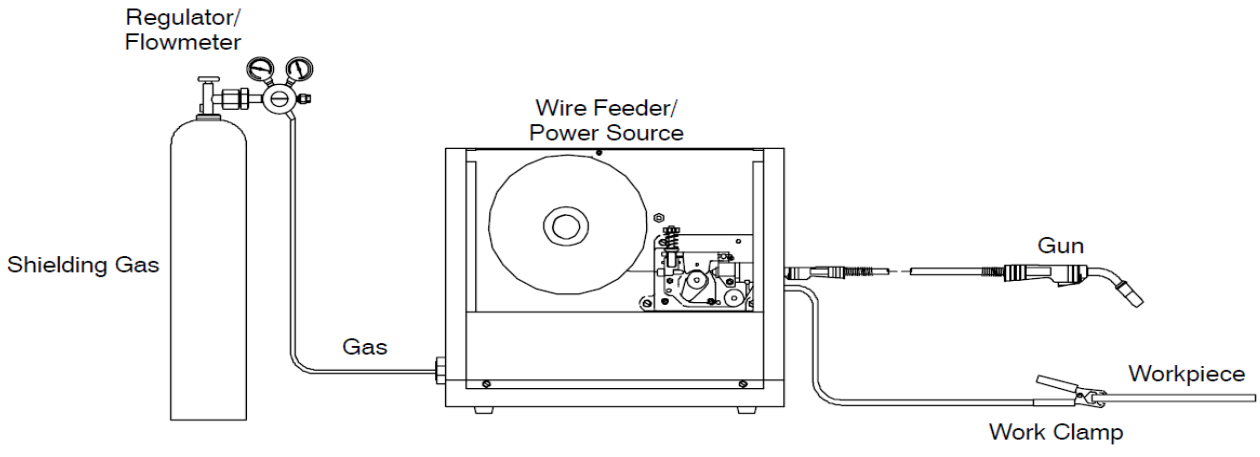

Figure 1.1 Typical MIG or “Wire Feed” welder [4]

Once powered, the MIG machine is activated by a trigger mechanism. As the trigger is pulled, electrode wire feeds from the gun tip, the power supply output becomes electrically hot and shielding gas flows from the gun nozzle. When contact is made with the weld material, current flows from the power source to the contact tip through the wire and arc, into the weld material and back to the power supply through a ground clamp. [2] Fig 1.2 shows the interaction of the weld gun with the material being bonded.

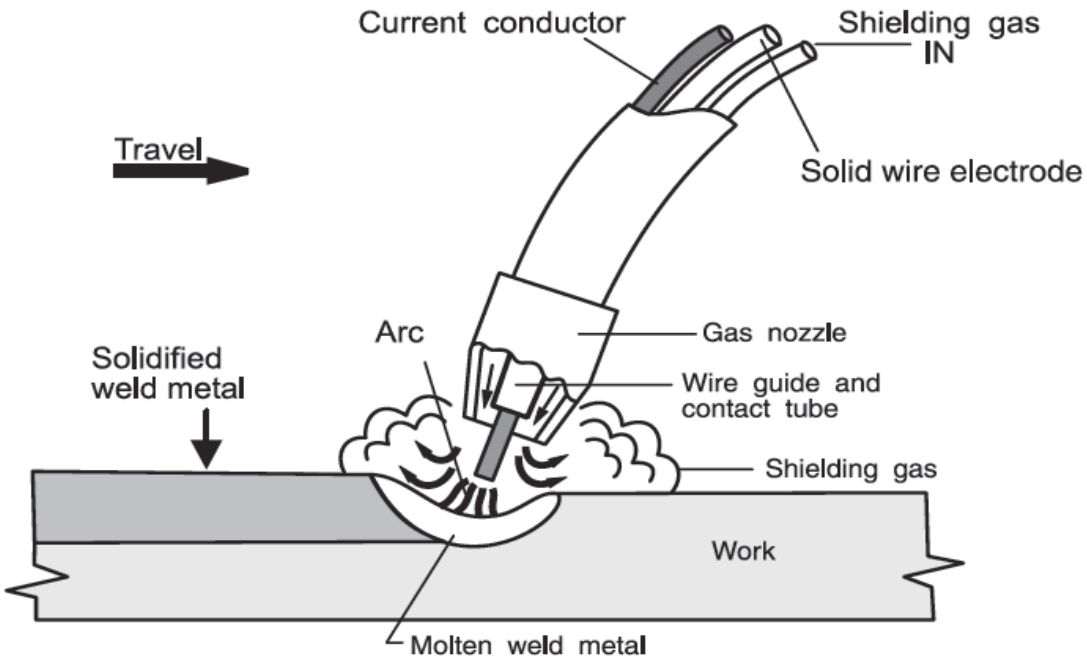

Figure 1.2 GMAW (MIG) welding [1]

MIG welders use a DC, constant voltage (CV) power supply, though welding can be done with various types of power supplies. MIG power supplies are designed to operate at low output voltages (10 V – 30 V) and high output currents (50 A – 300 A). [3] A basic MIG welder is influenced by two controls; wire speed and weld voltage. The weld arc is the load

seen by the power supply and the arc length (which by association the heat put into the weld) and is dictated by the output voltage. Because feedback is used to control the voltage, the device will maintain a near constant arc length during sudden load or wire speed changes because the wire burn off rate will adjust to maintain the arc length. [3, 5] Fig 1.3 shows a simplified electric model of the MIG power supply.

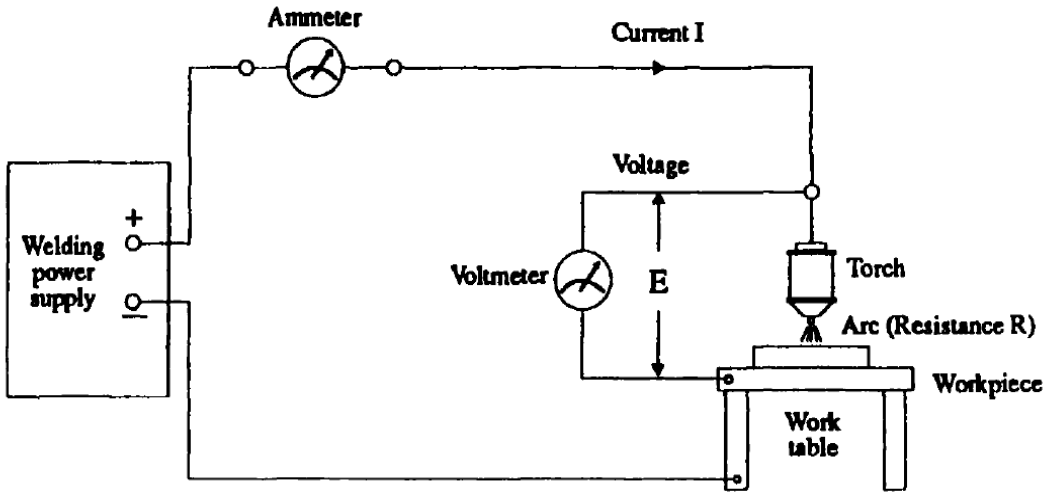

Figure 1.3 Simplified MIG power supply [3]

The average output current is dictated by the speed at which the wire is delivered to the weld arc. The actual output current can have spikes of several hundred amps that occur when the wire makes contact with the material, which then fall off as the wire burns away. The peaks are limited in rate of rise by an inductive choke on the output of the power supply. Messler describes this process as:

> "Short circuiting an electrode with such a [CV, MIG] power source would drop the arc length and the voltage to zero. This, in turn, would cause the current to rise to very high

values very rapidly, with the result of causing the electrode to heat by Joule heating with great rapidity and explosive force, causing severe spatter and, possibly, lengths of unmelted wire stuck in the weld pool. To prevent this from occurring, impedance is built into such power supplies to limit the rate of current change, thereby reducing the likelihood of electrode overheating and explosion, and allowing short-circuiting transfer to take place." [3]

Average welding current and wire burn-off are increased for welding of thicker base materials because greater amounts of filler material are needed. Subsequently, to accommodate the heat needed for joining thicker materials the user will usually have to increase the output voltage accordingly. [5] Fig 1.4 illustrates the relationship between output voltage and weld current.

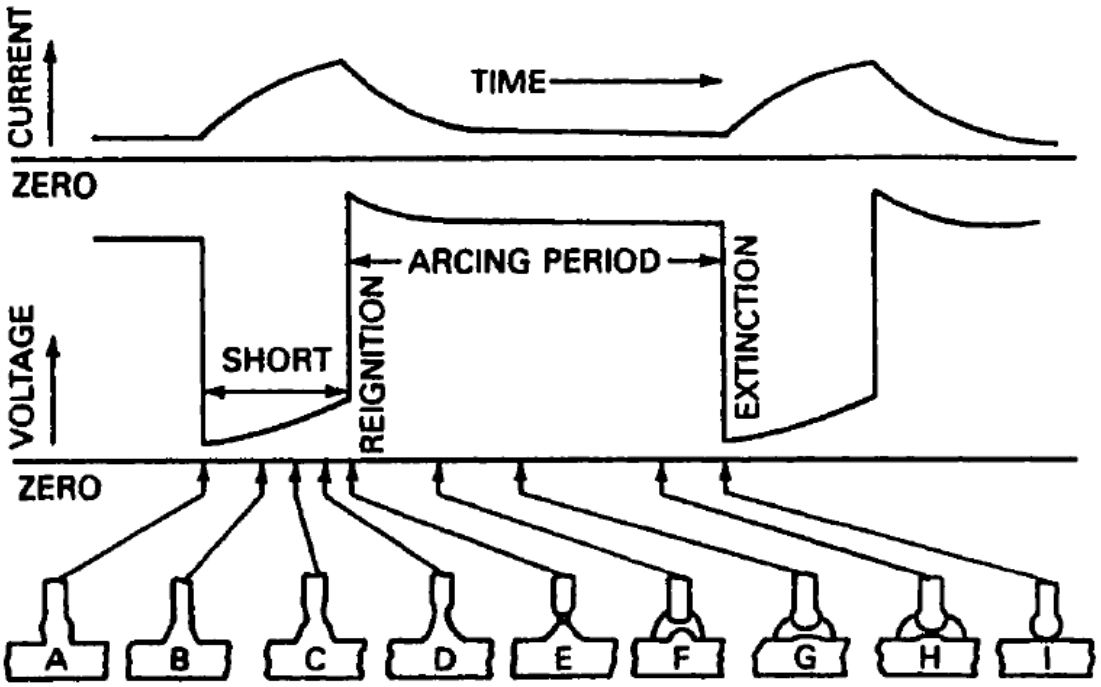

Figure 1.4 GMAW (MIG) current and voltage waveform [3]

There are well documented lists of voltage and current recommendations for MIG welding of standard materials of various size. The table in Appendix A shows one manufacturer's list of voltage and (average) current requirements for a standard MIG machine. Based on the table in Appendix A, a new welder design should be capable of delivering between 40 A and 250 A and operating between 14 V and 25 V output.

The term “MIG” has come to include all wire feed welders and as such, the industry requires that machines be capable of using various types of filler material. This includes flux-core wire that does not require a shielding gas. In order to accommodate both solid and flux-core wire, a new MIG design must include a feature to select polarity of the the electrode and work clamp. [4] Due to the kinetic energy associated with electron flow and the current limitations of the hollow-center wire [3] the machine must provide both direct current electrode negative (DCEN) for flux-cored wire and direct current electrode positive (DCEP) for solid wire. [4]

1.2 Motivation

Based on a gap in the consumer market, corporate direction was given to move forward with proof of concept for the PAWS design. The new design was built for a GMAW MIG machine because of the versatility and popularity of wire feed welders with both novice and experienced users. An entirely new switching power supply needed to be designed while existing “off the shelf” components could be used for the enclosure and wire feed mechanics.

As nearly all welders are powered by utility-supplied (AC) power, the primary component is a high power transformer to decrease the input voltage. This can be seen in Fig 1.5 which shows a conventional, AC-powered, CV MIG power supply. Multiple, switchable transformer taps are utilized to select the output voltage. To create a transformer machine with more voltage resolution, additional output taps are required in the main transformer. This is further complicated by the sag (or slight drop) that each tap will experience when under greater current load. [3] After the transformer, there are diodes to rectify the AC power as well as a capacitor to smooth the output of the rectifier. The final part of the power circuit is an output inductor used to limit splatter-causing current spikes. [3] Additional electrical components might include control circuits with over-current protection, gas valve and relay operations and wire feed motor drive.

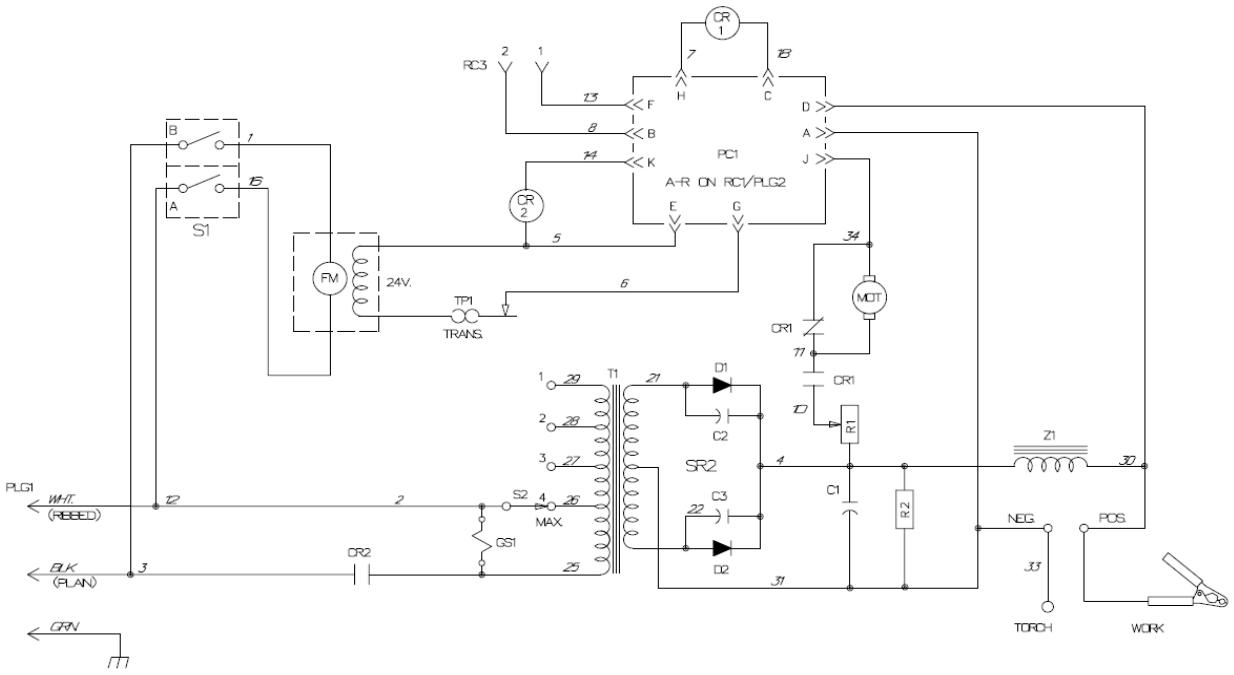

Figure 1.5 Constant Voltage power supply for MIG welder with multi-tap transformer (T1) and inductive choke (Z1) [6]

A portable welding machine promises to be a unique product as the consumer market for line-powered, transformer-based welders is established with many brands and models to choose from. Portability would be particularly useful at a construction site or when repairing a utility vehicle in a remote area. Transformer-based designs are heavy and require a utility power supply, making them unsuited for a portable application. Since welding requires up to several kilowatts of power, a portable welder requires a portable and energy dense power source. Thanks to their ready availability and familiarity in the consumer market, automotive batteries were chosen to power the new welder design. Two external 12 V, lead acid batteries connected in series supply a DC current. At full state of charge (SOC) their nominal voltage is approximately 25 V – 27 V, which is the upper voltage limit of most welding applications. From the battery supplied input, a silicon-based switching circuit can be used to germinate the adjustable voltage output.

Silicon based switching electronics have already been used to replace transformer-based designs in both AC powered and battery-powered welders. [7] As DC-DC and AC-DC switching technology is a new technology to the retail welding market, switching supplies are only seen in the high end, high cost machines. These machines are typically priced at $1,000 or more. An example of a high end portable welder with DC-DC converter can be seen outlined in Fig 1.6. The overhead costs of machines like this can include years of design time. They use expensive and complicated microprocessor-based control structures [7], power monitoring, and battery charging. Such complexity adds additional layers of development and debugging, often requiring more than one microprocessor and software level. The digital devices used to achieve such functionality also add additional susceptibility to electromagnetic interference, both from within and outside the device. Finally, higher

complexity machines are more difficult to assemble during manufacturing, require more complicated functionality tests and various levels of software installation, further increasing the price to consumers. Where high cost, complex machines have already been brought to market, simplicity and elegance of implementation represent the leading edge of design.

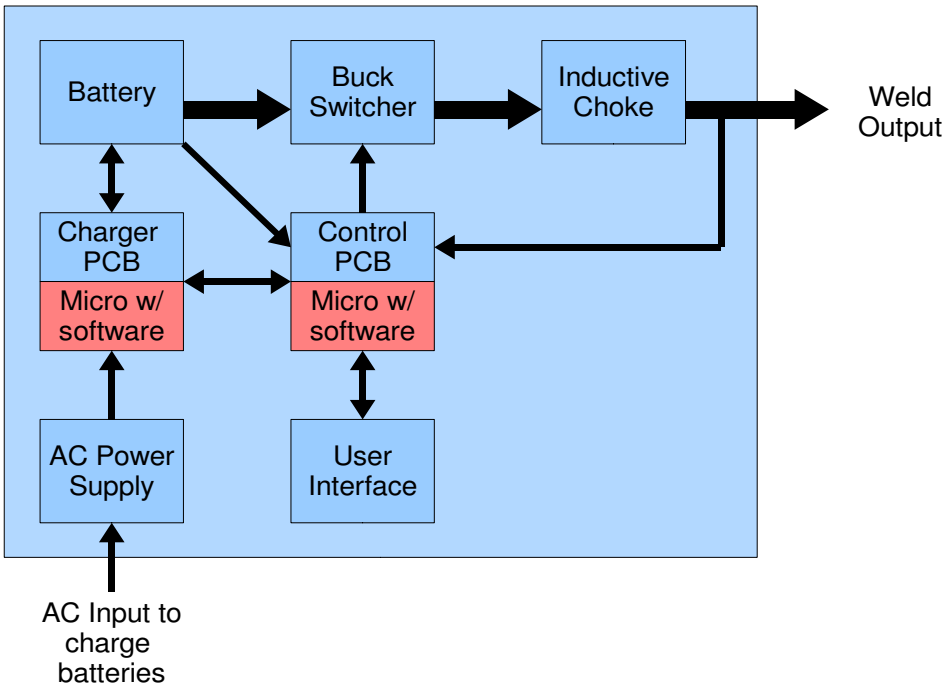

Figure 1.6 Diagram of existing, high-feature, battery powered welder

1.3 Objective

Considering the current state of switching power-supply-based welders in the retail industry, there exists an opportunity to introduce a low-cost, entry-level machines that utilize the benefits of DC-DC converters. The objective of the PAWS project is a wire-feed welder

capable of at least 250 A average output. The new design will be a lightweight, portable device with a 24 V DC input from two standard car batteries and benefit from a voltage regulated, pulse width modulation (PWM) controlled DC-DC converter with adjustable weld voltage of 14 V – 24 V.

Low-cost implementation is the highest priority in the new welder design. A minimalist design approach will be used for all systems and unnecessary features will be eliminated. Component count will be kept low in an attempt to minimize manufacturing costs. When possible, the new design will utilize components from the existing corporate library of part numbers to minimize component price and reduce design time. By revising the model in Fig 1.6 to the approximation model seen in Fig 1.7, the new design manufacturer can compete with their competitors low-cost overseas production.

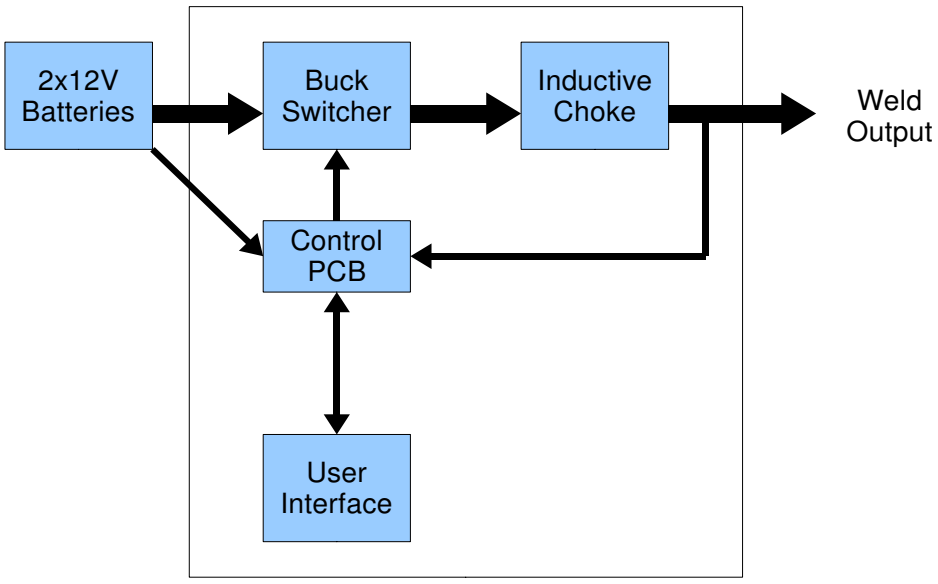

Figure 1.7 Diagram of proposed low cost switching battery welder

In order to be competitive, low cost products cannot have low quality performance. Some extremely low-cost welders are available with wire feed designs but no voltage output control. By using a switching power supply, the output voltage of the new design can be nearly infinitely controllable, unlike the tapped output of transformer designs. This will give the user finer control when adjusting for individual welding conditions. The power supply, when surrounded with quality mechanics, creates a system capable of meeting the quality requirements in terms of arc stability, absence of weld splatter, bead appearance, and the difficult to quantify “weld feel.” Such quality characteristics are defined by the whole system but particularly influenced by the voltage control system, output inductor and power circuit. By offering voltage control with a well-thought-out and thoroughly validated control circuit and output choke, the new design is assured to find the middle ground in terms of price and performance: Better control and weld quality at the same price as other low-cost machines that offer no voltage control, with the same weld quality as expensive, feature-rich machines.

In terms of portability, the new design is made inherently lighter-weight by eliminating the traditional power transformer and using switching power electronics. Also, because the automotive-grade batteries can weigh as much as 50 lbs each, they will be separate from the main welder body. In this way, the welding machine will exist as three distinct components (one welder and two batteries) for easy transportation, and then be combined for operation.

Lastly, as this design study is under the direction of a real-world welding products manufacturer, the ultimate goal is to deliver a design worthy of production for sale in the highly competitive consumer welding market. This requires that the new design be the best possible product, meeting the goals outlined above, for the lowest possible design and

production cost. The market also demands a limited design time within the scope of this project including at minimum a prototype welder that has been functionally tested, along with all associated drawings, documentation and intellectual knowledge.

Chapter 2 Design

The design process was dominated by the limited amount of time with the corporate sponsors engineering group. The initial prototype was needed to make an early case for the financial aspect of the project as well as demonstrating the quality of weld that could be achieved with this minimum cost design approach. With only six months to prove the validity of the concept, it was necessary to have a working prototype as soon as possible, knowing that component optimization and cost optimization would be revised in the future if or when the product was carried to production. The influence of time limitation is seen in the component choices and circuit simulation addressed later in section 2.3 and 2.5.

2.1 Power Circuit

The DC-DC power converter circuit is the key system in a compact and high-current power supply. There are various types of switching circuits that would work for this application, each of varying complexity. Development of switching technology for use in welding machines focuses mostly on circuits that electrically isolate the supply from the load and thus require the use of a transformer. Others use switching circuits to convert from AC to DC and possibly back again to AC, requiring bridge circuits with multiple high and low-side switches. Because of the unique configuration of the battery powered welder, a very simple

step down converter can be used to reduce the nominal 24V battery supply to a lower, variable DC voltage output. The practical efficiency of a step down converter can vary from 92 – 99%, making it ideal for an application where energy conservation is critical, such as when using batteries with limited power storage. [8] The simplest implementation of the step down converter can be seen in Fig 2.1(a) and consists of a pulsed semiconductor switch between the source voltage and the load.

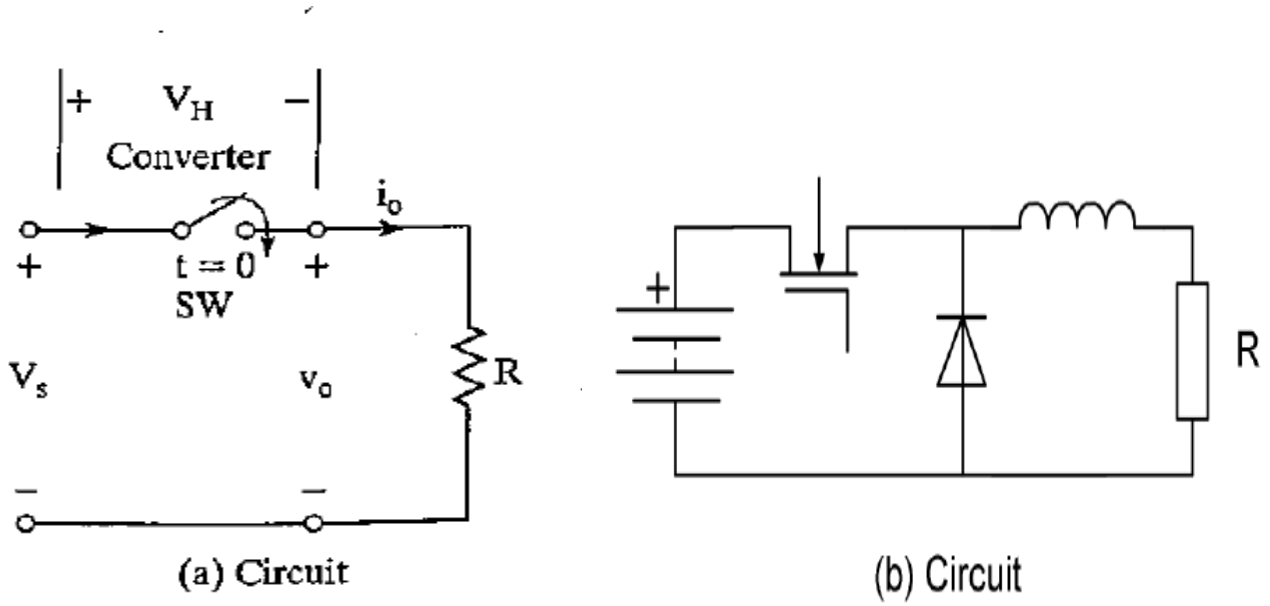

Figure 2.1 (a) Basic switching voltage step down circuit and (b) Switching circuit with energy storage component [8]

The switch, most often a metal oxide semiconductor field effect transistor (MOSFET) device, is turned on and off by a pulse width modulation (PWM) signal. The MOSFET is operated at a switching frequency, f_S, and duty cycle, D, which represents the ratio of switch on time to period, T. When the switch is closed, the output voltage, V_O, will equal V_S and when the switch is open, V_O is zero. The voltage chopping circuit in Fig 2.1(a) has a square and discontinuous output. For a continuous power output, an energy storage component is

necessary. By adding a choke with inductance, *L,* and diode (called the free wheeling diode), the circuit can be operated in the continuous current mode (CCM) which is needed to maintain a strong welding arc. The revised circuit with inductive energy storage component is shown in Fig 2.1(b).

Some power supplies feature an output capacitance to filter the voltage and current output, but because the welding power supply does not require a smooth output voltage, a filter capacitance was not installed. However, the current through the inductor of a step down converter has a saw tooth pattern. It can be described as being in CCM if the inductor current never reaches zero at the bottom of the saw tooth. Likewise, a switcher operating in discontinuous current mode (DCM) will spend some amount of time with zero current output, regardless of the peak current value. For the welder, the inductor current should be continuous because the current output of the inductor is the same current output to the weld arc. And because the weld load is nearly resistive, the current output will also be saw-toothed and potentially sporadic if the inductor current is discontinuous. By operating the power supply exclusively in CCM, a continuous weld arc can be ensured. In general, the current is continuous if $L/R >> T$ or $Lf_S >> R$. [9] The waveforms of these two modes of current conduction are shown in Fig 2.2(b) as well as the equivalent switching circuits with inductive load in Fig 2.2(a).

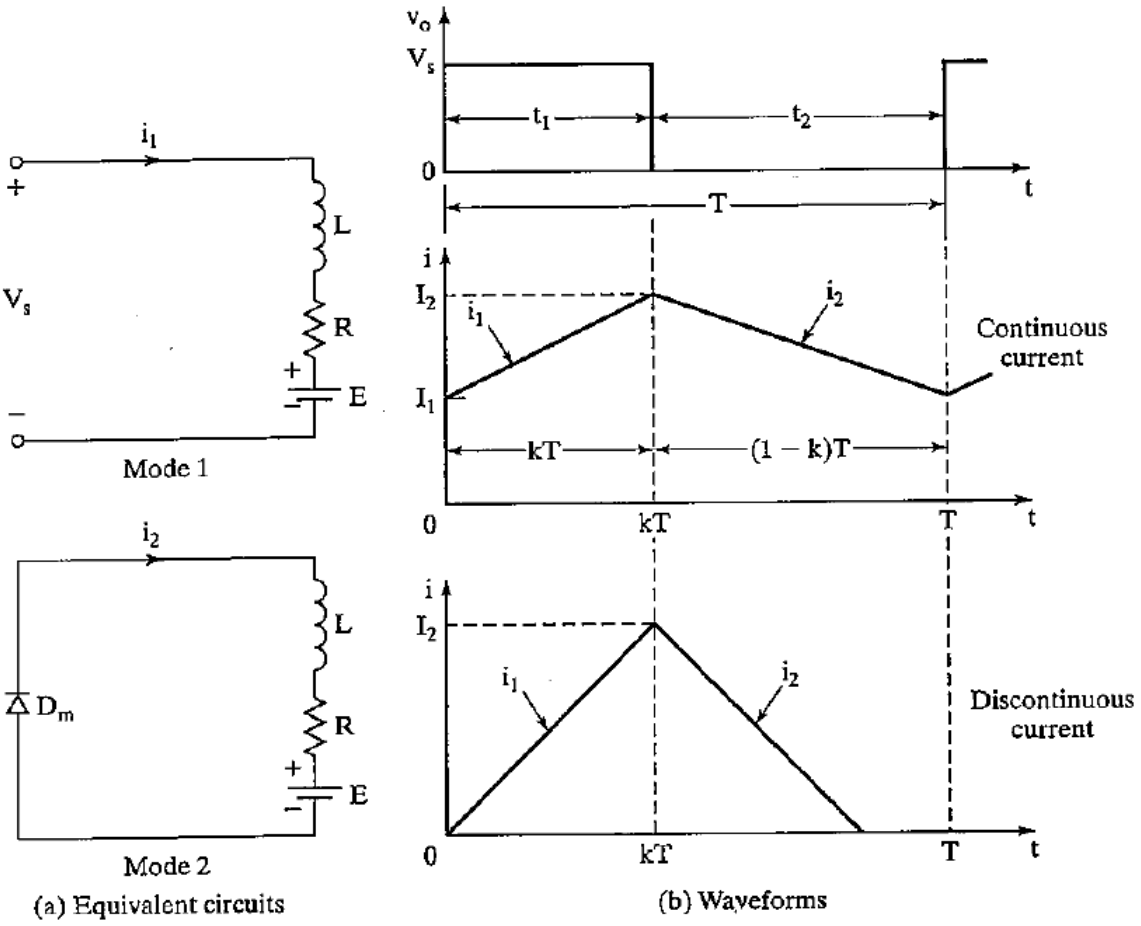

Figure 2.2 (a) Voltage chopper circuit with inductive load and (b) Continuous and discontinuous current mode waveforms [8]

During switching operation, the converter circuit can be represented with two separate equivalent circuits described as mode 1 and mode 2. In the first mode, the switch is closed and current, i_1, flows from the supply to the load. The current rise is limited by the presence of the inductor, which stores some of the energy in a magnetic field. During mode 2 the switch opens and the inductor releases energy to the load and back through the diode. [8] In this way, the amount of energy delivered to the load can be controlled via the duty cycle, D. [11] When in continuous mode, the minimum and maximum current levels, I_1 and I_2, can be

approximated with equations 2.1 and 2.2. Note that voltage supply, *E*, is included by Rashid to develop a series of generalized equations and for this application will be considered zero.

$$I_1 = \frac{V_{Source}}{R}\left(\frac{e^{Dz}-1}{e^{z}-1}\right) - \frac{E}{R} \quad \textbf{(2.1)}$$

$$I_2 = \frac{V_{Source}}{R}\left(\frac{e^{-Dz}-1}{e^{-z}-1}\right) - \frac{E}{R} \quad \textbf{(2.2)}$$

Where the Z coefficient is defined as,

$$Z = \frac{TR}{L}$$

Equations 2.1 and 2.2 only consider ideal components and as such do not account for the resistive and capacitive elements of the inductor. More importantly, ideal MOSFETs and diodes do not account for voltage spikes and energy losses that occur during transitional periods. However, these equations allow for an approximation of operating conditions. Through equations 2.1 and 2.2 above, both the average output current and source current can be computed, using equations 2.3 and 2.4 from Rashid.

$$I_{avg} \approx \frac{I_1 + I_2}{2} \quad \textbf{(2.3)}$$

and

$$I_{source} \approx D\, I_{avg} \quad \textbf{(2.4)}$$

Because the mobility of electrons (the majority carriers in N-MOS devices) is greater than the mobility of holes in P-MOS devices, N-mos components are generally faster and

more desirable for high power switching circuits. [9] To activate the N-channel device, a threshold gate-source voltage must be applied, V_{GS}, which for the circuit in Fig 2.1(a) would need to be higher than the source voltage supplied by the batteries. In Fig 2.3 the circuit is redrawn with a *common positive rail* configuration such that the source pin is tied to ground and V_{GS} << 24V.

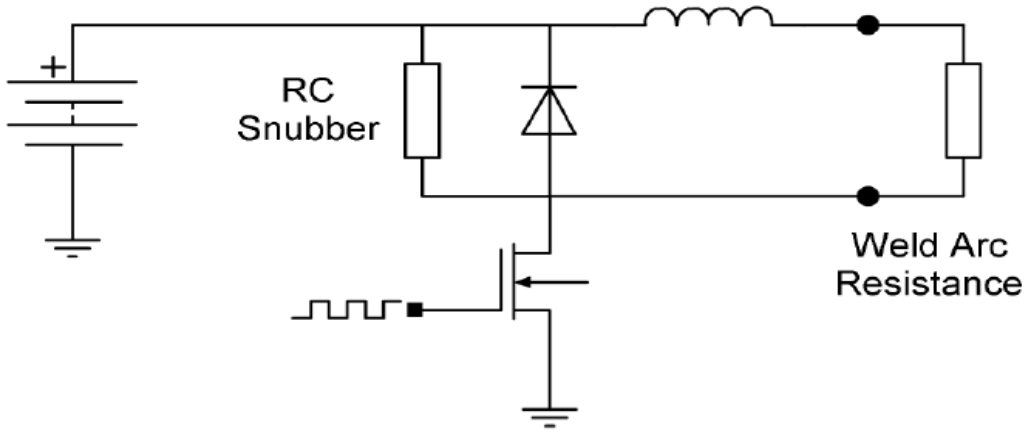

Figure 2.3 Common positive rail circuit, adapted from [11]

2.2 Switching Methodology

Choosing the switching frequency DC-DC converter is a process of compromise. High speed switching is often used to minimize the size of magnetic components such as transformers and inductors, while still maintaining CCM at the the inductor. It can be difficult to implement because of limitations inherent in the components, including noise issues and power requirements. The upper limit of the switching frequency is determined in part by the capacitance of the MOSFET gate. This capacitance is overcome by using a gate-driving circuit with a high power output to quickly charge and discharge the MOSFET gate. A bi-polar gate driver could be used to pull the FETs down faster during turn off, but it would add

unwanted cost and complexity.

Alternatively, slower switching speeds ensure a more square waveform and thus, fewer switching power loses. Because switching loses are greatest during the transition phase between the on state and off state of the devices, a slower frequency ensures a greater percentage of time is spent in a definitive state and out of transition. Equation 2.5 describes switching loss as a function of frequency, MOSFET output capacitance and input voltage. [9]

$$P_{SW} = f_S C_{out} V_I^2 \qquad \textbf{(2.5)}$$

From Equation 2.5, minimizing the switching frequency also minimizes the switching power loses. A converter switching frequency should not be lower than 20 KHz, or the approximate audio frequency limit for human hearing. [9] For the PAWS application, 25 KHz was chosen as a switching frequency slightly above the audible range, yet maximizing the squareness of the waveform with the knowledge that an inductive component would have to be sized appropriately. Early switching data (Appendix D) indicated that 25 KHz is a reasonable frequency for both the PWM controller and the MOSFET driver when in circuit with four parallel high power MOSFETs.

Duty cycle, *D*, will determine the ratio of time spent in mode 1 to the time spent in mode 2. Neglecting certain small losses, the steady state duty cycle can be approximated using in equation 2.6 below. [8]

$$D = \left(\frac{V_o}{V_I} \right)^2 \qquad \textbf{(2.6)}$$

The welder design incorporates a control circuit that will dictate the duty cycle. The characteristics of that system will be discussed in chapter 3. However from the welding voltage requirements in Appendix A and using the equation above, estimates can be made for the minimum duty cycle, D_{min}. At 14 V output (the approximate bottom of the voltage range), the welder will operate near 40% duty cycle. However considering the inherent losses that need to be overcome in a real device, the actual minimum duty cycle will probably be closer to 50%. It is also true that the output voltage will never be as high as the input, even at 100% duty cycle. This is because of the voltage drop across the inductor and closed MOSFETs, neither of which are perfect conductors.

2.3 Switching Components

This welder design was directed by a manufacturer with an existing library of products. For a company with established production, the fastest and lowest-cost way to create a new design is by using “off the shelf” components. By using general equations and approximations to understand the stresses that components are likely to see, parts can be chosen based on availability. After assembling a prototype the entire system can be evaluated. Validation data combined with simulation results can be used to determine if the cost of sourcing and validating new components is sufficiently offset by the per piece cost savings gained from using those new parts. Alternatively, the readily available but possibly over-engineered parts may be used even into production, because of the savings of scale and availability.

Considering the financial benefits of using parts from the corporate library, component choices were then made based on the worst case current and voltage stresses the individual component will experience during operation. Equations 2.7 and 2.8 describe the maximum current and voltage conditions experienced by the freewheeling diode and the switching MOSFET. [9]

$$I_{S(max)} = I_{D(max)} = I_{O(max)} + \frac{V_O\left(1 - D_{(min)}\right)}{2 f_s L} \quad \textbf{(2.7)}$$

$$V_{S(max)} = V_{D(max)} = V_{I(max)} \quad \textbf{(2.8)}$$

With the original requirement of 250 A average output current, the equations above indicate peak steady state currents approximately 10% higher than max output. Current output is the primary rating a commercial welder will receive, with the maximum current often embedded in the machine model number. As such current requirements for a welder in a commercial design setting are subject to change, depending on marketing requests. With potential for creepage in the requirements, plus a requisite margin of safety, it was considered prudent to maximize the current capacity of the switching circuit.

MOSFET # IRF2907 (Appendix B), is capable of 209 A continuous and 75 V breakdown voltage. It was available in the corporate part catalog and features a very low on resistance, R_{DS}, of 3.6 mΩ at 125 A. Also, because of the likelihood of stray inductance creating ringing and voltage spikes, the 75 V part offers good protection. Using four MOSFETs guarantees current requirements are met and the circuit will be constructed is if it

were four separate DC-DC converters, each wired in parallel to the next.

The high voltage power Schottky diode, # STPS40H100CW (Appendix C), is capable of 40 A average continuous forward current and 100 V reverse voltage protection. A traditional diode will create a storage charge when conducting that must be overcome before changing states. [9] The Schottky diode was chosen specifically because it does not exhibit the reverse recovery phenomenon of a standard junction diode. As a result, the Schottky diode can transition from conducting to blocking in tens of nanoseconds, where a traditional diode may require hundreds of nanoseconds. Faster transition times result in the ability to operate at a higher switching frequency, but more importantly, result in lower switching losses at all frequencies, as compared to junction diodes. [9]

As shown earlier, the freewheeling diode only conducts in mode 2 when the MOSFET is off. Because welding voltage is closely tied to weld current, the highest welder output currents will happen when the output voltage is near maximum and the duty cycle is near 100%. Equation 2.8 predicts peak *instantaneous* current of the diode but it is the *average* continuous current for which the device must be sized and thermally managed. Average current is a function of time and magnitude. When averaged over the entire switching period, the diode spends the most amount of time in conduction during the lowest duty cycle because that is when mode 2 is prevalent. Considering the previously calculated D_{min}, for this application the diode spends the most amount of time in conduction when operating at D = 0.5. Based on the weld requirements in Appendix A, user conditions should not demand more than 150 A at D = 0.5. Likewise, a 50% duty cycle means equal time spent in mode 1 and mode 2, so only half will the output (75 A) will be conducted through the diodes with the

rest conducted by the MOSFETS. Due to this unique voltage/current relationship in the welding power supply, the freewheeling diode can be sized to a lower current capacity than the switching MOSFET. As with the MOSFET, four diodes will be used in the circuit, all in parallel to maximize current capacity.

A PWM signal will be generated by the a PWM modulator which will be sent to a discrete MOSFET driver IC. The driver is needed to ensure that the V_{GS} switching signal to the MOSFET is able to overcome the combined gate capacitance of four parallel high power MOSFETs. The PWM module is capable of delivering only 200 mA to the switching signal output, which is sent to the driver chip rather than the MOSFETs directly. The driver will repeat the received signal and with the ability to drive the four parallel switches at 25 KHz with up to 9 A of current.

The printed circuit board (PCB) on which the welder circuit was built is a two-layer (top and bottom), through-hole component board. Surface mount component PCBs offer the benefit of a smaller overall board size due to smaller component size. And boards with more than two layers of copper are able to bury traces inside, further reducing the required surface area. Yet surface mount boards are much more difficult to work with, especially in the development phase when hand-rework and design revisions are likely. Also, choosing to not maximize the component density, makes component heat management easier to implement.

The four power MOSFETs and four diodes, each through-hole components in TO-247 packages, were mounted to the PCB so they were bent parallel to and touching the board surface. Hardware was used to retain the components to the board, offering additional stress

and vibration relief, and they were turned such that the metal sides were facing up. Aluminum heat sinks with conductive grease were mounted to both the diodes and MOSFETs to aid in heat dissipation. A 12 V fan was added to create forced air-cooling. At the time of the initial prototype the heat sinks and fan were not optimized for the particular application and instead a “cooler is better” methodology was used. Additional heating and power loss considerations were revisited in the simulations, but this approach should accommodate higher than expected power outputs while preventing heat damage to the components. The added complexity of large heat sinks and forced cooling may be abandoned as the design reaches maturity, but the added insurance is invaluable during development.

Last, in anticipation of future changes, a snubber circuit was added on the first prototype PCB. The snubber (seen in Fig 2.3) is a series resistor-capacitor network across the freewheeling diode, added to minimize potential voltage and current spikes. From supplier application notes of component manufacturer, Cornell Dubilier Electronics, a snubber network across the buck re-circulating diode reduces ringing and spikes at the switching node and spikes beyond the maximum voltage rating of the re-circulating diode, which can damage the device. Though the high power Schottky diode will not induce the effects of reverse recovery, it is likely that the traces and ground plane surrounding the switching components will induce parasitic inductive and capacitive elements. It was known that there would not be time for multiple PCB revisions, yet there was no way to know what parasitic effects would act on the DC-DC converter.

A resistor and capacitor snubber pair was added to the first prototype circuit board in parallel with the power diode, as a place holder for future revisions. Chosen specifically for

snubber applications were a 2 W non-inductive carbon resistor and 100 V film capacitor. The 4.7 Ω resistor and 0.1 µF capacitor values were taken from an existing product and once in place on the PCB, are easy values to change. Snubber circuit optimization and effectiveness will be discussed further in chapter 6.

Because the battery power source is DC, there is no input voltage ripple to filter, but initial testing showed that parasitic inductive loads between the battery and the switching circuit would increase the switching rise time. As shown, longer switching transitions cause higher losses during switching. For convenience to the user, the batteries are separated from the control board by as much as a dozen feet of high current cable. This means unwanted inductance can be present in the circuit before the switcher. To counter the effects of stray inductance, a large capacitance was added in front of the switching circuit. Capacitance can provide a stronger voltage supply to the switcher meaning less voltage sag under high loads and behaving more as an ideal voltage source. This addition will create better conditions for the initial arc-strike and during short circuit conditions. To implement the capacitance in the prototype PCB, five smaller capacitors were used in parallel rather than using a single large component. Using multiple smaller parts helped reduce the equivalent series resistance (ESR) and overall cost of the design. Fig 2.4 shows the final DC-DC switching circuit, as constructed on a PCB for initial evaluation. Note that the high current inductor is absent because this is an “off board” component, too large for the printed circuit board.

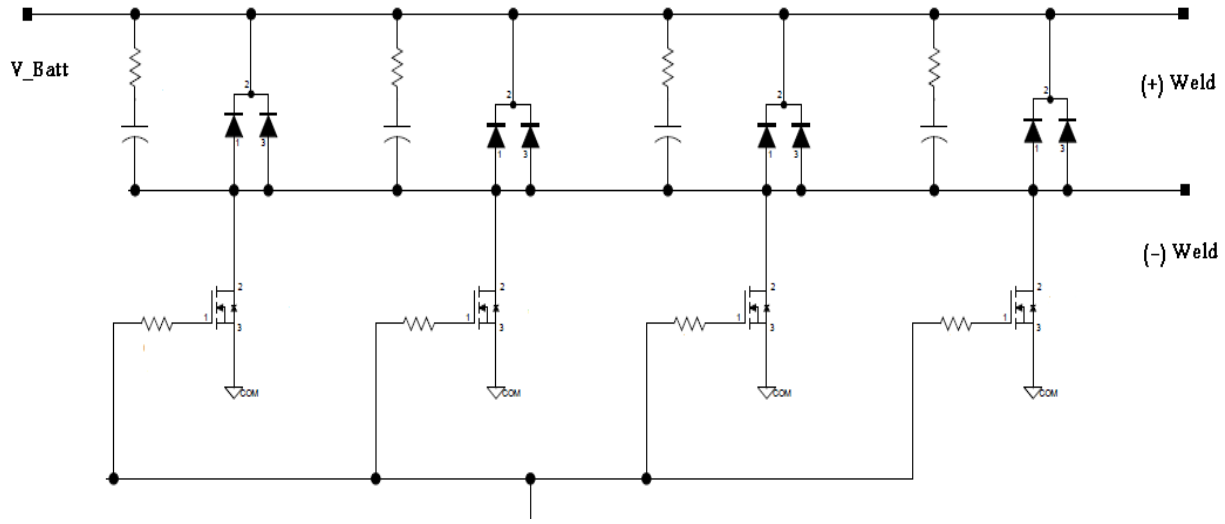

Figure 2.4 Switching circuit, as built and simulated, shown without output choke

2.4 Output Inductance

The amount of inductance in the weld circuit must be chosen carefully to ensure ideal operation. As seen in Fig 2.3, inductance is added to the power supply by installing a choke at the output terminals of the switching circuit. The inductance controls the rate of current rise during a short circuit and stores energy to maintain current flow in mode 2, when the MOSFET switch opens. In general terms, more inductance is better, yet weld-start problems can be caused by having too much inductance as well as not having any at all. [5] The inductance of the choke is generally determined by the number of conductor turns in the choke, but there are other important factors must be considered when choosing a choke.

Core saturation occurs when the choke can no longer store additional magnetic energy and is associated with a maximum current amplitude. Operating near or beyond the

saturation point will cause the device to cease providing linear control of the current rise. Saturation is mainly a feature of the inductor core size and material. Also the choke current carrying capacity must be considered. At DC and low frequency conditions, current capacity is determined by the cross sectional area of the winding wire and must be sized in accordance with the high-current output cables and switching components. [10]

Due to limited project time, designing a completely new choke was not possible. An existing part was chosen from a high-end, 180 A MIG welding machine. The chosen choke was previously pulse-tested with a voltage burst. Using equation 2.9 and observing the waveforms of a high current pulse test, the choke was shown to have a core saturation beyond 300 A (the maximum anticipated current at that time) and an approximate inductance of 15 uH.

$$V_L = L\frac{di_L}{dt} \qquad \textbf{(2.9)}$$

Equation 2.10 from Kazimierczuk approximates the minimum inductance, *L,* necessary for the DC-DC converter to operate in CCM mode.

$$L_{min} = \frac{R_{L(max)}(1 - D_{min})}{2 f_S} \qquad \textbf{(2.10)}$$

Where $R_{L(max)} = \frac{V_{O(max)}}{I_{O(min)}}$

The inductance equation above with steady state conditions (R_L = 0.25 Ω, D = 0.4) returns a value near 6 μH, implying the inductor choice of 15 μH is more than sufficient. However, a strong inductance is also necessary to prevent weld splatter, which occurs when the welding wire briefly contacts the work material, causing the load resistance to approach zero. [3] Short circuit conditions create variables beyond the steady state calculations. This is why the welding characteristics of a new machine are often “tuned” through real world testing. The test results of using this inductor will be discussed further in Chapters 5 and 6.

With a known switching frequency, output inductance and approximate output load, equations 2.1 and 2.2 from above can be revisited. By plugging these values into the upper and lower current level equations, the current bounds are explored in terms of output resistance and duty cycle. This relationship can be clearly seen in the MATLAB simulation of Fig 2.5 below. Several operating characteristics can be seen in Fig 2.5 below, including the minimum impact that duty cycle will have on output current, particularly considering the welder's ability to effectively vary the load resistance through control of wire feed speed. The figure below also indicates that the machine will operate in CCM even at the lowest duty cycles and highest load resistance. Lastly it is confirmed that the 50% duty cycle condition sees the greatest current swings.

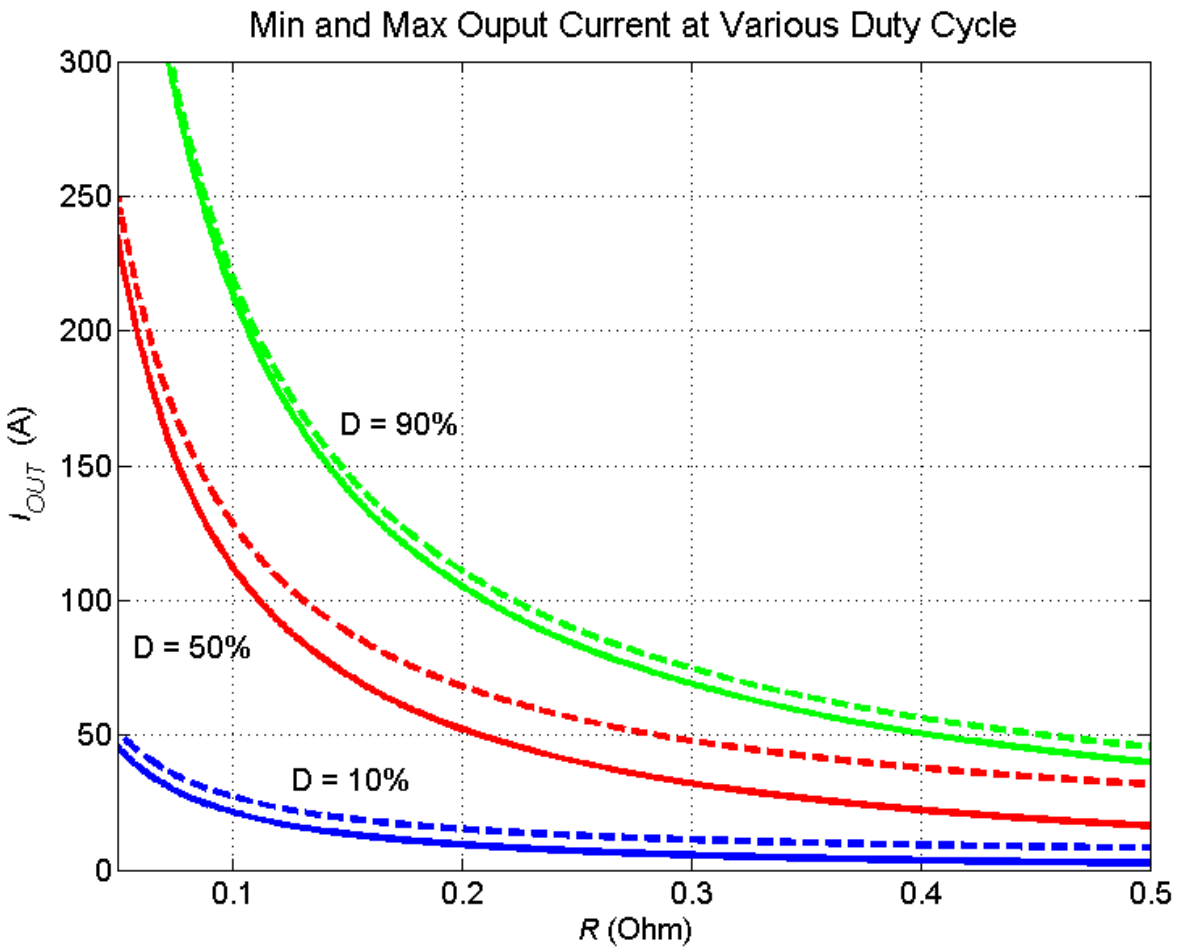

Fig 2.5 Minimum and Maximum output current at various duty cycles and loads

2.5 Power Simulations

The easiest and most accurate way to estimate switching and power losses in a DC-DC converter is through computer simulation. By constructing a computerized version of the circuit with manufacture supplied models of the actual components, modern software packages can quickly derive the complicated operating conditions. Once the initial design was finalized, the circuit was assembled digitally in the Saber Sketch Software package. Though more advanced than standard equations, the simulation software also has some

limitations. Because the new design features four sets of parallel components and wide, thick, traces between components, stray inductance and capacitance will play a large role in the real world performance of the device. These parasitic components can be added to the computer model but the real world values would be extremely difficult to derive or measure.

The greatest unknown of simulating the weld circuit comes with accounting for the output load, or the arc itself. The welding arc is often approximated with a purely restive load, but in the real world behaves slightly as an energy storage element. Messler attempt to describe the nature of the weld arc in terms of thermal activity, including variables such as arc length, temperature and metallurgical characteristics. However complex arc models are beyond the scope of this design. A limited trial revealed that a very slightly inductive component (0.2 mH) used with a series resistive element (between 0.05 Ω for short circuit and 0.5 Ω for steady state) worked well in the Saber simulations.

An additional complication of the weld arc is the choppy and non-linear nature of the current draw, shown in Fig 1.4. Rather than trying to simulate a circuit with a variable load, separate simulations were conducted, one for the steady state, or arcing condition, and another for the short circuit, high current rise condition. By combining the two separate models, both a steady state and a transitional condition can be observed. Because of the shortfalls inherent in all software packages, performance of a new design is gauged by a combination of simulations and real-world testing. The predicted simulations will be compared with the real-world data in Chapter 5.

Chapter 3 Control Circuit Design

The control circuit is responsible for creating the 25 KHz switching frequency, f_S, and controlling the duty cycle, D. By using a feedback loop, the control circuit will ensure the desired output voltage is maintained by adjusting the PWM duty cycle, particularly when the load and welding conditions vary. To meet the goal of a low cost and minimalist design, the control circuit must be simple, straightforward, and scalable.

Control can be implemented with a microprocessor, dedicated analog circuit, or combination of both. [11] Analog control circuits have been used extensively in the consumer welding industry while microprocessor control has been limited to high-cost, feature-rich units. Microprocessor-based controllers can be hugely flexible and offer near infinite tuning of the weld performance. However, a microprocessor requires specialized software, which requires investing more time and possibly more expertise during the development process. Additionally, it has been shown by Priewasser that microprocessor-based control circuits will respond to changes slower than analog equivalents, due to the delays inherent analog-to-digital conversion process. [12]

For advanced welding applications such as an industrial setting, where extremely precise welding is more important than cost, digital control offers the high level of configuration necessary. [11] However, considering the less demanding requirements of the consumer market and the priority of reduced cost for this design, analog control was the best fit for the PAWS project. With the exception of a slight voltage droop when the batteries are under severe load, the input voltage will be nearly constant. This means the control loop will

only need to account for changes in the output. The CV power supply used by MIG machines allows current to fluctuate as demanded by the user (via wire speed) so only the output voltage must be regulated. Based on these requirements and limitations, an adjustable voltage-based control feedback loop was used. A hugely beneficial secondary effect from choosing this particular analog control topology is the ability to use those same components and layout to control the 24 V brushed DC wire feed motor. This was a major step towards reducing the overall development time and complexity, as the two circuits, though tuned to their respective applications, are essentially the same.

An adjustable, voltage-regulated DC-DC feedback loop uses a closed-loop voltage mode control. The voltage mode control hardware implementation was based on a simple fixed frequency, multipurpose pulse width modulator (Appendix E). Featuring an analog, 1 V to 3.5 V input reference, part # LM2524D will produce a scaled 0 – 100% duty cycle output. The PWM module for this purpose can be considered a prepackaged PWM generator based on a saw-tooth signal and set/reset (SR) latch. The duty cycle is in turn determined by the intersect of an externally supplied (1 V – 3.5 V) reference signal, which is compared against an internally generated saw tooth (1 V – 3.5 V, peak to peak). The switching frequency of the output pulse is determined by an external resistor-capacitor pair.

The voltage feedback circuit for the PAWS machine was implemented in a traditional way, as it is a well studied and proven design. The voltage feedback loop employs a reference voltage, V_R, and compares it against a feedback voltage, V_F. The feedback is related to the output voltage by the beta network, β, and equation 3.1: [9]

$$V_F = \beta V_O \quad \textbf{(3.1)}$$

The error voltage, V_E, is created with a comparator or full-gain operational amplifier (also know as the error amplifier, or compensator) and describes the difference between the desired output voltage and the actual output voltage [9]

$$V_E = V_R - V_F \quad \textbf{(3.2)}$$

Finally the error, V_E, is used to derive the duty cycle by comparing it to a ramp voltage with a op-amp based comparator. This final step is the process that takes place within the PWM module. [9] Table 3.1 describes the cause and effect relationship at work in the voltage feedback control loop.

	System Change →	**Effect on Voltage →**	**Effect on Compensator →**	**Effect on PWM →**	**Effect on Voltage →**	
System Stability →	Short Circuit or Heavy Motor Load	Output Voltage Drops	More Time Output High	Pulse Width Increases	Voltage Increases	**System Stability →**
	Open Circuit or Light Motor Load	Output Voltage Spikes	More Time Output Low	Pulse Width Decreases	Voltage Drops	

Table 3.1 Control Loop Action Table

For this particular application, the output voltage is across the freewheeling diode and is not referenced to system ground. To account for this condition, a differential voltage

amplifier circuit was installed to measure the voltage output between the positive weld terminal and the negative weld terminal. This circuit also scaled the output to 10% of its original value, (making $\beta = 0.1$) and provides the V_F signal to the negative pin of the error amplifier. This yields a feedback signal that varies from 1.4 V – 2. 5 V as the welder output adjusts from 14 V – 25 V. In standard control applications the output signal from a DC-DC converter is filtered with a large output capacitor, making for a smooth V_O and relatively small AC component in the feedback voltage. Since the welder output is unfiltered, it was necessary to filter the feedback instead. A very small capacitance was added across the negative input and output of the error compensator. In this case, a 0.033 µF ceramic cap was sufficient to filter the large AC component from the feedback without slowing down the system response.

The positive input of the error amplifier is supplied the reference voltage to which the control loop will try to push the welder output voltage. Recall that the feedback voltage is scaled by the beta network to vary from 1.4 V - 2.5 V. The reference signal is compared against the feedback by the error compensator, so the reference must also have the same dynamic voltage range. Since the output voltage is a user-defined level, a 10 KΩ potentiometer was incorporated into a voltage-divider network. It was adjusted such that adjusting the potentiometer from full 0 Ω to 10 KΩ, would adjust the reference voltage from 1.4 V to 2.5 V.

3.1 Over Current Protection

The voltage feedback loop is a single-loop control circuit. For safety purposes and to

protect the welding circuit components, a pseudo second-loop was added for over current conditions. An inductive current sensor capable of measuring +/-500 A (for short periods) is used to monitor the output of the machine. The inductive sensor is used because it does not require breaking the output circuit and can measure current flow without a loss-inducing shunt resistor. When subject to positive current flow, the sensor will produce a scaled, positive 0 V – 5 V signal, corresponding to a 0 A – 500 A current. When the output of the transducer exceeds the preset threshold (3.0 V scaled to correspond to 300 A) the over-current comparator will switch low, momentarily pulling down the PWM reference signal. As the current retards, the comparator will return high and the machine will immediately recover to the user defined settings. This arrangement should allow the welder to operate at the very limit without completely killing the output or shutting down the weld, creating an undesirable "start-stop-start" condition. The a block diagram of the full control scheme is shown in Fig 3.1

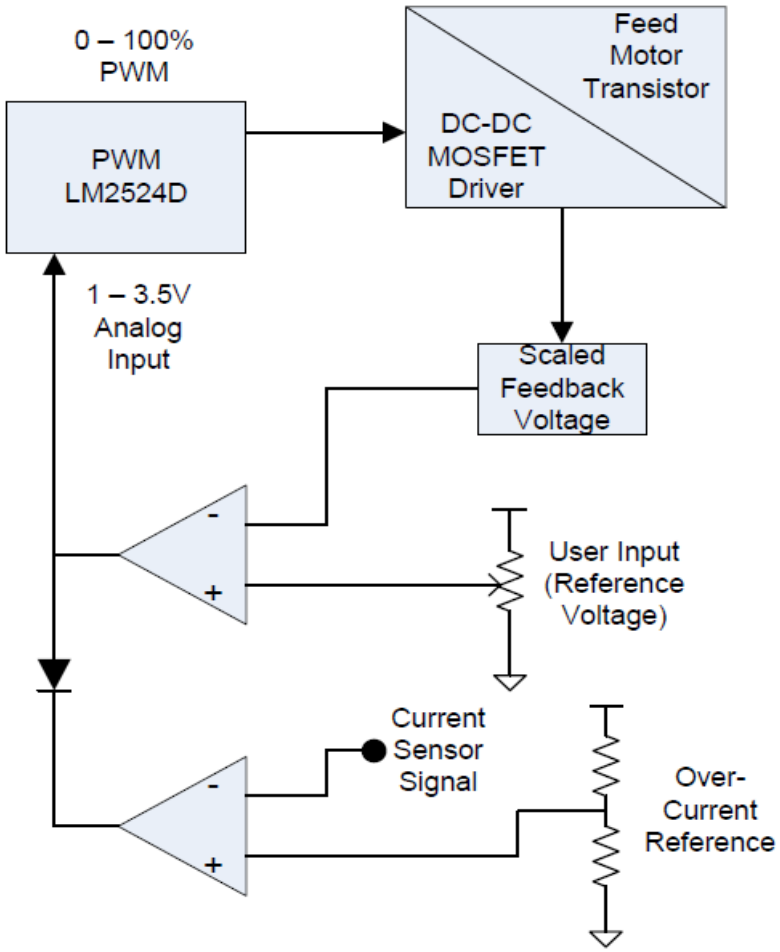

Figure 3.1 Analog voltage mode PWM control circuit as used for DC-DC converter and wire feed motor speed control

Chapter 4 Additional Design

The DC-DC switching circuit and associated control scheme represent a third of the total design effort to create the complete welding machine package. Most of the additional design work is beyond the scope of this project but what follows is a brief description of the major sections. Table 4.1 outlines the major design areas, followed by a brief description of the on-board power supplies.

Feed Motor Control	Use voltage-based feedback to vary motor speed Provide over-current protection and dynamic brake to prevent coasting
Pre-charge Circuit	Limit inrush current to input capacitors and prevent contact closure if batteries connected in reverse polarity
Gun Trigger Control	Simultaneously engage all power relays, switching circuits and feed motor. Delay switching circuit turn-off to allow for wire “burn back”
Contactor Economizer	Use full voltage to pull in main contactor coil and then switch to limit circuit to contactor coil

Table 4.1 Additional circuitry in the PAWS design

To power the controls and ancillary devices contained within the welding machine, two linear power regulators were used to create a +15 V and +12 V supply from the 24 V input. Recall that the battery voltage will sag when subject to the high power loads of the weld circuit, so it was necessary to have stable supplies present on the PCB. To minimize design time of the first revision, standard linear regulators were used with the appropriate filtering capacitor installed as directed in the manufacturer application notes. Using separate supplies, +12 V for the electromechanical devices, and +15 V for logic devices, decreased likelihood of noise propagation between the two.

4.1 Wire Feed Motor

The wire feed motor is a 24 V brushed DC motor. Like the rest of the PAWS design,

the wire feed motor is a minimum cost device, meaning it lacks a speed or position feedback signal. Instead a PWM signal is used to control a medium-current MOSFET that in turn creates a pulsed signal to the motor. The motor behaves similar to the weld circuit because of its own internal inductance and the switched MOSFET behaves like a variable voltage output. Using a repeat of the control circuit described in Chapter 3, the voltage feedback is compared to a reference signal. Like the weld voltage control, wire speed is also a user-controlled reference signal. Unlike the weld output voltage, the user may want to vary the motor speed from 0 – 100%, so the reference voltage must have a range between 0.1 V and 2.5 V (corresponding to a 1 V to 25 V signal to the motor). Again, like the DC-DC control circuit, over-current protection is included for the motor drive. By routing the motor current through a very low resistance shunt resistor, the feedback voltage from the shunt can be compared to a set reference point. When the shunt resistance surpasses the set references, the over-current circuit will pull down the feedback to the PWM module.

Chapter 5 Simulation and Test Results

Once the first level of design for the DC-DC power converter and control circuitry was finalized, a small number of PCBs were made and populated with components. A second satellite board was assembled with the two user-control potentiometers plus three light emitting diodes (LEDs) to indicate status of “power,” “low battery voltage” and “battery reverse polarity.” Heat sinks were attached to the high power components and wire harnesses were assembled to connect the main PCBs to the control interface. The prototype power and control board is shown in Fig 5.1.

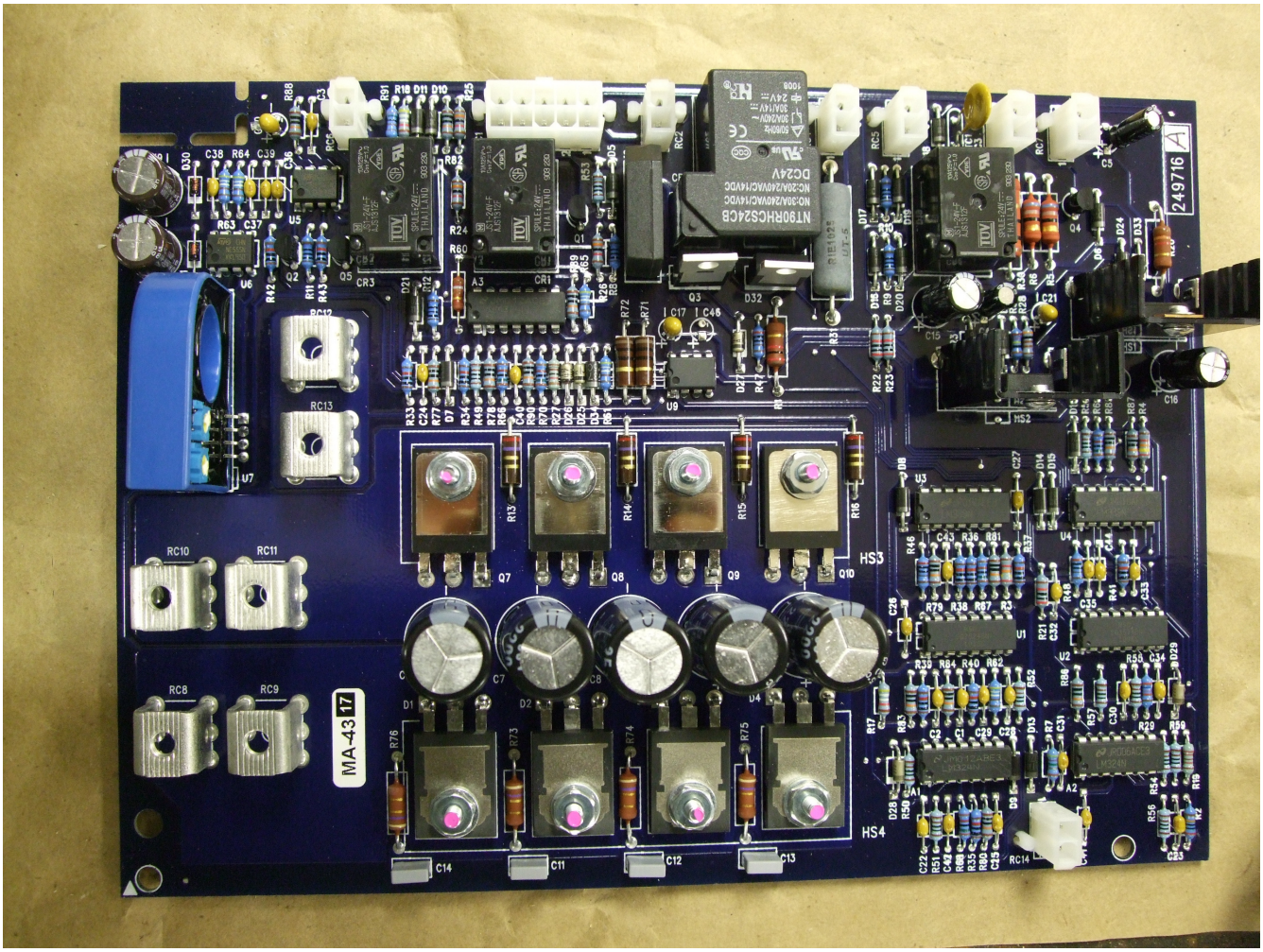

Figure 5.1 Prototype power and control PCB for PAWS design

An plastic enclosure was adapted to hold both PCBs plus high current cabling, main electrical contactor, cooling fan and wire feed motor with mechanism. As each step progressed in the initial assembly, intermediate functionality tests were performed to check the wiring of each subsection. Mistakes in the schematic manifested themselves in functionality failures that required physical modification of the PCB. Once the errors were corrected and documented, the final assembled prototype welder was ready for weld testing. An image of the prototype welder is shown in Fig 5.2.

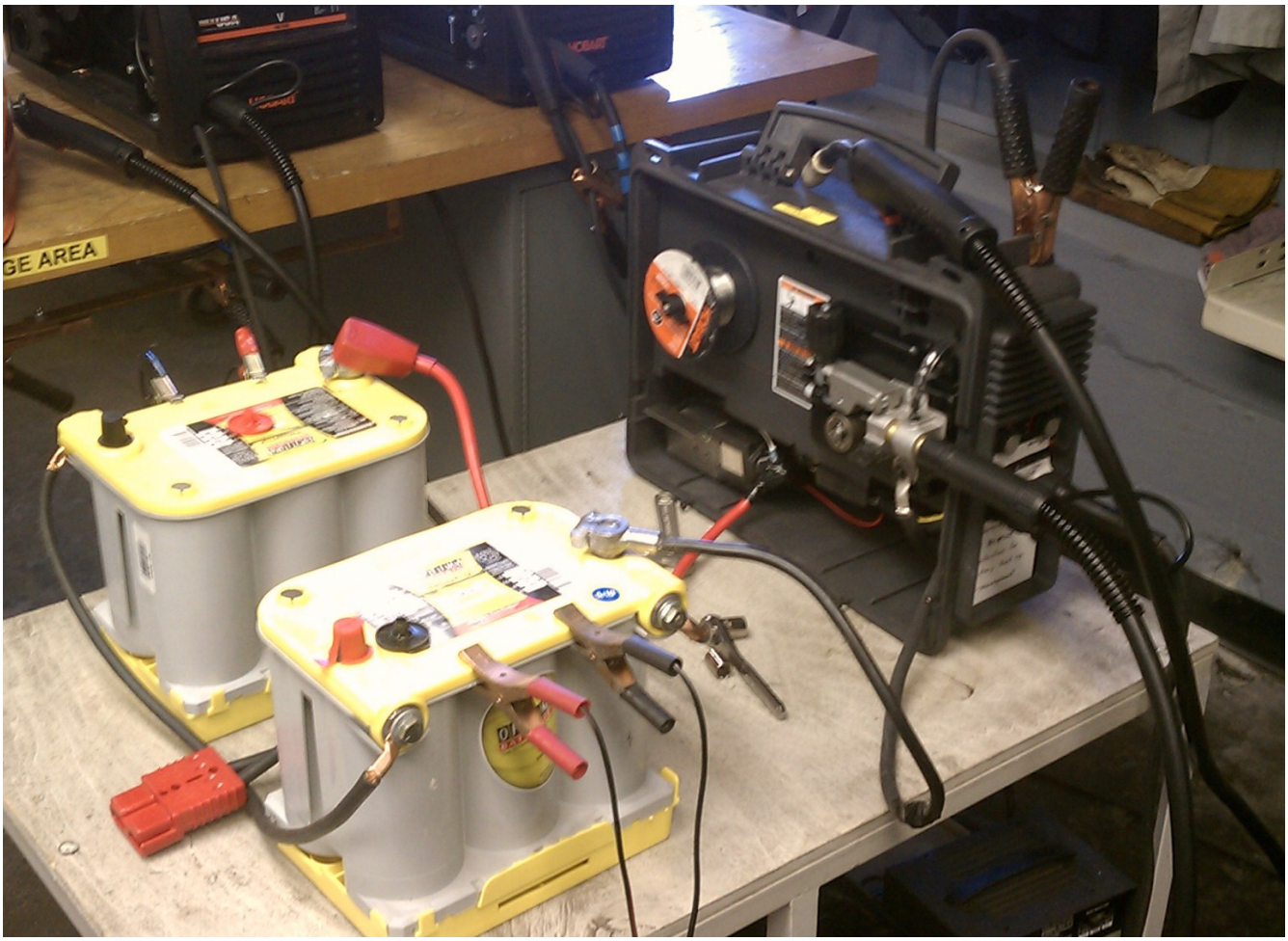

Figure 5.2 Working prototype of the PAWS design

Before computer simulations were attempted, welder functionality was tested. As neither the control scheme nor switching topography had been seen in this application, it would not be possible to say whether the simulations were realistic. First, the machine was used on an assortment of materials, from small to large, gradually increasing the voltage and current. Confidence needed to be established that the machine was safe for use by an operator and did not exhibit self destructive behavior, such as excessive component heating. The new machine was put in the hands of several experienced operators and received a

consensus of good usability. Weld tests show it is capable of welding material from 22 guage (0.8 mm) to 3/8” (9.5 mm) steel, as designed and weld quality varied from “medium” to “excellent,” depending on application.

Once the welder function was demonstrated, general waveforms of the output voltage and current were collected. Using 0.030” solid core wire, shielding gas and 12 gauge steel, an oscilloscope was used to record data during a test weld. The general welding voltage and current waveforms described in Chapter 1 is mirrored in Fig 5.3.

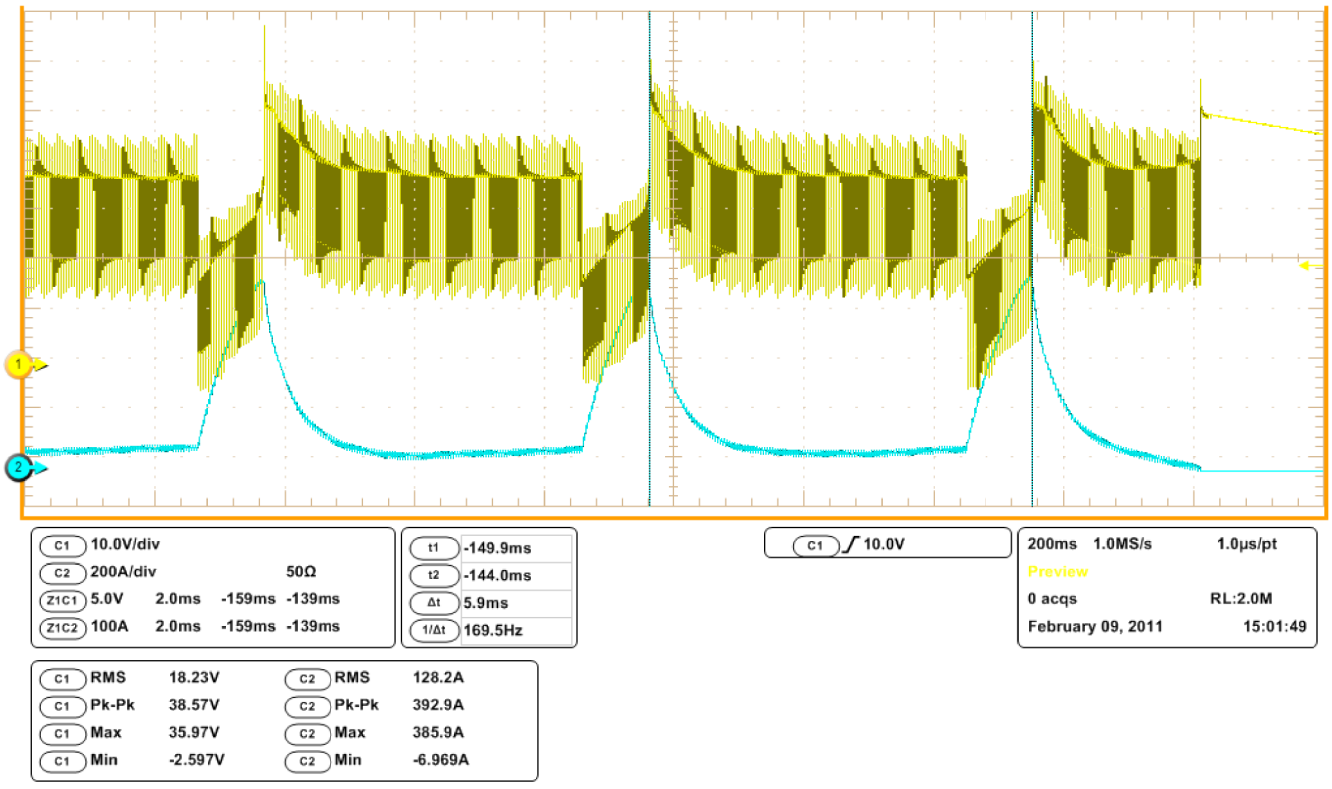

Figure 5.3 Current (bottom, blue) and voltage (top, yellow) output of the PAWS design

This is a clear representation of the high current peaks that occur during short circuit states

and steady state arc conditions that exist between shorts. By zooming into the waveform in Fig 5.3, an enhanced close up of the CCM current and individual switching waveforms is shown in Fig 5.4. Additional welder waveforms can be found in Appendix G.

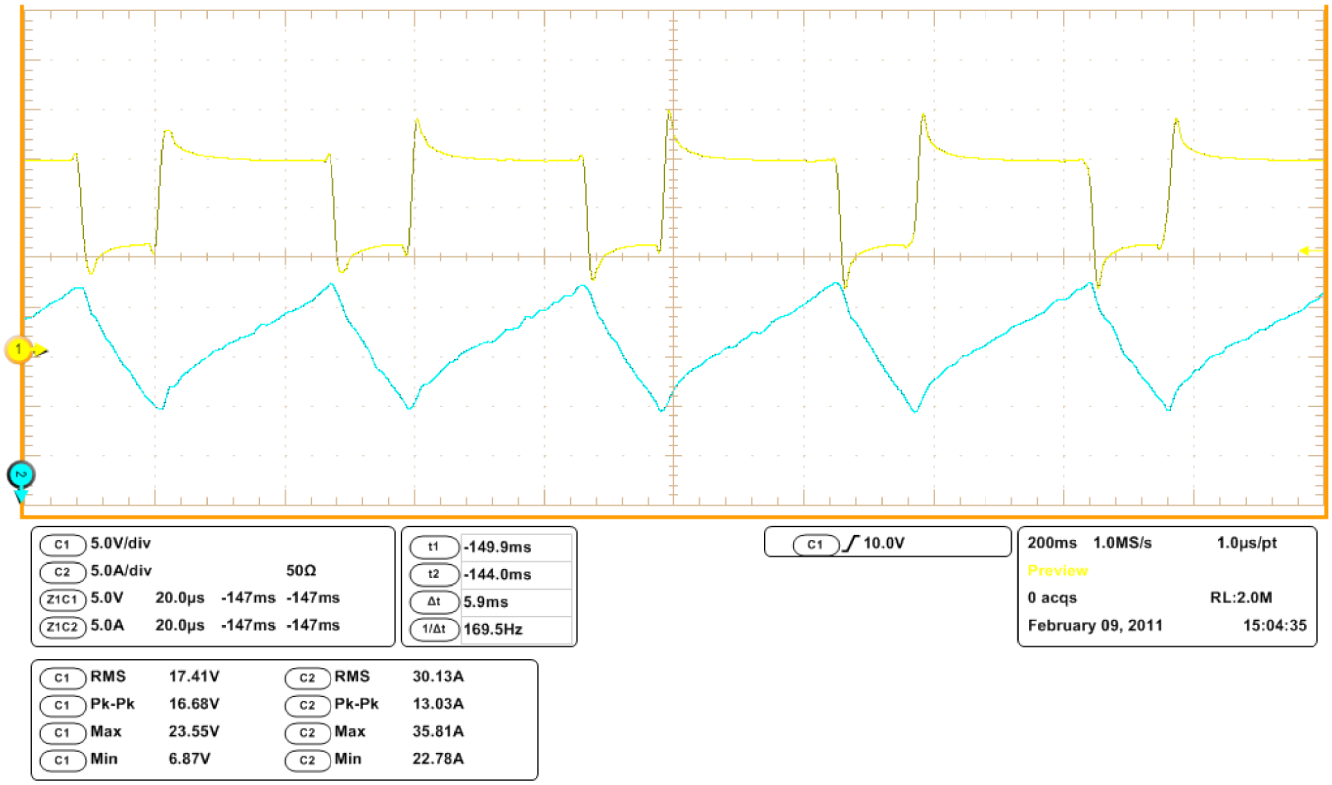

Figure 5.4 Enhanced zoom of current (bottom, blue) and voltage (top, yellow) output of the PAWS prototype design

From the images above it is seen that the PAWS machine performs generally as expected and the output current exhibits a classical CCM form. There is a fair amount of overshoot and undershoot in the output voltage switching waveform, the cause of which was not immediately evident. The high power Schottky diodes are known to not exhibit reverse recovery effects so the peaks were assumed to be a result of parasitic losses in the hardware,

In respect to the control circuit, the voltage response during massive current spikes indicates the feedback loop is managing output voltage well. Armed with performance data, a simulation was constructed in an attempt to understand the intricacies of the weld circuit.

As discussed in Section 2.5, the Saber Sketch circuit simulation software package was used to construct a digital version of the DC-DC switching circuit. Initial tests of the real weld circuit (Appendix G.5) revealed a 66% duty cycle should correspond to an output of approximately 30 A (RMS) and 17 V (RMS). With this knowledge, the simulated circuit was also set to switch at $D = 0.66$ and a starting output resistance of $V_O / I_O = 30\ V / 17\ A = 0.5\ \Omega$. Some tuning of the load was required to achieve similar voltage and current output. As expected, by simply recreating the design in software and using the manufacturer models of the components (Appendix J.1), the simulated voltage and current waveforms did not match perfectly the real world data. Fig 5.5 shows the current and voltage output of the ideal switching circuit using non-ideal components. Though not a perfect match with real data in Fig 5.4, the current waveform is shaped properly and RMS current is correct, though the peak-to-peak current is slightly low. The simulated voltage is less perfect, with an overly square shape, but it too has the proper RMS value and min/max levels are similar to the real welder data.

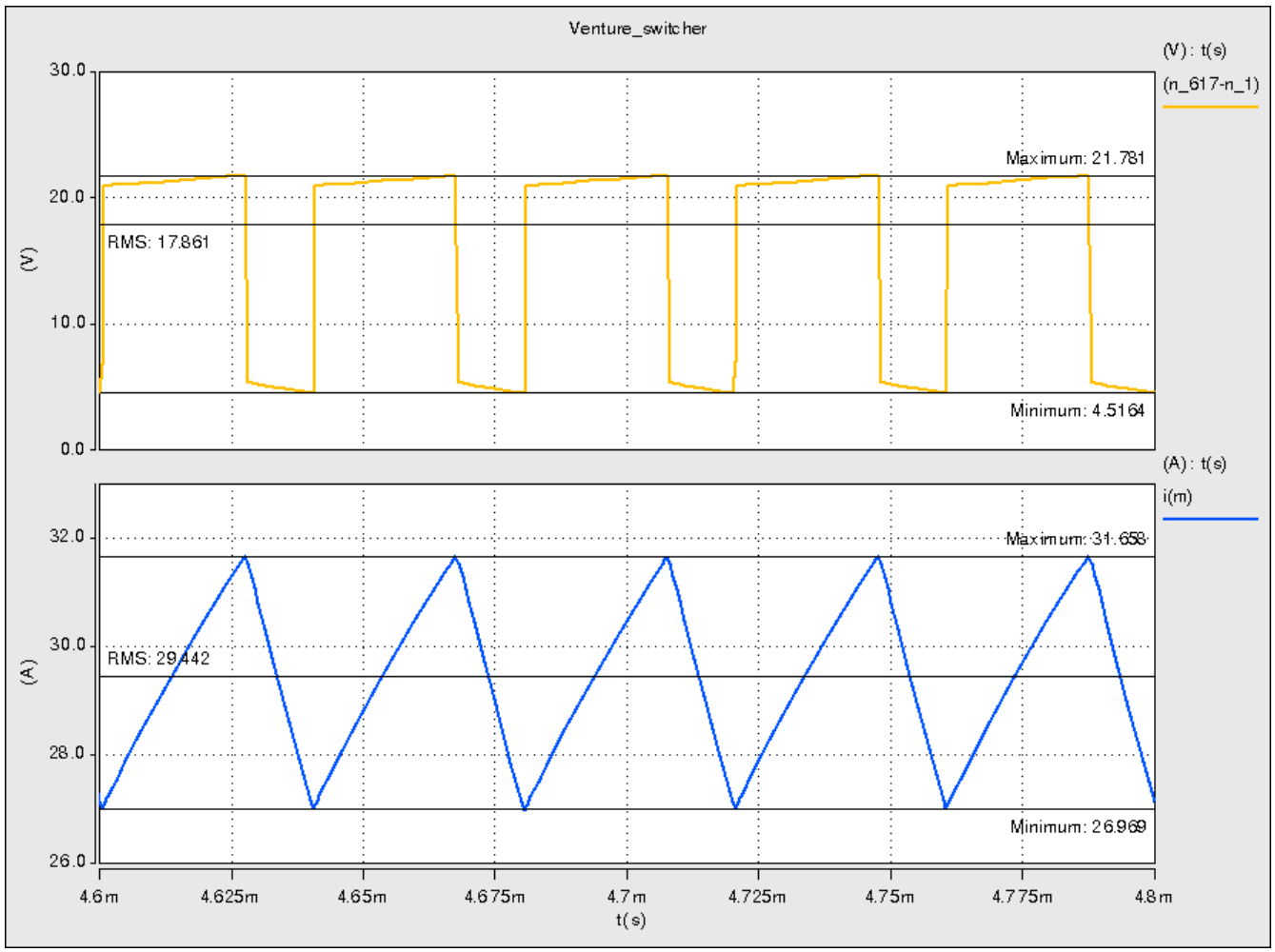

Figure 5.5 Simulated welder output, ideal circuit with non-ideal components

An attempt was made to refine the Saber simulation circuit. The MOSFET and diode manufacturers provide non-ideal simulation components. These models can account for the parasitic components noted in the device data sheet info (Appendix B and C). Because the simulated circuit had the non-ideal component models, the difference in real and simulated waveforms was presumed to be caused by inductance and capacitance in the physical interconnects surrounding the components. These interconnects include the high current cables, connectors, and PCB traces and planes. As Williams describes, overvoltages are

generated when current flowing through an inductive load is switched off quickly, and stray inductance may cause significant transients. [13] This, combined with the fact that all surrounding interconnects are large conductors sized for high currents, suggested the parasitic components were mostly inductive.

Assuming stray inductance was causing the voltage transients, the leads connected to the MOSFETs and diodes would be the most susceptible to high *di/dt* switching. Simulation trials revealed that extra inductance on the drain pin of the MOSFETs caused the overshoots on top of the voltage waveform to increase. Likewise, inductance on the anode of the freewheeling diodes caused the undershoot on the bottom of the voltage wave form to increase. It is worthwhile to note these relationships as they identify areas in the physical design that can be addressed to create cleaner switching waveforms. The model was revised (Appendix J.2) to include inductors of 1 µH on the MOSFET source and drain pins and 0.5 µH on the anode of the diodes. Each parasitic inductor also included a 0.01 Ω resistance. The revised output from these modifications is shown in Fig 5.6. Although the voltage shape is not completely in line with the real world data presented in Fig 5.4, the overall approximation is very similar.

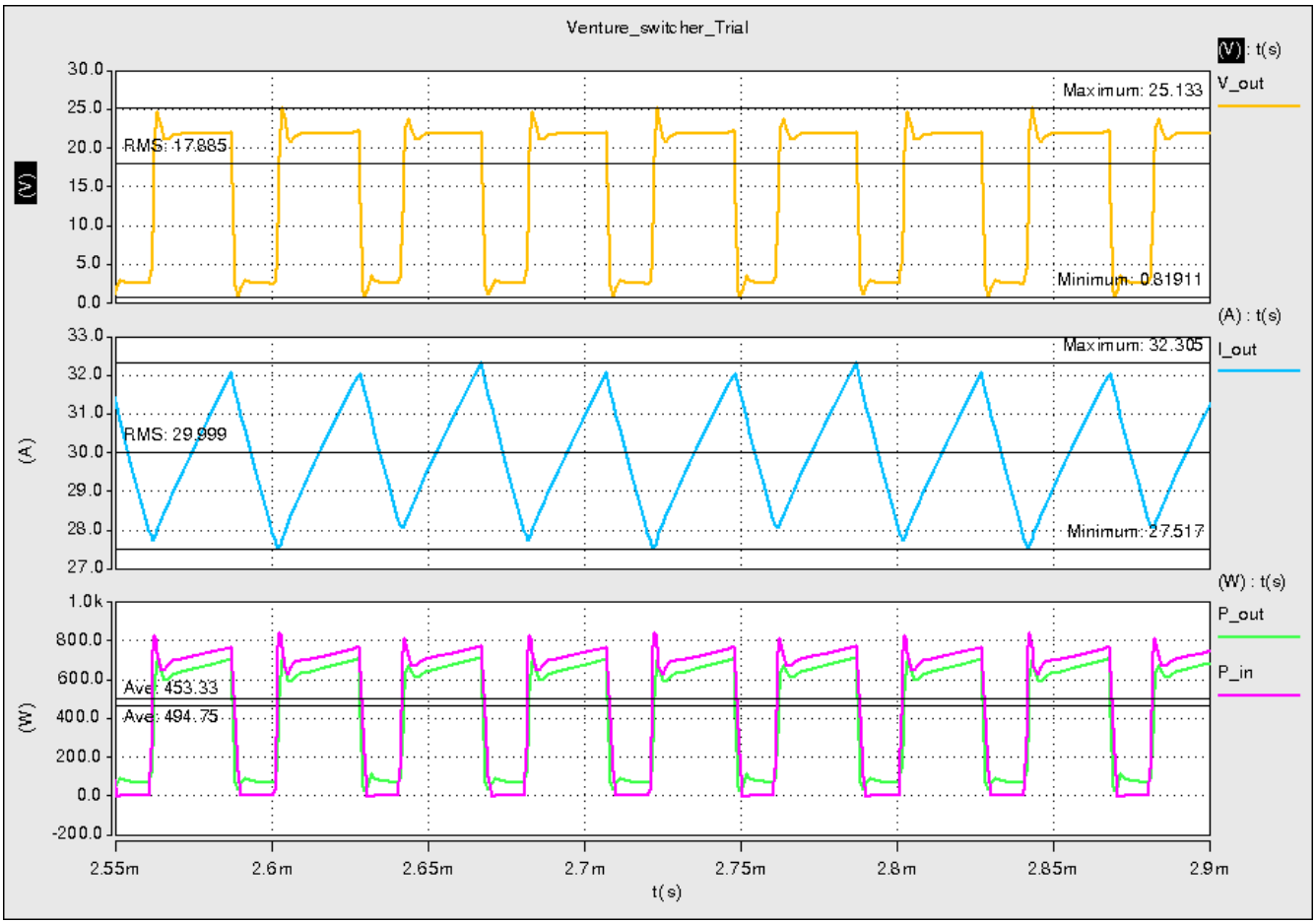

Figure 5.6 Simulated welder output, non-ideal circuit with non-ideal components

The revised simulation model was next tuned to produce input and output power waveform for purposes of predicting the converter efficiency, also seen in Fig 5.6. Again using the 17 V and 30 A (RMS) output condition, the model predicts an efficiency of 91.6% at 453 W output power. When the Saber software was adjusted to simulate a near short circuit, 400A condition, the power efficiency prediction dropped to 51% at 2.7 KW output. (Appendix J.3 and J.4) this dramatic drop appears unrealistic, especial when compared to the real world data, obtained In a second set of welder tests.

Welder test data comparing the real world input voltage and current to the output voltage and current are shown in Appendix G.11 – G.14. These tests reveal 92% and 96% efficiency, respectively, the second occurring at 1.5 KW average output power. As Kazimierczuk shows, power losses in the diode and inductance both increase as the output current increases. [9] It is not unreasonable to expect a slightly lower efficiency at a higher power load, particularly when parasitic inductance is prevalent. However data from the prototype (Appendix G) suggests that the actual efficiency never drops below 90%, while the simulation predicts only 50% at high power draw. This disparity shows that the inductance-heavy adjusted Saber model which was appropriate for a 30 A load, does not work well when asked to simulate a 400 A load. This is a strong argument for the use of real world data for predicting system losses and designing thermal management of power components.

Chapter 6 Summary and Conclusion

The design and feasibility study for a portable, affordable welding system (PAWS) reveals that it is possible to create a quality, high-power welder based on a minimal-cost approach, using analog controls without any microprocessors. Where costly, complex machines exist the market, there remains an opportunity for a simple, elegant design. The PAWS prototype demonstrated very good weld quality when using flux-core wire with welding material between 16 GA and 3/8”. It is also capable with solid core down to 22 GA material thickness, and market research suggests these are the two most likely uses for a portable welder design.

Limitations remain in the ability to use Saber Sketch simulation software to mirror the real world waveforms, but much of this variability may lie in the use of a simplified arc simulation model. Accurately modeling the parasitic inductance in high current devices and PCBs is key to creating a viable simulation model, and it is difficult to create a model that works at both high and low power levels. And though the prototype machine works well in most conditions, there is a fair amount of weld splatter when using solid core wire with medium to thick material.

6.1 Recommendations for Future Work

Further engineering work is necessary for the PAWS design study to be carried to production. The question of thermal management is complicated by the nature of welding specifications. Most welders are rated at full output power for only a short duration, expressed as a duty cycle. Neglecting usage duty cycle and assuming the PAWS design loses 10% of the output to internal loses in the form of heating (~500 W at full power), it is still not known for how long the batteries can maintain that output. (Recall that the batteries are supplied by the operator.) The prudent approach would be to imporve the ability of the power components to reject heat, by maximizing the thermal conductivity of the heat sinks. Forced cooling increase the rejection and can be achieved with a small fan. To preserve battery power during idle times, the fan can be designed to operate only when a critical temperature has been reach. Implementing this functionality can be done with one of the remaining unused op-amps (Appendix F) on the control board.

Because the prototype is exhibiting splatter when welding solid core wire with thicker

material, the output inductor is not inhibiting spikes during the highest current levels. Recall from Section 2.4, the existing choke was shown to have a saturation point above 300 A, yet the output current in Fig 5.3 shows momentary spikes as high as 400 A. An inductor with a larger core would raise the saturation level and help alleviate weld splatter, but this would also require a physically larger part. It should be studied whether a larger air gap in the core would create a sufficient increase in saturation.

As discussed in chapter 2.3, the snubber circuit was not optimized for the switching characteristics of the particular application. Component manufacturer Application notes show that refinement of the snubber components is best achieved through empirical methods but there are general procedures for a quick design process. As noted,

> *"Resistance should be less than the ratio of the off-voltage across the switch over the on current through the switch. with a 2 W resistor, the capacitor should be chosen such that 1 W of energy is dissipated across the resistor. The capacitor should equal the inverse of f_S multiplied by the output voltage, squared. These values should then be empirically evaluated. Increasing the value of the snubber capacitor results in more damping, however the snubber losses increase. Select a minimum value of the capacitor that provides adequate clamping of the diode waveform at maximum load." [14]*

Refinement of the DC-DC switching circuit should include adaptation of the above procedure. By optimizing the snubber circuit and minimizing the switched voltage peaks, it may be possible to use less durable and less expensive switching components.

The easy to implement +12 V and +15 V linear power supplies are inefficient (as low as 50%) and require an aluminum heat sink that adds cost and demands board space. By converting the entire system to +12 V and sourcing 12 V relays, power contactor, gas valve, fan, the two linear regulators and associated heat-sinks can be replaced by a single variable-input, fixed-output DC-DC switcher. A single National Semiconductor (part number LM 3151) I.C. can provide 12 A of current and would require a small inductor and two small MOSFETs. This solution would offer more power at a higher efficiency, in a smaller footprint and approximately equivalent cost of the existing linear supplies. Implementing a universal +12 V supply throughout the entire control board would require adjustment to all voltage dividing resistor networks, but this modification should be rolled into a second revision of the control board.

Finally, per Williams, all traces with high di/dt switching should be revisited to ensure they are as short as possible, to minimize stray inductance. [13] Particularly as the simulations revealed, the drain pin of the MOSFETs and the anode of the freewheeling diodes seem to be causing overshoot in the waveforms seen throughout the design and those areas should be made as short as possible.

6.2 Acknowledgments

I would like to thank Hobart Welding Equipment for providing the means and background to complete this project, but especially the time and insight of Darrell Sickels, engineering manager.

I would also like to thank the department of electrical engineering and the faculty of Wright State, especially my adviser, Dr. Kazimierczuk.

Finally, thanks to the support of my lovely and outstanding girlfriend Allison, who still has more degrees than me.

REFERNCES

[1] Miller, Duane K. *Welded Connections - A Primer For Engineers.* The Lincoln Electric Company. Cleveland, Ohio: American Institute of Steel Construction (AISC) Inc., 2006.

[2] Lincoln Electric Company. “Welding Connects Your World: GMAW (MIG Welding).” E-Learning Course. No date. Available online: http://www.lincolnelectric.com/en-us/education-center/Documents/GMAWMIGWelding.ppt

[3] Messler, Robert W. Jr. *Principles of Welding, Processes, Physics, Chemistry and Metallurgy*. Troy, New York: Wiley-VCH, 2004.

[4] *Model Handler 210 Owners Manual.* OM-227 978D. Hobart Welding Products, 2010. Available online: http://www.hobartwelders.com/om/6digit/o227978d_hob.pdf

[5] ESAB North America Welding and Cutting. *MIG Handbook*. Available online: http://www.esabna.com/EUWeb/MIG_handbook/592mig1_1.htm

[6] *Model Handler 130XL Owners Manual.* OM-210082B. Hobart Welding Products, 2010. Available online: http://www.hobartwelders.com/om/6digit/o210082b_hob.pdf

[7] Vogel, B.J. and R.W. Beeson. U.S. Patent No. 0181547. Washington DC: U.S. Patent and Trademark Office, 2007.

[8] Rashid, Muhammad H. *Power Electronics, Circuits Devices and Applications.* Upper Saddle River, New Jersey: Person Prentice Hall, 2003.

[9] Kazimierczuk, Marian K. *Pulse-Width Modulated DC-DC Power Converters.* West Sussex: John Wiley & Sons Ltd., 2008.

[10] Kazimierczuk, Marian K. *High-Frequency Magnetic Components*. West Sussex: John Wiley & Sons Ltd., 2009.

[11] Oshaben, Edward J. *DC-DC Power Converter Design For Application In Welding Power Source For The Retail Market*. MS Thesis, Cleveland State University, Cleveland, Ohio, December 2010.

[12] Priewasser, R., M. Agostinelli, S. Marsili, D. Straeussnigg, and M. Huemer OVE. "Comparative study of linear and non-linear integrated control scheme applied to a buck converter for mobile applications," *Elektrotechnick & Informationstechnik,* 127/4: 103-108 (2010).

[13] Williams, Tim. *The Circuit Designer's Companion.* Oxford, UK: Elsevier, 2005.

[14] CDE Cornell Dubilier, Application Guide Snubber Capacitors. Available online: http://www.cde.com/catalogs/igbtAPPguide.pdf.

Appendix A - Voltage and Current for GMAW Welding

Gas-Shielded, Solid Wire			Self-Shielded, Flux-Cored Wire		
Material Size	**Current**	**Voltage**	**Material Size**	**Current**	**Voltage**
22 GA (0.8 mm)	40 - 55 A	16 - 17 V			
20 GA (0.9 mm)	50 - 60 A	17 - 18 V			
18 GA (1.2 mm)	70 - 80 A	18 - 19 V			
16 GA (1.6 mm)	90 - 110 A	19 - 20 V			
14 GA (2.0 mm)	120 - 130 A	20 - 21 V	3/32” (2.4 mm)	110 – 125 A	14 - 15 V
1/8” (3.2 mm)	140 - 150 A	21 - 22 V	1/8” (3.2 mm)	140 - 155 A	14 - 15 V
3/16” (4.8 mm)	160 - 170 A	21 - 22 V	3/16” (4.8 mm)	155 - 170 A	15 - 16 V
1/4” (6.4 mm)	180 - 190 A	23 - 24 V	1/4” (6.4 mm)	170 - 190 A	15 - 16 V
5/16” (7.9 mm)	200 - 210 A	23 - 24 V	5/16” (7.9 mm)	190 - 205 A	16 - 17 V
3/8” (9.5 mm)	220 - 250 A	24 - 25 V			

Source: http://www.millerwelds.com/resources/calculators/

Appendix B – IRFP2907 MOSFET Abridged Data Sheet

International
IOR Rectifier

PD-93906C

AUTOMOTIVE MOSFET

IRFP2907

HEXFET® Power MOSFET

Typical Applications
- Integrated Starter Alternator
- 42 Volts Automotive Electrical Systems

Benefits
- Advanced Process Technology
- Ultra Low On-Resistance
- Dynamic dv/dt Rating
- 175°C Operating Temperature
- Fast Switching
- Repetitive Avalanche Allowed up to Tjmax

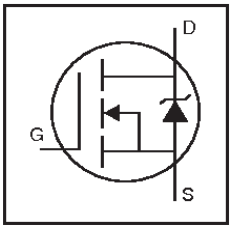

V_{DSS} = 75V

$R_{DS(on)}$ = 4.5mΩ

I_D = 209A⑥

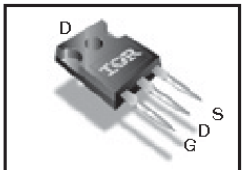

TO-247AC

Description
Specifically designed for Automotive applications, this Stripe Planar design of HEXFET® Power MOSFETs utilizes the lastest processing techniques to achieve extremely low on-resistance per silicon area. Additional features of this HEXFET power MOSFET are a 175°C junction operating temperature, fast switching speed and improved repetitive avalanche rating. These benefits combine to make this design an extremely efficient and reliable device for use in Automotive applications and a wide variety of other applications.

G	D	S
Gate	Drain	Source

Absolute Maximum Ratings

	Parameter	Max.	Units
I_D @ T_C = 25°C	Continuous Drain Current, V_{GS} @ 10V	209⑥	A
I_D @ T_C = 100°C	Continuous Drain Current, V_{GS} @ 10V	148⑥	
I_{DM}	Pulsed Drain Current ①	840	
P_D @T_C = 25°C	Power Dissipation	470	W
	Linear Derating Factor	3.1	W/°C
V_{GS}	Gate-to-Source Voltage	± 20	V
E_{AS}	Single Pulse Avalanche Energy②	1970	mJ
I_{AR}	Avalanche Current	See Fig.12a, 12b, 15, 16	A
E_{AR}	Repetitive Avalanche Energy⑦		mJ
dv/dt	Peak Diode Recovery dv/dt ③	5.0	V/ns
T_J T_{STG}	Operating Junction and Storage Temperature Range	-55 to + 175	°C
	Soldering Temperature, for 10 seconds	300 (1.6mm from case)	
	Mounting Torque, 6-32 or M3 screw	10 lbf•in (1.1N•m)	

Thermal Resistance

	Parameter	Typ.	Max.	Units
$R_{\theta JC}$	Junction-to-Case	—	0.32	°C/W
$R_{\theta CS}$	Case-to-Sink, Flat, Greased Surface	0.24	—	
$R_{\theta JA}$	Junction-to-Ambient	—	40	

Electrical Characteristics @ T_J = 25°C (unless otherwise specified)

	Parameter	Min.	Typ.	Max.	Units	Conditions
$V_{(BR)DSS}$	Drain-to-Source Breakdown Voltage	75	—	—	V	V_{GS} = 0V, I_D = 250µA
$\Delta V_{(BR)DSS}/\Delta T_J$	Breakdown Voltage Temp. Coefficient	—	0.085	—	V/°C	Reference to 25°C, I_D = 1mA
$R_{DS(on)}$	Static Drain-to-Source On-Resistance	—	3.6	4.5	mΩ	V_{GS} = 10V, I_D = 125A ④
$V_{GS(th)}$	Gate Threshold Voltage	2.0	—	4.0	V	V_{DS} = 10V, I_D = 250µA
g_{fs}	Forward Transconductance	130	—	—	S	V_{DS} = 25V, I_D = 125A
I_{DSS}	Drain-to-Source Leakage Current	—	—	20	µA	V_{DS} = 75V, V_{GS} = 0V
		—	—	250		V_{DS} = 60V, V_{GS} = 0V, T_J = 150°C
I_{GSS}	Gate-to-Source Forward Leakage	—	—	200	nA	V_{GS} = 20V
	Gate-to-Source Reverse Leakage	—	—	-200		V_{GS} = -20V
Q_g	Total Gate Charge	—	410	620	nC	I_D = 125A
Q_{gs}	Gate-to-Source Charge	—	92	140		V_{DS} = 60V
Q_{gd}	Gate-to-Drain ("Miller") Charge	—	140	210		V_{GS} = 10V ④
$t_{d(on)}$	Turn-On Delay Time	—	23	—	ns	V_{DD} = 38V
t_r	Rise Time	—	190	—		I_D = 125A
$t_{d(off)}$	Turn-Off Delay Time	—	130	—		R_G = 1.2Ω
t_f	Fall Time	—	130	—		V_{GS} = 10V ④
L_D	Internal Drain Inductance	—	5.0	—	nH	Between lead, 6mm (0.25in.) from package and center of die contact
L_S	Internal Source Inductance	—	13	—		
C_{iss}	Input Capacitance	—	13000	—	pF	V_{GS} = 0V
C_{oss}	Output Capacitance	—	2100	—		V_{DS} = 25V
C_{rss}	Reverse Transfer Capacitance	—	500	—		f = 1.0MHz, See Fig. 5
C_{oss}	Output Capacitance	—	9780	—		V_{GS} = 0V, V_{DS} = 1.0V, f = 1.0MHz
C_{oss}	Output Capacitance	—	1360	—		V_{GS} = 0V, V_{DS} = 60V, f = 1.0MHz
C_{oss} eff.	Effective Output Capacitance ⑤	—	2320	—		V_{GS} = 0V, V_{DS} = 0V to 60V

Source-Drain Ratings and Characteristics

	Parameter	Min.	Typ.	Max.	Units	Conditions
I_S	Continuous Source Current (Body Diode)	—	—	209⑥	A	MOSFET symbol showing the integral reverse p-n junction diode.
I_{SM}	Pulsed Source Current (Body Diode) ①	—	—	840		
V_{SD}	Diode Forward Voltage	—	—	1.3	V	T_J = 25°C, I_S = 125A, V_{GS} = 0V ④
t_{rr}	Reverse Recovery Time	—	140	210	ns	T_J = 25°C, I_F = 125A
Q_{rr}	Reverse RecoveryCharge	—	880	1320	nC	di/dt = 100A/µs ④
t_{on}	Forward Turn-On Time	Intrinsic turn-on time is negligible (turn-on is dominated by L_S+L_D)				

Notes:

① Repetitive rating; pulse width limited by max. junction temperature. (See fig. 11).

② Starting T_J = 25°C, L = 0.25mH R_G = 25Ω, I_{AS} = 125A. (See Figure 12).

③ I_{SD} ≤ 125A, di/dt ≤ 260A/µs, V_{DD} ≤ $V_{(BR)DSS}$, T_J ≤ 175°C

④ Pulse width ≤ 400µs; duty cycle ≤ 2%.

⑤ C_{oss} eff. is a fixed capacitance that gives the same charging time as C_{oss} while V_{DS} is rising from 0 to 80% V_{DSS} .

⑥ Calculated continuous current based on maximum allowable junction temperature. Package limitation current is 90A.

⑦ Limited by T_{Jmax} , see Fig.12a, 12b, 15, 16 for typical repetitive avalanche performance.

Appendix C – STPS40H100CW Diode Abridged Data Sheet

STPS40H100CW

HIGH VOLTAGE POWER SCHOTTKY RECTIFIER

MAIN PRODUCT CHARACTERISTICS

$I_{F(AV)}$	2 x 20 A
V_{RRM}	100 V
Tj (max)	175 °C
V_F (max)	0.61 V

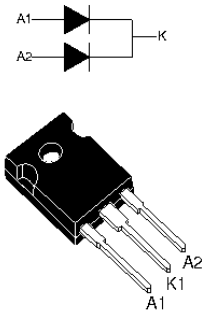

TO-247

FEATURES AND BENEFITS

- NEGLIGIBLE SWITCHING LOSSES
- LOW LEAKAGE CURRENT
- GOOD TRADE OFF BETWEEN LEAKAGE CURRENT AND FORWARD VOLTAGE DROP
- LOW THERMAL RESISTANCE
- AVALANCHE CAPABILITY SPECIFIED

DESCRIPTION

Dual center tap Schottky rectifier suited for Switch Mode Power Supplies and high frequency DC to DC converters.

Packaged in TO-247, this device is intended for use in high frequency inverters.

ABSOLUTE RATINGS (limiting values, per diode)

Symbol	Parameter			Value	Unit
V_{RRM}	Repetitive peak reverse voltage			100	V
$I_{F(RMS)}$	RMS forward current			30	A
$I_{F(AV)}$	Average forward current	Tc = 160°C δ = 0.5	Per diode Per device	20 40	A
I_{FSM}	Surge non repetitive forward current	tp = 10 ms sinusoidal		300	A
I_{RRM}	Repetitive peak reverse current	tp = 2 µs F = 1kHz square		1	A
I_{RSM}	Non repetitive peak reverse current	tp = 100 µs square		4	A
E_{AS}	Non repetitive avalanche energy	Tj = 25°C L= 60 mH I_{as} = 3 A		36	mJ
P_{ARM}	Repetitive peak avalanche power	tp = 1µs Tj = 25°C		26400	W
T_{stg}	Storage temperature range			- 65 to + 175	°C
Tj	Maximum operating junction temperature			175	°C
dV/dt	Critical rate of rise of rise voltage			10000	V/µs

THERMAL RESISTANCES

Symbol	Parameter		Value	Unit
$R_{th\ (j-c)}$	Junction to case	Per diode Total	0.9 0.55	°C/W
$R_{th\ (c)}$		Coupling	0.1	

When the diodes 1 and 2 are used simultaneously :
Δ Tj(diode 1) = P(diode1) x $R_{th(j-c)}$(Per diode) + P(diode 2) x $R_{th(c)}$

STATIC ELECTRICAL CHARACTERISTICS

Symbol	Parameter	Tests Conditions		Min.	Typ.	Max.	Unit
I_R *	Reverse leakage current	Tj = 25°C	$V_R = V_{RRM}$			10	µA
		Tj = 125°C			5	15	mA
V_F **	Forward voltage drop	Tj = 25°C	I_F = 20 A			0.73	V
		Tj = 125°C	I_F = 20 A		0.58	0.61	
		Tj = 25°C	I_F = 40 A			0.85	
		Tj = 125°C	I_F = 40 A		0.67	0.72	

Pulse test : * tp = 5 ms, δ < 2%
** tp = 380 µs, δ < 2%

To evaluate the maximum conduction losses use the following equation :
$P = 0.5 \times I_{F(AV)} + 0.0055 \times I_{F}^{2}{}_{(RMS)}$

Fig. 1: Average forward power dissipation versus average forward current (per diode).

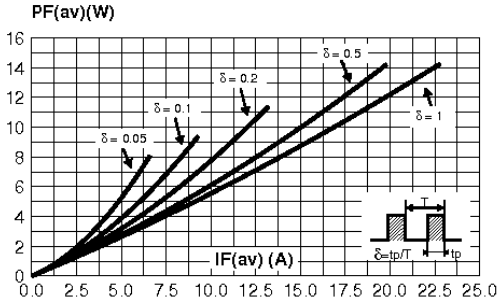

Fig. 2: Average forward current versus ambient temperature (δ=0.5, per diode).

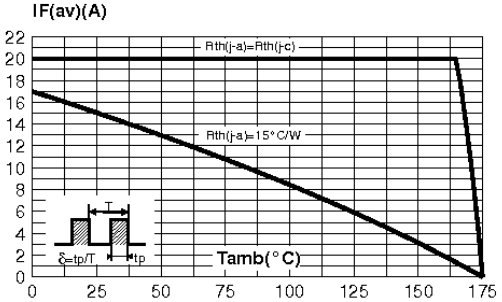

Fig. 3: Normalized avalanche power derating versus pulse duration.

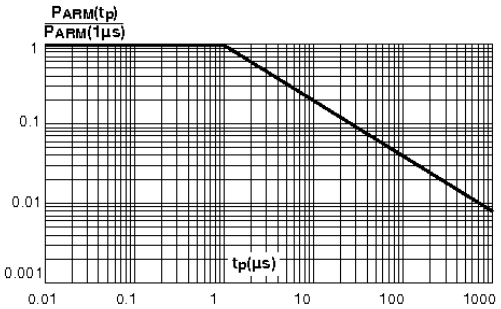

Fig. 4: Normalized avalanche power derating versus junction temperature.

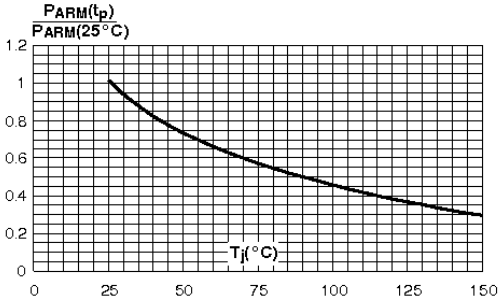

National Semiconductor

May 2, 2008

LM2524D/LM3524D
Regulating Pulse Width Modulator

General Description

The LM3524D family is an improved version of the industry standard LM3524. It has improved specifications and additional features yet is pin for pin compatible with existing 3524 families. New features reduce the need for additional external circuitry often required in the original version.

The LM3524D has a ±1% precision 5V reference. The current carrying capability of the output drive transistors has been raised to 200 mA while reducing V_{CEsat} and increasing V_{CE} breakdown to 60V. The common mode voltage range of the error-amp has been raised to 5.5V to eliminate the need for a resistive divider from the 5V reference.

In the LM3524D the circuit bias line has been isolated from the shut-down pin. This prevents the oscillator pulse amplitude and frequency from being disturbed by shut-down. Also at high frequencies (300 kHz) the max. duty cycle per output has been improved to 44% compared to 35% max. duty cycle in other 3524s.

In addition, the LM3524D can now be synchronized externally, through pin 3. Also a latch has been added to insure one pulse per period even in noisy environments. The LM3524D includes double pulse suppression logic that insures when a shut-down condition is removed the state of the T-flip-flop will change only after the first clock pulse has arrived. This feature prevents the same output from being pulsed twice in a row, thus reducing the possibility of core saturation in push-pull designs.

Features

- Fully interchangeable with standard LM3524 family
- ±1% precision 5V reference with thermal shut-down
- Output current to 200 mA DC
- 60V output capability
- Wide common mode input range for error-amp
- One pulse per period (noise suppression)
- Improved max. duty cycle at high frequencies
- Double pulse suppression
- Synchronize through pin 3

Connection Diagram

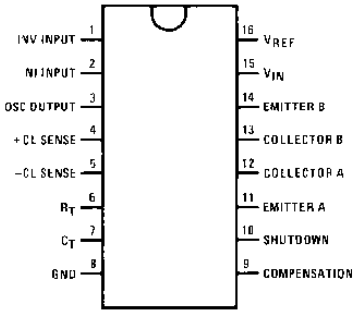

Top View
Order Number LM2524DN or LM3524DN
See NS Package Number N16E
Order Number LM3524DM
See NS Package Number M16A

Block Diagram

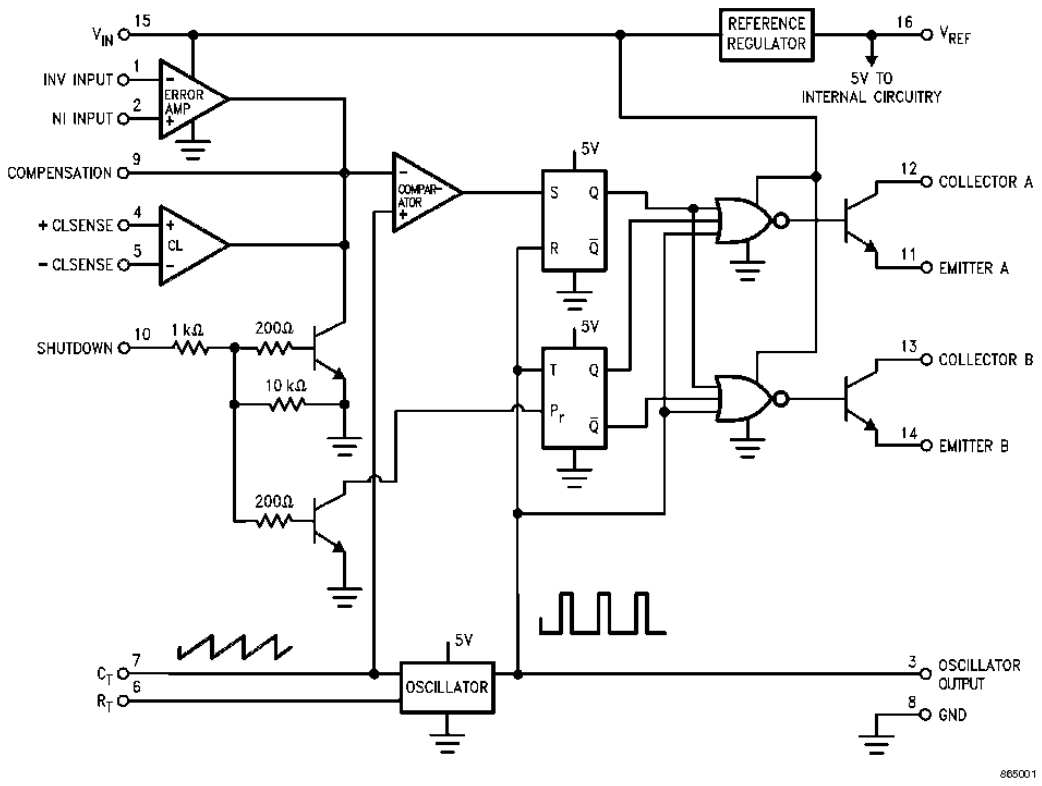

Absolute Maximum Ratings (Note 5)

If Military/Aerospace specified devices are required, please contact the National Semiconductor Sales Office/ Distributors for availability and specifications.

Supply Voltage	40V
Collector Supply Voltage	
(LM2524D)	55V
(LM3524D)	40V
Output Current DC (each)	200 mA
Oscillator Charging Current (Pin 7)	5 mA
Internal Power Dissipation	1W
Operating Junction Temperature Range (Note 2)	
LM2524D	−40°C to +125°C
LM3524D	0°C to +125°C
Maximum Junction Temperature	150°
Storage Temperature Range	−65°C to +150°C
Lead Temperature (Soldering 4 sec.)	
M, N Pkg.	260°C

Electrical Characteristics

(Note 1)

Symbol	Parameter	Conditions	LM2524D			LM3524D			Units
			Typ	Tested Limit (Note 3)	Design Limit (Note 4)	Typ	Tested Limit (Note 3)	Design Limit (Note 4)	
REFERENCE SECTION									
V_{REF}	Output Voltage		5	4.85	**4.80**	5	4.75		V_{Min}
				5.15	**5.20**		5.25		V_{Max}
V_{RLine}	Line Regulation	V_{IN} = 8V to 40V	10	15	**30**	10	25	50	mV_{Max}
V_{RLoad}	Load Regulation	I_L = 0 mA to 20 mA	10	15	**25**	10	25	50	mV_{Max}
$\frac{\Delta V_{IN}}{\Delta V_{REF}}$	Ripple Rejection	f = 120 Hz	66			66			dB
I_{OS}	Short Circuit Current	V_{REF} = 0	50	25 180		50	25 200		mA Min mA Max
N_O	Output Noise	10 Hz ≤ f ≤ 10 kHz	40		100	40		100	$\mu V_{rms\ Max}$
	Long Term Stability	T_A = 125°C	20			20			mV/kHr
OSCILLATOR SECTION									
f_{OSC}	Max. Freq.	R_T = 1k, C_T = 0.001 µF (Note 7)	550		500	350			kHz_{Min}
f_{OSC}	Initial Accuracy	R_T = 5.6k, C_T = 0.01 µF (Note 7)	20	17.5 22.5		20	17.5 22.5		kHz_{Min} kHz_{Max}
		R_T = 2.7k, C_T = 0.01 µF (Note 7)	38	34 42		38	30 46		kHz_{Min} kHz_{Max}
Δf_{OSC}	Freq. Change with V_{IN}	V_{IN} = 8 to 40V	0.5	1		0.5	1.0		$\%_{Max}$
Δf_{OSC}	Freq. Change with Temp.	T_A = −55°C to +125°C at 20 kHz R_T = 5.6k, C_T = 0.01 µF	5			5			%
V_{OSC}	Output Amplitude (Pin 3) (Note 8)	R_T = 5.6k, C_T = 0.01 µF	3	2.4		3	2.4		V_{Min}
t_{PW}	Output Pulse Width (Pin 3)	R_T = 5.6k, C_T = 0.01 µF	0.5	1.5		0.5	1.5		μs_{Max}
	Sawtooth Peak Voltage	R_T = 5.6k, C_T = 0.01 µF	3.4	3.6	**3.8**		3.8		V_{Max}

Symbol	Parameter	Conditions	LM2524D			LM3524D			Units
			Typ	Tested Limit (Note 3)	Design Limit (Note 4)	Typ	Tested Limit (Note 3)	Design Limit (Note 4)	
	Sawtooth Valley Voltage	R_T = 5.6k, C_T = 0.01 µF	1.1	0.8	**0.6**		0.6		V_{Min}
ERROR-AMP SECTION									
V_{IO}	Input Offset Voltage	V_{CM} = 2.5V	2	8	**10**	2	10		mV_{Max}
I_{IB}	Input Bias Current	V_{CM} = 2.5V	1	8	**10**	1	10		μA_{Max}
I_{IO}	Input Offset Current	V_{CM} = 2.5V	0.5	1.0	**1**	0.5	1		μA_{Max}
I_{COSI}	Compensation Current (Sink)	$V_{IN(I)} - V_{IN(NI)}$ = 150 mV	95	65 125		95	65 125		μA_{Min} μA_{Max}
I_{COSO}	Compensation Current (Source)	$V_{IN(NI)} - V_{IN(I)}$ = 150 mV	–95	–125 –65		–95	–125 –65		μA_{Min} μA_{Max}
A_{VOL}	Open Loop Gain	$R_L = \infty$, V_{CM} = 2.5 V	80	74	**60**	80	70	60	dB_{Min}
VCMR	Common Mode Input Voltage Range			1.5 5.5	**1.4** **5.4**		1.5 5.5		V_{Min} V_{Max}
CMRR	Common Mode Rejection Ratio		90	80		90	80		dB_{Min}
G_{BW}	Unity Gain Bandwidth	A_{VOL} = 0 dB, V_{CM} = 2.5V	3			2			MHz
V_O	Output Voltage Swing	$R_L = \infty$		0.5 5.5			0.5 5.5		V_{Min} V_{Max}
PSRR	Power Supply Rejection Ratio	V_{IN} = 8 to 40V	80		70	80	65		db_{Min}
COMPARATOR SECTION									
$\frac{t_{ON}}{t_{OSC}}$	Minimum Duty Cycle	Pin 9 = 0.8V, [R_T = 5.6k, C_T = 0.01 µF]	0	0		0	0		$\%_{Max}$
$\frac{t_{ON}}{t_{OSC}}$	Maximum Duty Cycle	Pin 9 = 3.9V, [R_T = 5.6k, C_T = 0.01 µF]	49	45		49	45		$\%_{Min}$
$\frac{t_{ON}}{t_{OSC}}$	Maximum Duty Cycle	Pin 9 = 3.9V, [R_T = 1k, C_T = 0.001 µF]	44	35		44	35		$\%_{Min}$
V_{COMPZ}	Input Threshold (Pin 9)	Zero Duty Cycle	1			1			V
V_{COMPM}	Input Threshold (Pin 9)	Maximum Duty Cycle	3.5			3.5			V
I_{IB}	Input Bias Current		–1			–1			µA
CURRENT LIMIT SECTION									
V_{SEN}	Sense Voltage	$V_{(Pin\ 2)} - V_{(Pin\ 1)} \geq$ 150 mV	200	180 220		200	180 220		mV_{Min} mV_{Max}
TC-V_{sense}	Sense Voltage T.C.		0.2			0.2			mV/°C

Symbol	Parameter	Conditions	LM2524D			LM3524D			Units
			Typ	Tested Limit (Note 3)	Design Limit (Note 4)	Typ	Tested Limit (Note 3)	Design Limit (Note 4)	
	Common Mode Voltage Range	$V_5 - V_4 = 300$ mV	−0.7 1			−0.7 1			V_{Min} V_{Max}
SHUT DOWN SECTION									
V_{SD}	High Input Voltage	$V_{(Pin\ 2)} - V_{(Pin\ 1)} \geq$ 150 mV	1	0.5 1.5		1	0.5 1.5		V_{Min} V_{Max}
I_{SD}	High Input Current	$I_{(pin\ 10)}$	1			1			mA
OUTPUT SECTION (EACH OUTPUT)									
V_{CES}	Collector Emitter Voltage Breakdown	$I_C \leq 100$ µA		55			40		V_{Min}
I_{CES}	Collector Leakage Current	$V_{CE} = 60V$							
		$V_{CE} = 55V$	0.1	50					μA_{Max}
		$V_{CE} = 40V$				0.1	50		
V_{CESAT}	Saturation Voltage	$I_E = 20$ mA	0.2	0.5		0.2	0.7		V_{Max}
		$I_E = 200$ mA	1.5	2.2		1.5	2.5		
V_{EO}	Emitter Output Voltage	$I_E = 50$ mA	18	17		18	17		V_{Min}
t_R	Rise Time	$V_{IN} = 20V$, $I_E = -250$ µA $R_C = 2k$	200			200			ns
t_F	Fall Time	$R_C = 2k$	100			100			ns
SUPPLY CHARACTERISTICS SECTION									
V_{IN}	Input Voltage Range	After Turn-on		*8* 40			*8* 40		V_{Min} V_{Max}
T	Thermal Shutdown Temp.	(Note 2)	160			160			°C
I_{IN}	Stand By Current	$V_{IN} = 40V$ (Note 6)	5	10		5	10		mA

Note 1: Unless otherwise stated, these specifications apply for $T_A = T_J = 25°C$. Boldface numbers apply over the rated temperature range: LM2524D is −40° to 85°C and LM3524D is 0°C to 70°C. $V_{IN} = 20V$ and $f_{OSC} = 20$ kHz.

Note 2: For operation at elevated temperatures, devices in the N package must be derated based on a thermal resistance of 86°C/W, junction to ambient. Devices in the M package must be derated at 125°C/W, junction to ambient.

Note 3: Tested limits are guaranteed and 100% tested in production.

Note 4: Design limits are guaranteed (but not 100% production tested) over the indicated temperature and supply voltage range. These limits are not used to calculate outgoing quality level.

Note 5: Absolute maximum ratings indicate limits beyond which damage to the device may occur. DC and AC electrical specifications do not apply when operating the device beyond its rated operating conditions.

Note 6: Pins 1, 4, 7, 8, 11, and 14 are grounded; Pin 2 = 2V. All other inputs and outputs open.

Note 7: The value of a C_t capacitor can vary with frequency. Careful selection of this capacitor must be made for high frequency operation. Polystyrene was used in this test. NPO ceramic or polypropylene can also be used.

Note 8: OSC amplitude is measured open circuit. Available current is limited to 1 mA so care must be exercised to limit capacitive loading of fast pulses.

Appendix E – HTB 200-P LEM Current Transducer Abridged Data Sheet

Current Transducers HTB 50..400-P and HTB 50..100-TP

$I_{PN\,DC}$ = ± 50 .. 400 A

For the electronic measurement of currents: DC, AC, pulsed, mixed, with a galvanic isolation between the primary circuit (high power) and the secondary circuit (electronic circuit).

Electrical data

Primary continuous direct current (nominal) $I_{PN\,DC}$ (A)	Primary current, measuring range I_{PM} (A)	Type	RoHS since date code
± 50	± 150	**HTB 50-P, HTB 50-TP**[1]	46104, 46166
± 100	± 300	**HTB 100-P, HTB 100-TP**[1]	45178, 46183
± 200	± 500	**HTB 200-P**	45198
± 300	± 600	**HTB 300-P**	45225
± 400	± 600	**HTB 400-P**	46224

V_C	Supply voltage (± 5 %)[2]	± 12 .. 15	V
I_C	Current consumption	< ± 15	mA
V_d	Rms voltage for AC isolation test, 50 Hz, 1 min	2.5	kV
R_{IS}	Isolation resistance @ 500 VDC	> 500	MΩ
V_{OUT}	Output voltage (Analog) @ $\pm I_{PN\,DC}$, R_L = 10 kΩ, T_A = 25°C	± 4	V
R_{OUT}	Output internal resistance	100	Ω
R_L	Load resistance	≥ 10	kΩ

Accuracy - Dynamic performance data

X	Accuracy @ $I_{PN\,DC}$, T_A = 25°C (excluding offset)	< ± 1 % of $I_{PN\,DC}$	
ε_L	Linearity error (0 .. ± $I_{PN\,DC}$)	< ± 1 % of $I_{PN\,DC}$	
V_{OE}	Electrical offset voltage, T_A = 25°C	< ± 30	mV
V_{OH}	Hysteresis offset voltage @ I_P = 0; after an excursion of 1 x $I_{PN\,DC}$	< ± 1 % of $I_{PN\,DC}$	
TCV_{OE}	Temperature coefficient of V_{OE} HTB 50-(T)P	< ± 2.0	mV/K
	HTB 100-(T)P..400-P	< ± 1.0	mV/K
TCV_{OUT}	Temperature coefficient of V_{OUT} (% of reading)	< ± 0.1	%/K
t_r	Response time to 90% of $I_{PN\,DC}$	< 3	µs
BW	Frequency bandwidth (0..-3 dB)[3]	DC .. 50	kHz

General data

T_A	Ambient operating temperature	- 20 .. + 80	°C
T_S	Ambient storage temperature	- 25 .. + 85	°C
m	Mass (-TP version)	< 30 (< 36)	g
	Standards	EN 50178: 1997	
	2 pins of Ø2mm diameter are available on transducer for PCB soldering.		

Notes :

[1] -TP version is equipped with a primary bus bar.

[2] Operating at ±12V ≤ Vc < ±15V will reduce measuring range.

[3] Derating is needed to avoid excessive core heating at high frequency.

Features

- Hall effect measuring principle
- Galvanic isolation between primary and secondary circuit
- Isolation voltage 2500V
- Low power consumption
- Wide power supply: ±12V to ±15V
- Primary bus bar option for 50A and 100A version for ease of connection

Advantages

- Small size and space saving
- Only one design for wide current ratings range
- High immunity to external interference.

Applications

- AC variable speed drives
- Static converters for DC motor drives
- Battery supplied applications
- Uninterruptible Power Supplies (UPS)
- Switched Mode Power Supplies (SMPS)
- Power supplies for welding applications.

Application domain

- Industrial

National Semiconductor

August 2000

LM124/LM224/LM324/LM2902
Low Power Quad Operational Amplifiers

General Description

The LM124 series consists of four independent, high gain, internally frequency compensated operational amplifiers which were designed specifically to operate from a single power supply over a wide range of voltages. Operation from split power supplies is also possible and the low power supply current drain is independent of the magnitude of the power supply voltage.

Application areas include transducer amplifiers, DC gain blocks and all the conventional op amp circuits which now can be more easily implemented in single power supply systems. For example, the LM124 series can be directly operated off of the standard +5V power supply voltage which is used in digital systems and will easily provide the required interface electronics without requiring the additional ±15V power supplies.

Unique Characteristics

- In the linear mode the input common-mode voltage range includes ground and the output voltage can also swing to ground, even though operated from only a single power supply voltage
- The unity gain cross frequency is temperature compensated
- The input bias current is also temperature compensated

Advantages

- Eliminates need for dual supplies
- Four internally compensated op amps in a single package
- Allows directly sensing near GND and V_{OUT} also goes to GND
- Compatible with all forms of logic
- Power drain suitable for battery operation

Features

- Internally frequency compensated for unity gain
- Large DC voltage gain 100 dB
- Wide bandwidth (unity gain) 1 MHz (temperature compensated)
- Wide power supply range:
  Single supply 3V to 32V
  or dual supplies ±1.5V to ±16V
- Very low supply current drain (700 µA)—essentially independent of supply voltage
- Low input biasing current 45 nA (temperature compensated)
- Low input offset voltage 2 mV and offset current: 5 nA
- Input common-mode voltage range includes ground
- Differential input voltage range equal to the power supply voltage
- Large output voltage swing 0V to V^+ – 1.5V

Connection Diagrams

Dual-In-Line Package

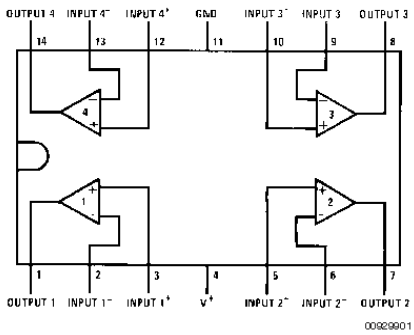

00929901

Top View

Order Number LM124J, LM124AJ, LM124J/883 (Note 2), LM124AJ/883 (Note 1), LM224J, LM224AJ, LM324J, LM324M, LM324MX, LM324AM, LM324AMX, LM2902M, LM2902MX, LM324N, LM324AN, LM324MT, LM324MTX or LM2902N LM124AJRQML and LM124AJRQMLV(Note 3)

See NS Package Number J14A, M14A or N14A

Absolute Maximum Ratings (Note 12)

If Military/Aerospace specified devices are required, please contact the National Semiconductor Sales Office/ Distributors for availability and specifications.

	LM124/LM224/LM324 LM124A/LM224A/LM324A	LM2902
Supply Voltage, V^+	32V	26V
Differential Input Voltage	32V	26V
Input Voltage	−0.3V to +32V	−0.3V to +26V
Input Current		
(V_{IN} < −0.3V) (Note 6)	50 mA	50 mA
Power Dissipation (Note 4)		
Molded DIP	1130 mW	1130 mW
Cavity DIP	1260 mW	1260 mW
Small Outline Package	800 mW	800 mW
Output Short-Circuit to GND		
(One Amplifier) (Note 5)		
$V^+ \le 15V$ and $T_A = 25^\circ C$	Continuous	Continuous
Operating Temperature Range		−40°C to +85°C
LM324/LM324A	0°C to +70°C	
LM224/LM224A	−25°C to +85°C	
LM124/LM124A	−55°C to +125°C	
Storage Temperature Range	−65°C to +150°C	−65°C to +150°C
Lead Temperature (Soldering, 10 seconds)	260°C	260°C
Soldering Information		
Dual-In-Line Package		
Soldering (10 seconds)	260°C	260°C
Small Outline Package		
Vapor Phase (60 seconds)	215°C	215°C
Infrared (15 seconds)	220°C	220°C
See AN-450 "Surface Mounting Methods and Their Effect on Product Reliability" for other methods of soldering surface mount devices.		
ESD Tolerance (Note 13)	250V	250V

Electrical Characteristics

$V^+ = +5.0V$, (Note 7), unless otherwise stated

Parameter	Conditions	LM124A			LM224A			LM324A			Units
		Min	Typ	Max	Min	Typ	Max	Min	Typ	Max	
Input Offset Voltage	(Note 8) $T_A = 25^\circ C$		1	2		1	3		2	3	mV
Input Bias Current (Note 9)	$I_{IN(+)}$ or $I_{IN(-)}$, $V_{CM} = 0V$, $T_A = 25^\circ C$		20	50		40	80		45	100	nA
Input Offset Current	$I_{IN(+)}$ or $I_{IN(-)}$, $V_{CM} = 0V$, $T_A = 25^\circ C$		2	10		2	15		5	30	nA
Input Common-Mode Voltage Range (Note 10)	$V^+ = 30V$, (LM2902, $V^+ = 26V$), $T_A = 25^\circ C$	0		$V^+-1.5$	0		$V^+-1.5$	0		$V^+-1.5$	V
Supply Current	Over Full Temperature Range $R_L = \infty$ On All Op Amps										mA
	$V^+ = 30V$ (LM2902 $V^+ = 26V$)		1.5	3		1.5	3		1.5	3	
	$V^+ = 5V$		0.7	1.2		0.7	1.2		0.7	1.2	
Large Signal Voltage Gain	$V^+ = 15V$, $R_L \ge 2k\Omega$, ($V_O = 1V$ to 11V), $T_A = 25^\circ C$	50	100		50	100		25	100		V/mV
Common-Mode	DC, $V_{CM} = 0V$ to $V^+ - 1.5V$,	70	85		70	85		65	85		dB

Electrical Characteristics (Continued)

V^+ = +5.0V, (Note 7), unless otherwise stated

Parameter		Conditions		LM124A			LM224A			LM324A			Units
				Min	Typ	Max	Min	Typ	Max	Min	Typ	Max	
Rejection Ratio		T_A = 25˚C											
Power Supply Rejection Ratio		V^+ = 5V to 30V (LM2902, V^+ = 5V to 26V), T_A = 25˚C		65	100		65	100		65	100		dB
Amplifier-to-Amplifier Coupling (Note 11)		f = 1 kHz to 20 kHz, T_A = 25˚C (Input Referred)			−120			−120			−120		dB
Output Current	Source	V_{IN}^+ = 1V, V_{IN}^- = 0V, V^+ = 15V, V_O = 2V, T_A = 25˚C		20	40		20	40		20	40		mA
	Sink	V_{IN}^- = 1V, V_{IN}^+ = 0V, V^+ = 15V, V_O = 2V, T_A = 25˚C		10	20		10	20		10	20		mA
		V_{IN}^- = 1V, V_{IN}^+ = 0V, V^+ = 15V, V_O = 200 mV, T_A = 25˚C		12	50		12	50		12	50		µA
Short Circuit to Ground		(Note 5) V^+ = 15V, T_A = 25˚C			40	60		40	60		40	60	mA
Input Offset Voltage		(Note 8)				4			4			5	mV
V_{OS} Drift		R_S = 0Ω			7	20		7	20		7	30	µV/˚C
Input Offset Current		$I_{IN(+)} - I_{IN(-)}$, V_{CM} = 0V				30			30			75	nA
I_{OS} Drift		R_S = 0Ω			10	200		10	200		10	300	pA/˚C
Input Bias Current		$I_{IN(+)}$ or $I_{IN(-)}$			40	100		40	100		40	200	nA
Input Common-Mode Voltage Range (Note 10)		V^+ = +30V (LM2902, V^+ = 26V)		0		V^+−2	0		V^+−2	0		V^+−2	V
Large Signal Voltage Gain		V^+ = +15V (V_OSwing = 1V to 11V) R_L ≥ 2 kΩ		25			25			15			V/mV
Output Voltage Swing	V_{OH}	V^+ = 30V	R_L = 2 kΩ	26			26			26			V
		(LM2902, V^+ = 26V)	R_L = 10 kΩ	27	28		27	28		27	28		
	V_{OL}	V^+ = 5V, R_L = 10 kΩ			5	20		5	20		5	20	mV
Output Current	Source	V_O = 2V	V_{IN}^+ = +1V, V_{IN}^- = 0V, V^+ = 15V	10	20		10	20		10	20		mA
	Sink		V_{IN}^- = +1V, V_{IN}^+ = 0V, V^+ = 15V	10	15		5	8		5	8		

Electrical Characteristics

V^+ = +5.0V, (Note 7), unless otherwise stated

Parameter	Conditions	LM124/LM224			LM324			LM2902			Units
		Min	Typ	Max	Min	Typ	Max	Min	Typ	Max	
Input Offset Voltage	(Note 8) T_A = 25˚C		2	5		2	7		2	7	mV
Input Bias Current (Note 9)	$I_{IN(+)}$ or $I_{IN(-)}$, V_{CM} = 0V, T_A = 25˚C		45	150		45	250		45	250	nA
Input Offset Current	$I_{IN(+)}$ or $I_{IN(-)}$, V_{CM} = 0V, T_A = 25˚C		3	30		5	50		5	50	nA
Input Common-Mode Voltage Range (Note 10)	V^+ = 30V, (LM2902, V^+ = 26V), T_A = 25˚C	0		V^+−1.5	0		V^+−1.5	0		V^+−1.5	V

Electrical Characteristics (Continued)

V^+ = +5.0V, (Note 7), unless otherwise stated

Parameter		Conditions		LM124/LM224			LM324			LM2902			Units
				Min	Typ	Max	Min	Typ	Max	Min	Typ	Max	
Supply Current		Over Full Temperature Range $R_L = \infty$ On All Op Amps V^+ = 30V (LM2902 V^+ = 26V)			1.5	3		1.5	3		1.5	3	mA
		V^+ = 5V			0.7	1.2		0.7	1.2		0.7	1.2	
Large Signal Voltage Gain		V^+ = 15V, $R_L \geq 2k\Omega$, (V_O = 1V to 11V), T_A = 25˚C		50	100		25	100		25	100		V/mV
Common-Mode Rejection Ratio		DC, V_{CM} = 0V to $V^+ - 1.5V$, T_A = 25˚C		70	85		65	85		50	70		dB
Power Supply Rejection Ratio		V^+ = 5V to 30V (LM2902, V^+ = 5V to 26V), T_A = 25˚C		65	100		65	100		50	100		dB
Amplifier-to-Amplifier Coupling (Note 11)		f = 1 kHz to 20 kHz, T_A = 25˚C (Input Referred)			−120			−120			−120		dB
Output Current	Source	V_{IN}^+ = 1V, V_{IN}^- = 0V, V^+ = 15V, V_O = 2V, T_A = 25˚C		20	40		20	40		20	40		mA
	Sink	V_{IN}^- = 1V, V_{IN}^+ = 0V, V^+ = 15V, V_O = 2V, T_A = 25˚C		10	20		10	20		10	20		
		V_{IN}^- = 1V, V_{IN}^+ = 0V, V^+ = 15V, V_O = 200 mV, T_A = 25˚C		12	50		12	50		12	50		µA
Short Circuit to Ground		(Note 5) V^+ = 15V, T_A = 25˚C			40	60		40	60		40	60	mA
Input Offset Voltage		(Note 8)				7			9			10	mV
V_{OS} Drift		R_S = 0Ω			7			7			7		µV/˚C
Input Offset Current		$I_{IN(+)} - I_{IN(-)}$, V_{CM} = 0V				100			150		45	200	nA
I_{OS} Drift		R_S = 0Ω			10			10			10		pA/˚C
Input Bias Current		$I_{IN(+)}$ or $I_{IN(-)}$			40	300		40	500		40	500	nA
Input Common-Mode Voltage Range (Note 10)		V^+ = +30V (LM2902, V^+ = 26V)		0		$V^+ - 2$	0		$V^+ - 2$	0		$V^+ - 2$	V
Large Signal Voltage Gain		V^+ = +15V (V_OSwing = 1V to 11V) $R_L \geq 2$ kΩ		25			15			15			V/mV
Output Voltage Swing	V_{OH}	V^+ = 30V	R_L = 2 kΩ	26			26			22			V
		(LM2902, V^+ = 26V)	R_L = 10 kΩ	27	28		27	28		23	24		
	V_{OL}	V^+ = 5V, R_L = 10 kΩ			5	20		5	20		5	100	mV
Output Current	Source	V_O = 2V	V_{IN}^+ = +1V, V_{IN}^- = 0V, V^+ = 15V	10	20		10	20		10	20		mA
	Sink		V_{IN}^- = +1V, V_{IN}^+ = 0V, V^+ = 15V	5	8		5	8		5	8		

Note 4: For operating at high temperatures, the LM324/LM324A/LM2902 must be derated based on a +125˚C maximum junction temperature and a thermal resistance of 88˚C/W which applies for the device soldered in a printed circuit board, operating in a still air ambient. The LM224/LM224A and LM124/LM124A can be derated based on a +150˚C maximum junction temperature. The dissipation is the total of all four amplifiers—use external resistors, where possible, to allow the amplifier to saturate of to reduce the power which is dissipated in the integrated circuit.

Note 5: Short circuits from the output to V^+ can cause excessive heating and eventual destruction. When considering short circuits to ground, the maximum output current is approximately 40 mA independent of the magnitude of V^+. At values of supply voltage in excess of +15V, continuous short-circuits can exceed the power dissipation ratings and cause eventual destruction. Destructive dissipation can result from simultaneous shorts on all amplifiers.

Appendix G – Switching Waveforms of Prototype Welder

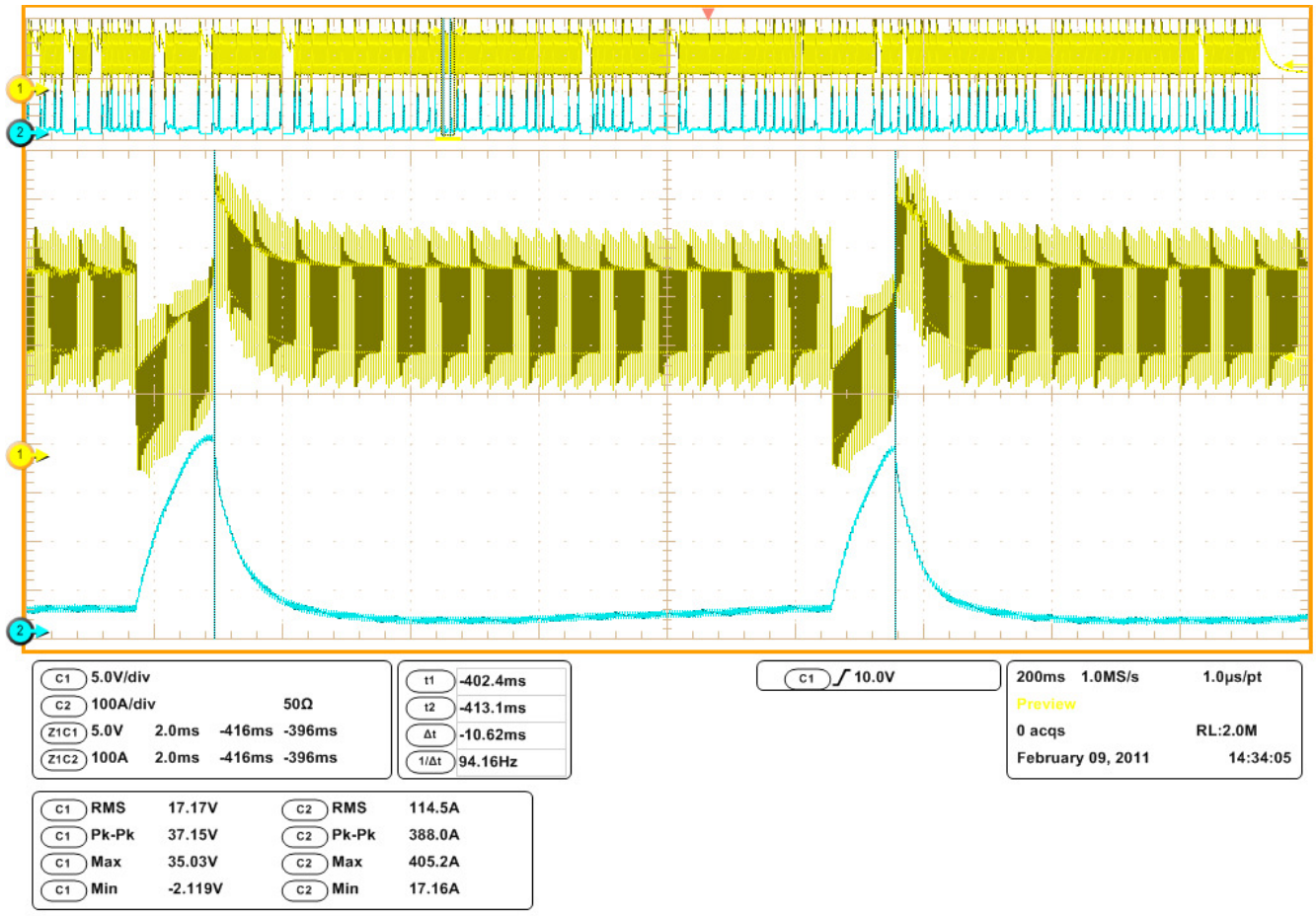

Fig G.1 Weld output voltage (yellow, top) and current (blue, bottom) using shielded 0.030" wire on 12 GA (0.109") steel with 25% CO_2 gas

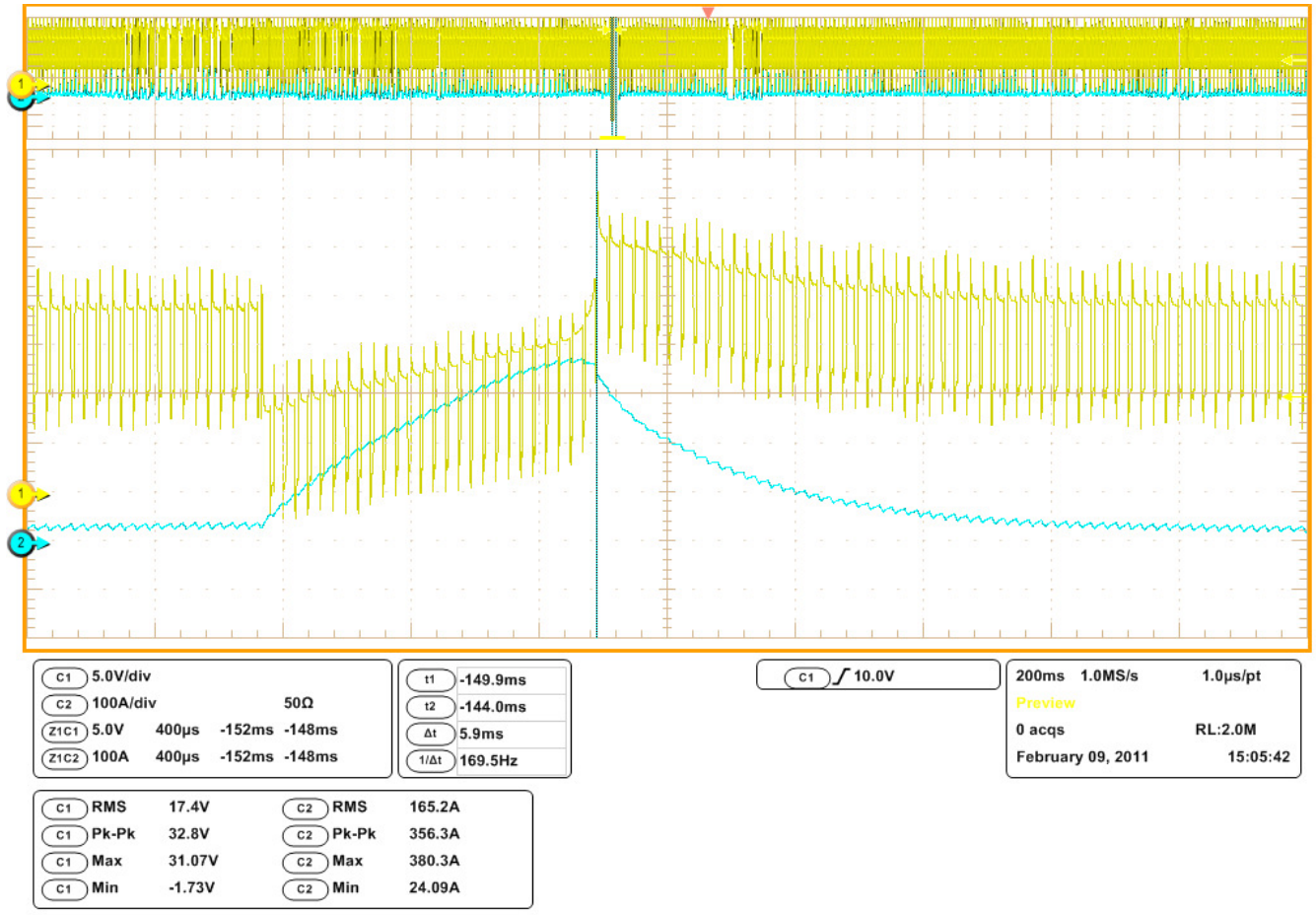

Fig G.2 Weld output voltage (yellow, top) and current (blue, bottom) using shielded 0.030" wire on 12 GA (0.109") steel with 25% CO_2 gas [Shown during current spike]

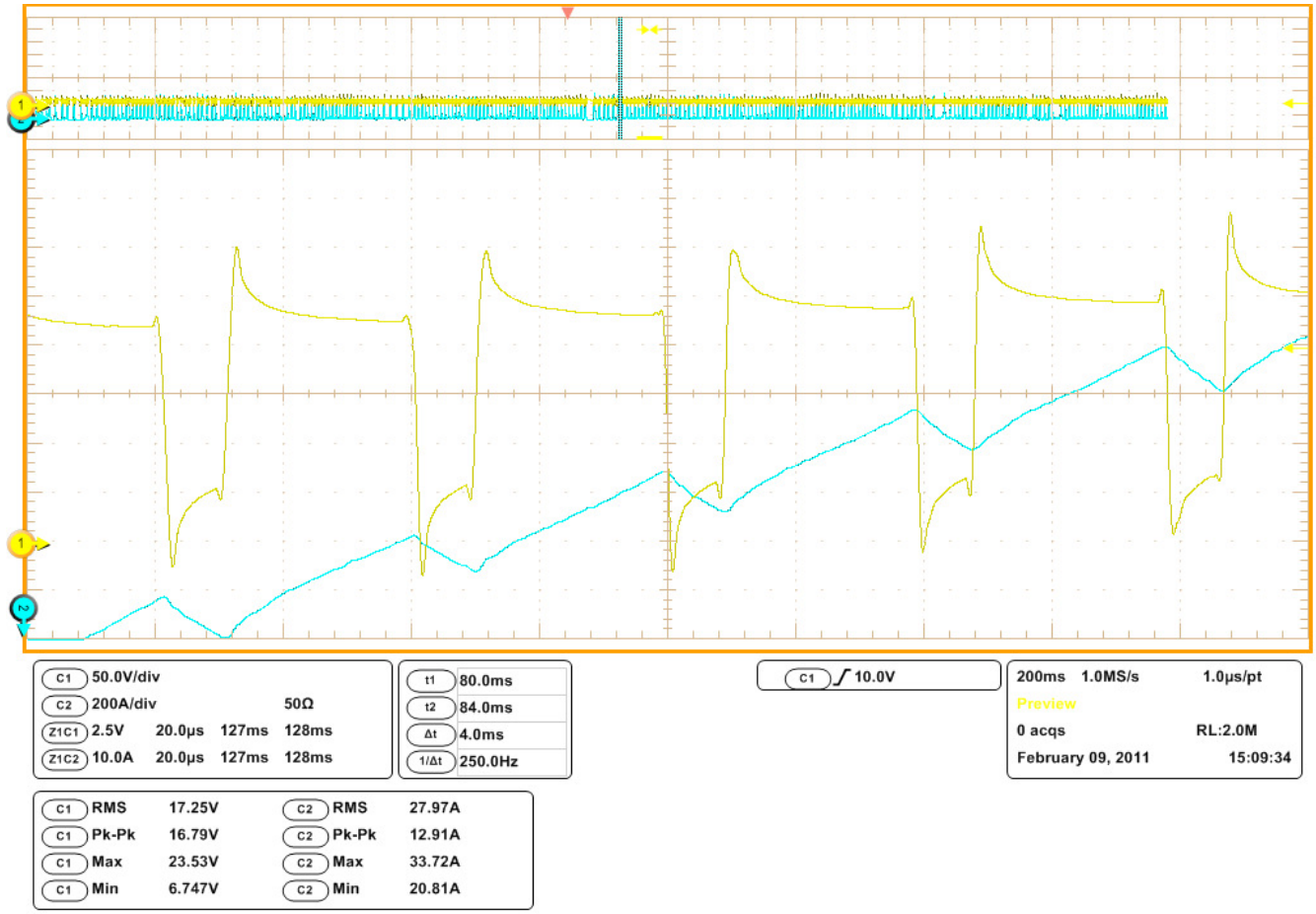

Fig G.3 Weld output voltage (yellow, top) and current (blue, bottom) using shielded 0.030" wire on 12 GA (0.109") steel with 25% CO_2 gas [Shown during current rise]

Fig G.4 Weld output voltage (yellow, top) and current (blue, bottom) using shielded 0.030" wire on 12 GA (0.109") steel with 25% CO_2 gas [Shown during steady state current]

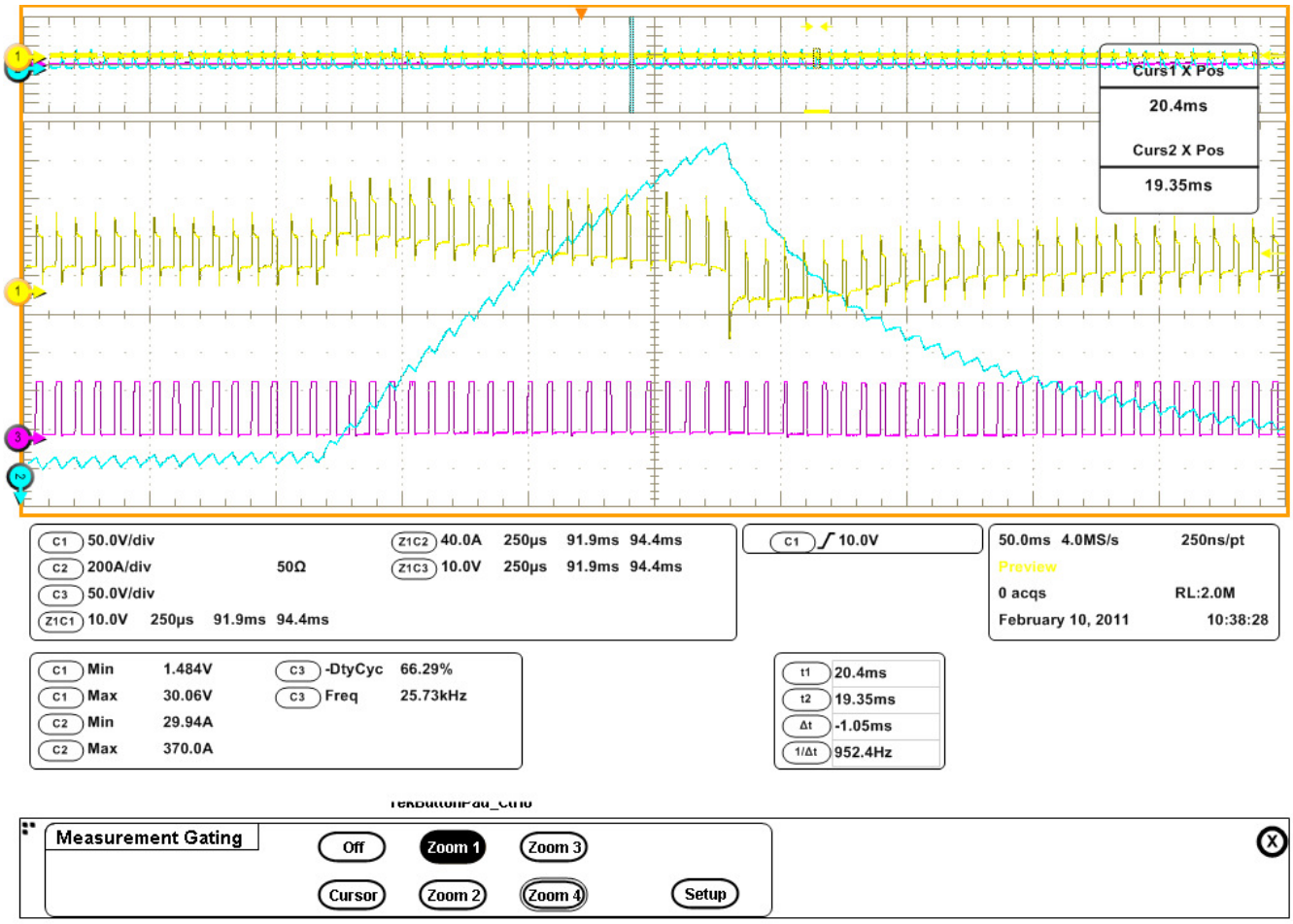

Fig G.5 MOSFET Voltage (yellow, top), weld output current (blue, middle) and PWM signal (purple, bottom) using shielded 0.030” wire on 12 GA (0.109”) steel with 25% CO_2 gas [Shown during current spike]

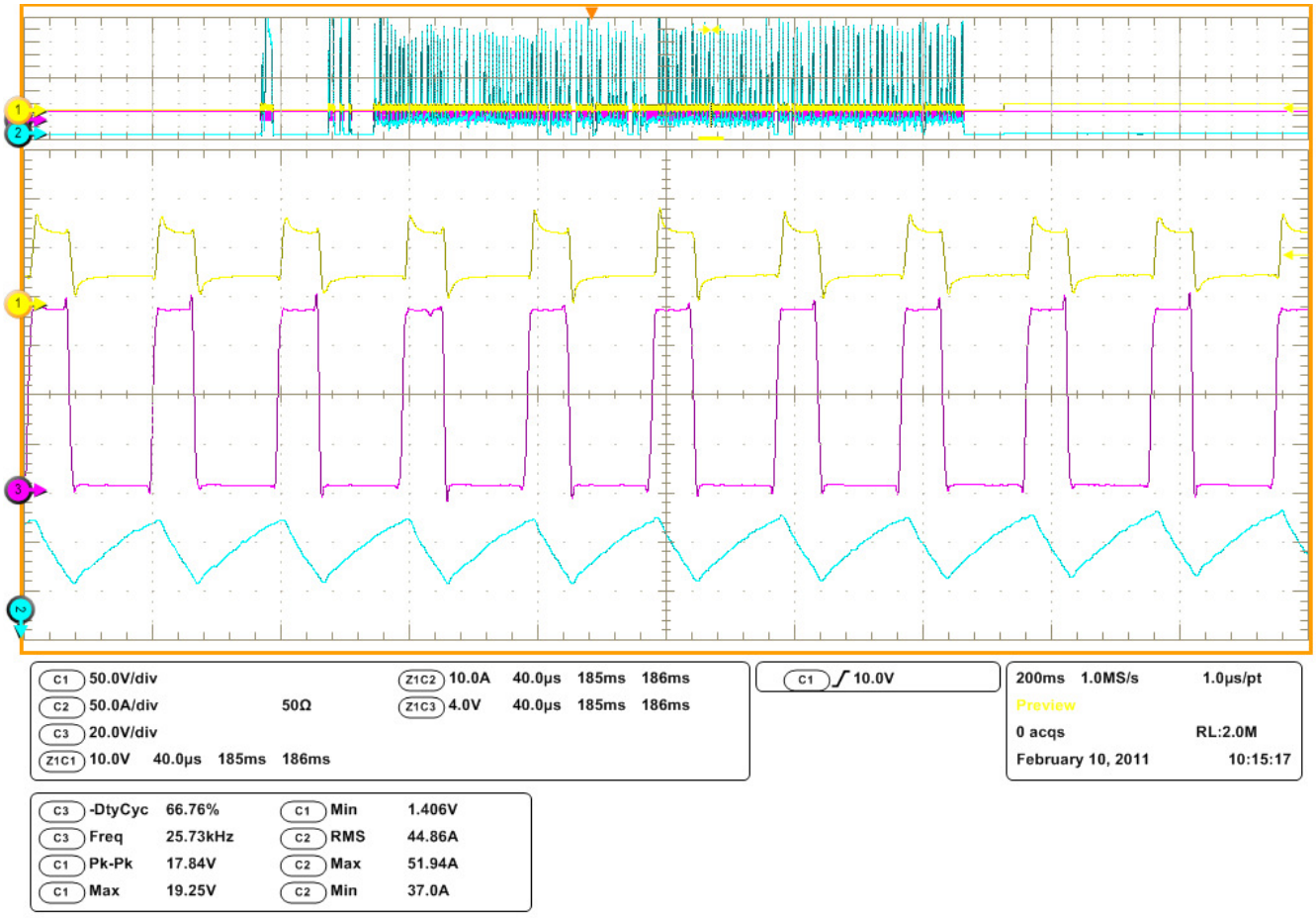

Fig G.6 MOSFET Voltage (yellow, top), weld output current (blue, bottom) and PWM signal (purple, middle) using shielded 0.030” wire on 12 GA (0.109”) steel with 25% CO_2 gas [shown during steady state current]

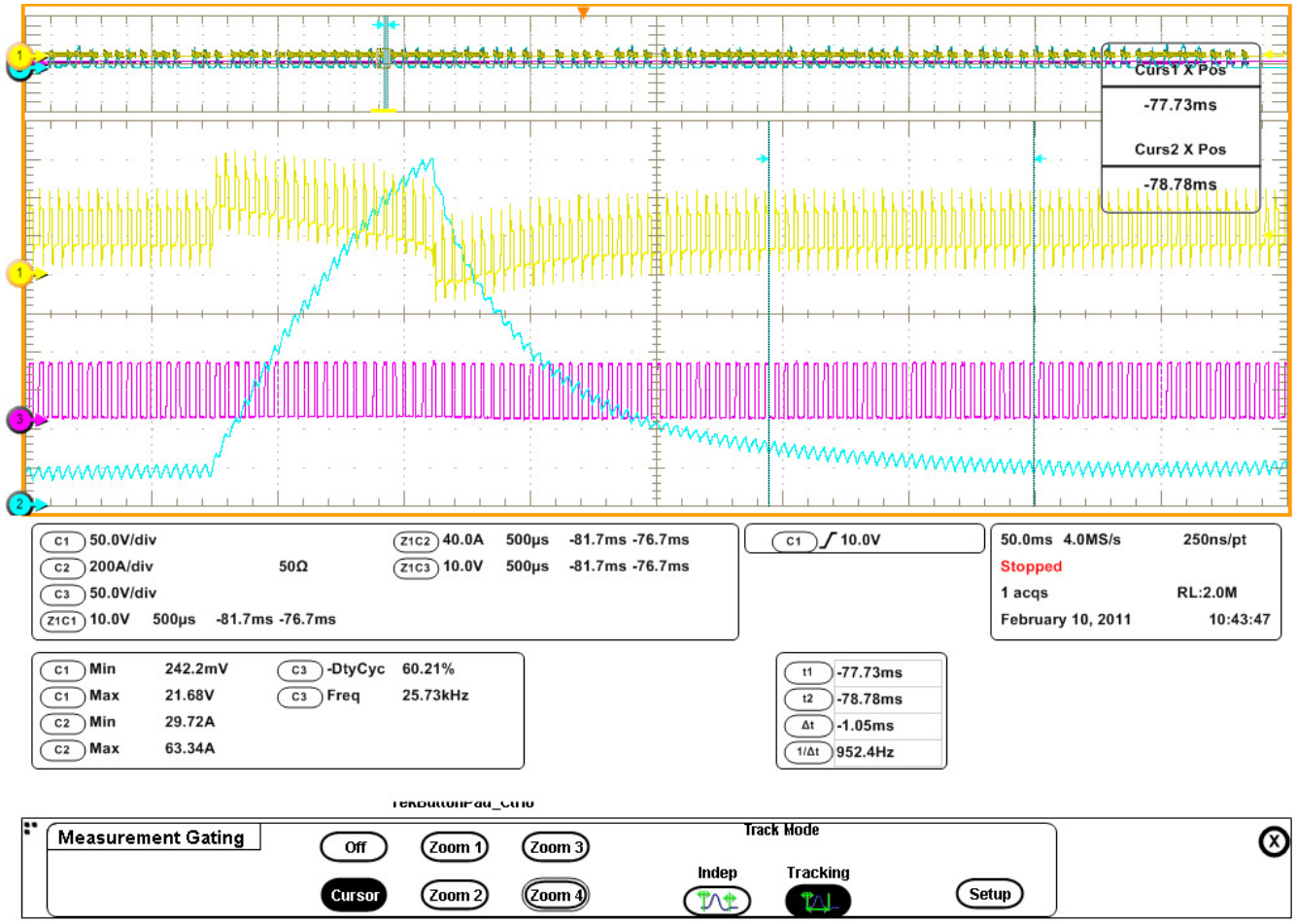

Fig G.7 MOSFET Voltage (yellow, top), weld output current (blue, bottom) and PWM signal (purple, bottom) using shielded 0.030” wire on 12 GA (0.109”) steel with 25% CO_2 gas [commanded V_{min} + 20% voltage, yields 60% PWM duty cycle]

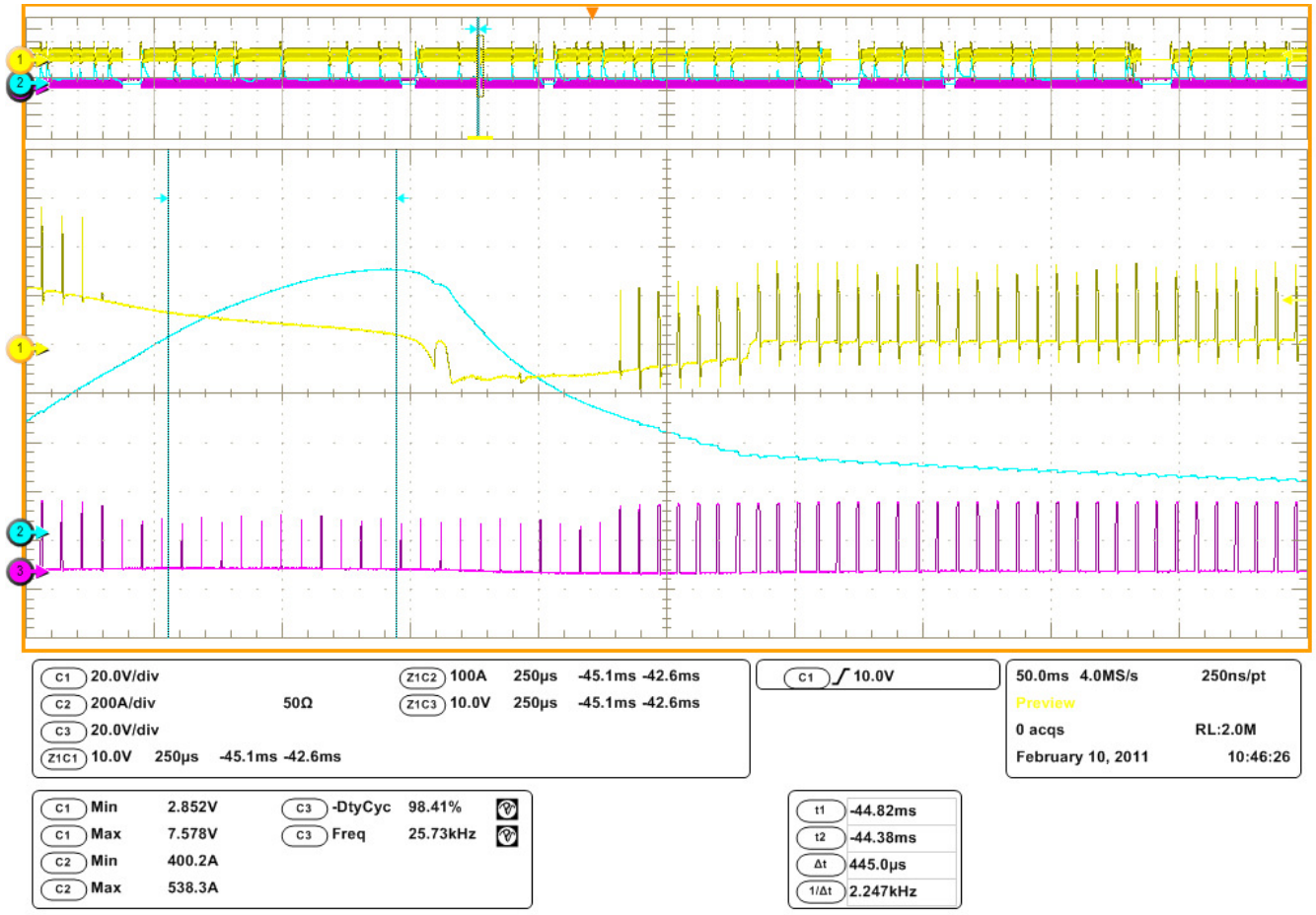

Fig G.8 MOSFET voltage (yellow, top), weld output current (blue, middle) and PWM signal (purple, bottom) using shielded 0.030” wire on 12 GA (0.109”) steel with 25% CO_2 gas [commanding V_{min} + 80% voltage yields 98% PWM duty cycle at current spike]

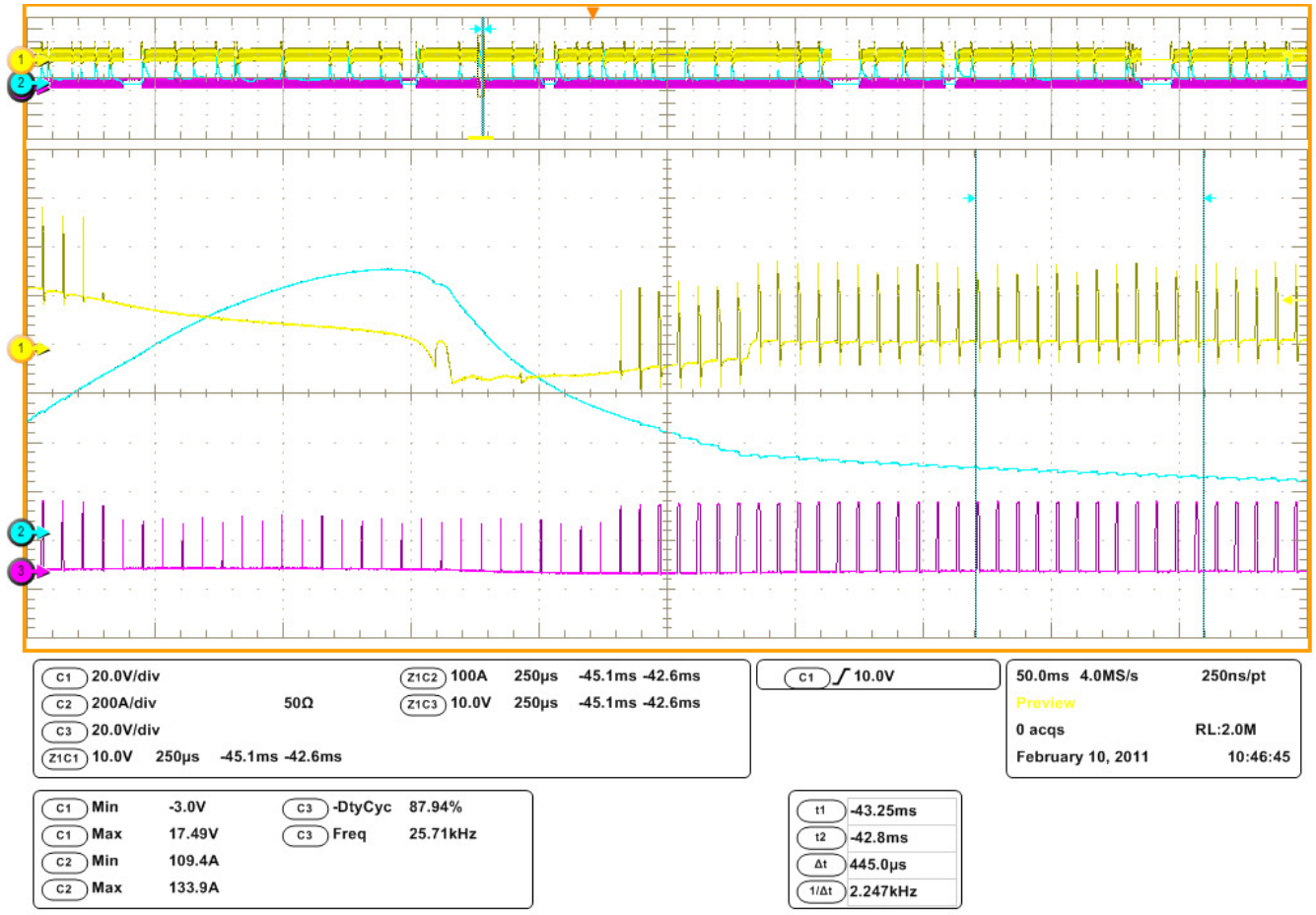

Fig G.9 MOSFET voltage (yellow, top), weld output current (blue, middle) and PWM signal (purple, bottom) using shielded 0.030” wire on 12 GA (0.109”) steel with 25% CO_2 gas [commanding V_{min} + 80% voltage yields 88% PWM duty cycle at steady state current]

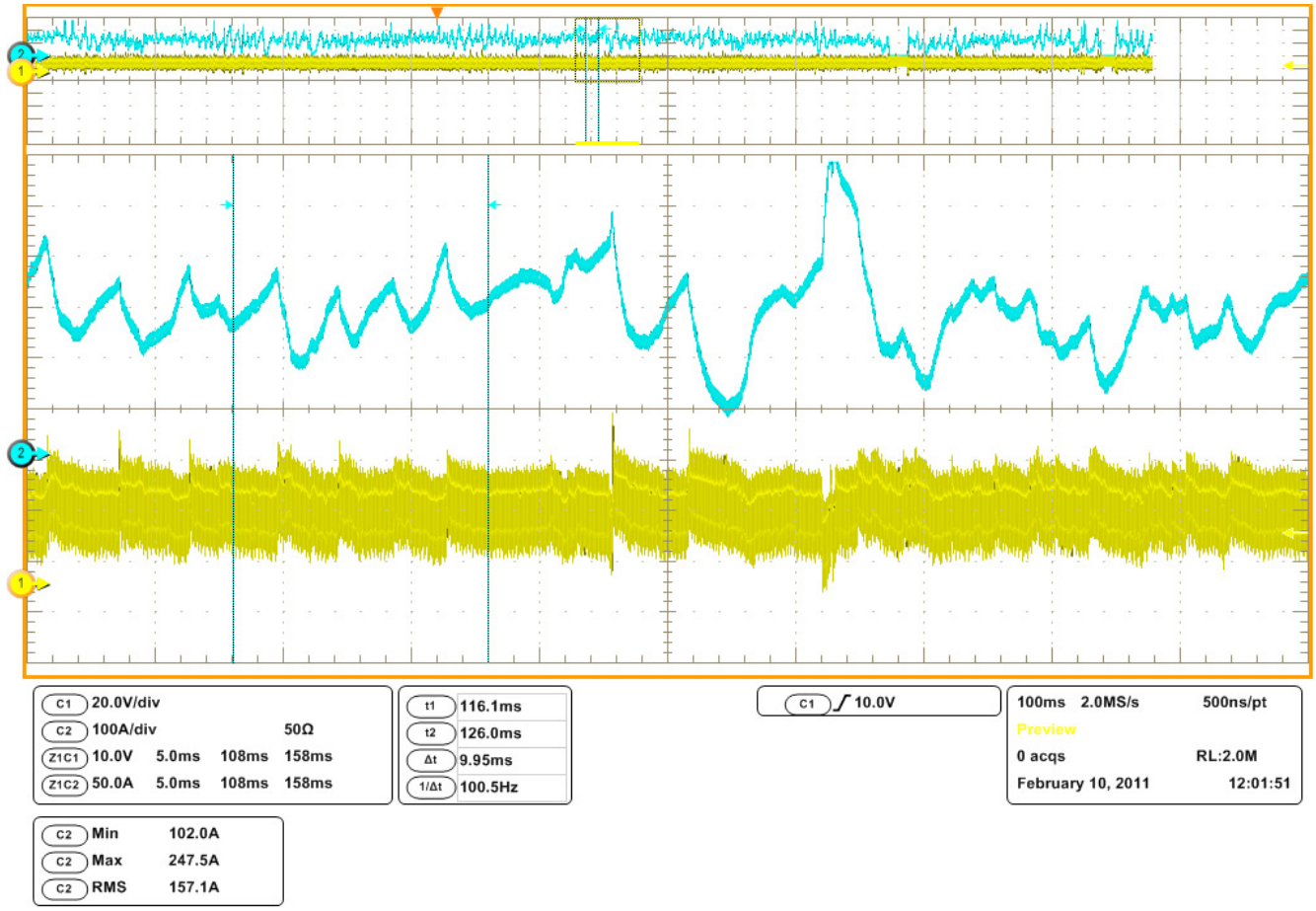

Fig G.10 Weld output voltage (yellow, bottom) and current (blue, top) using flux-core (self-shielded) 0.030” wire on 12 GA (0.109”) steel [Irregular current spikes even with optimized voltage and wire speed]

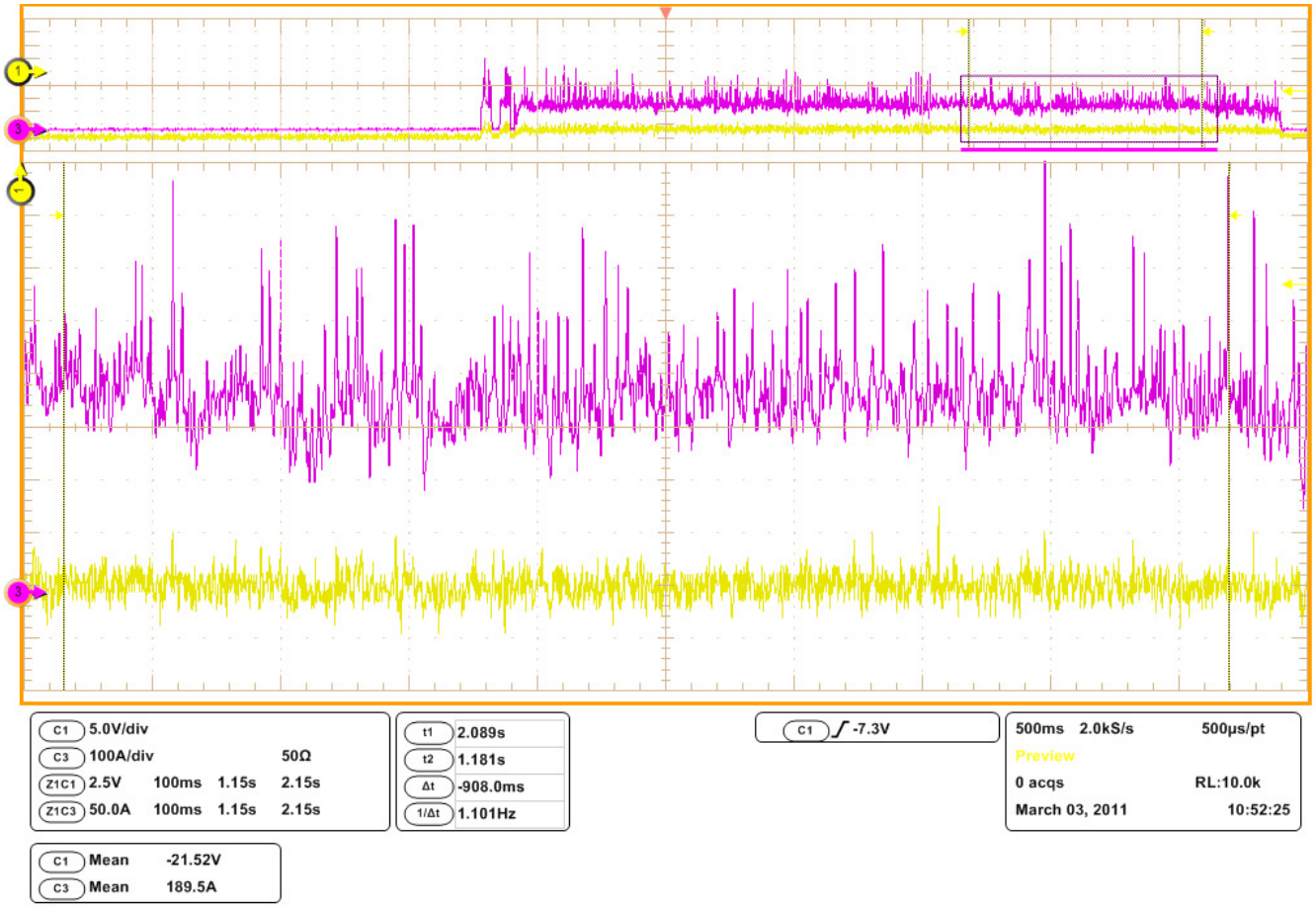

Fig G.11 Welder input average voltage (yellow, bottom) and average current (purple, top) using flux-core (self-shielded) 0.035” wire on 3/16” steel shows 4.08 KW average input power

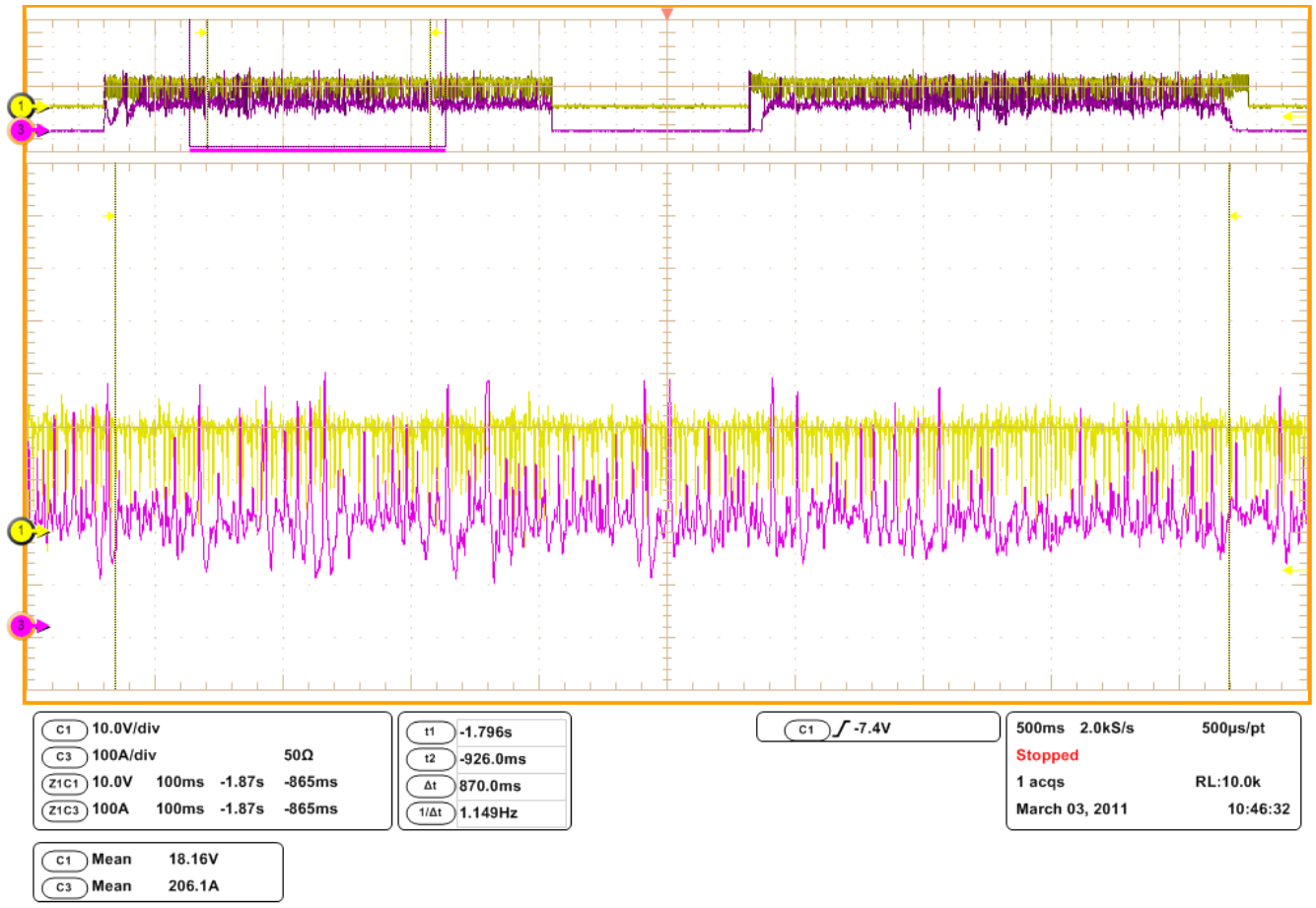

Fig G.12 Welder output average voltage (yellow, top) and average current (purple, bottom) using flux-core (self-shielded) 0.035” wire on 3/16” steel shows 3.74 KW average output power

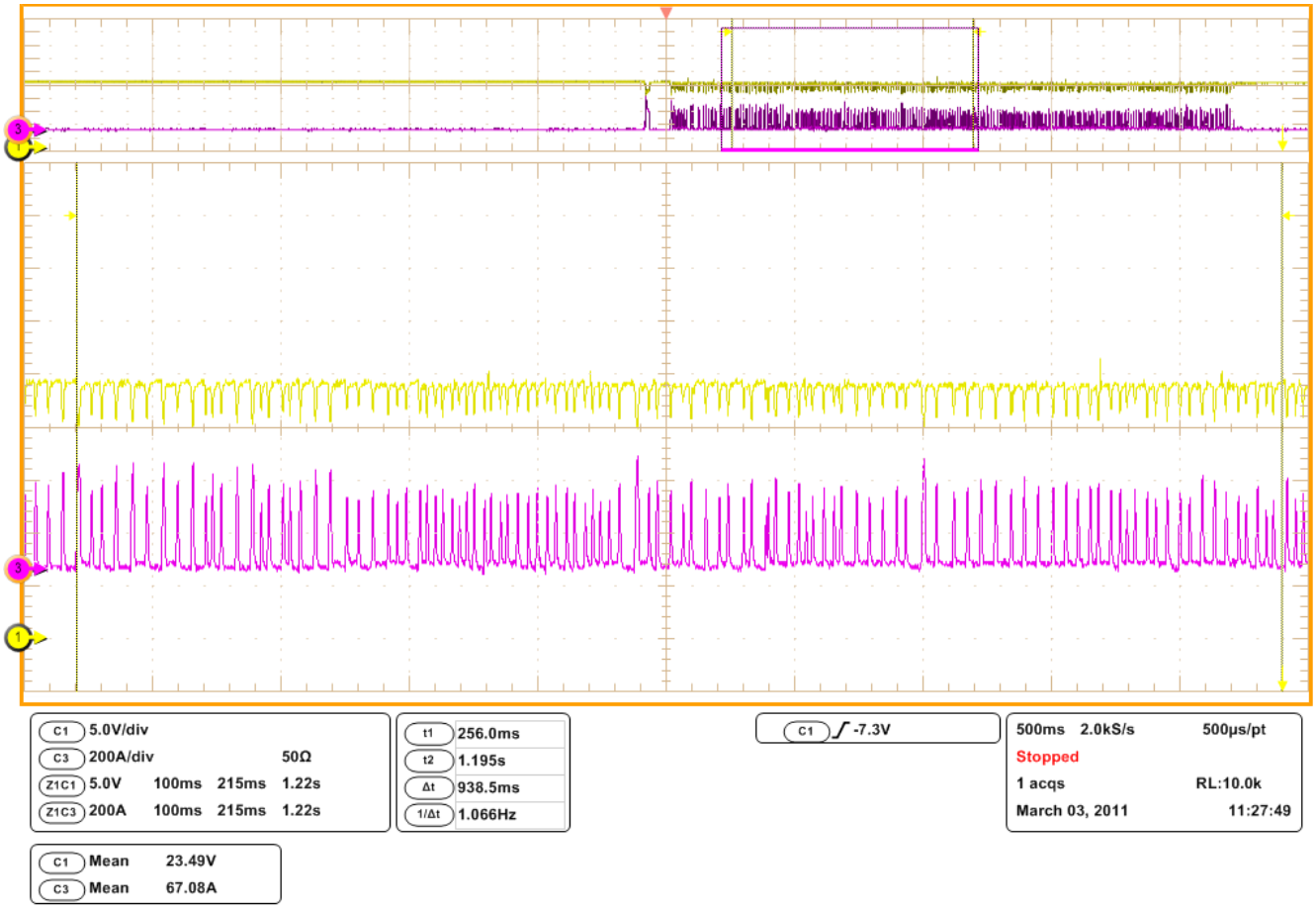

Fig G.13 Welder input average voltage (yellow, top) and average current (purple, bottom) using shielded 0.030” wire on 12 GA (0.109”) steel with 25% CO_2 gas shows 1.58 KW average input power

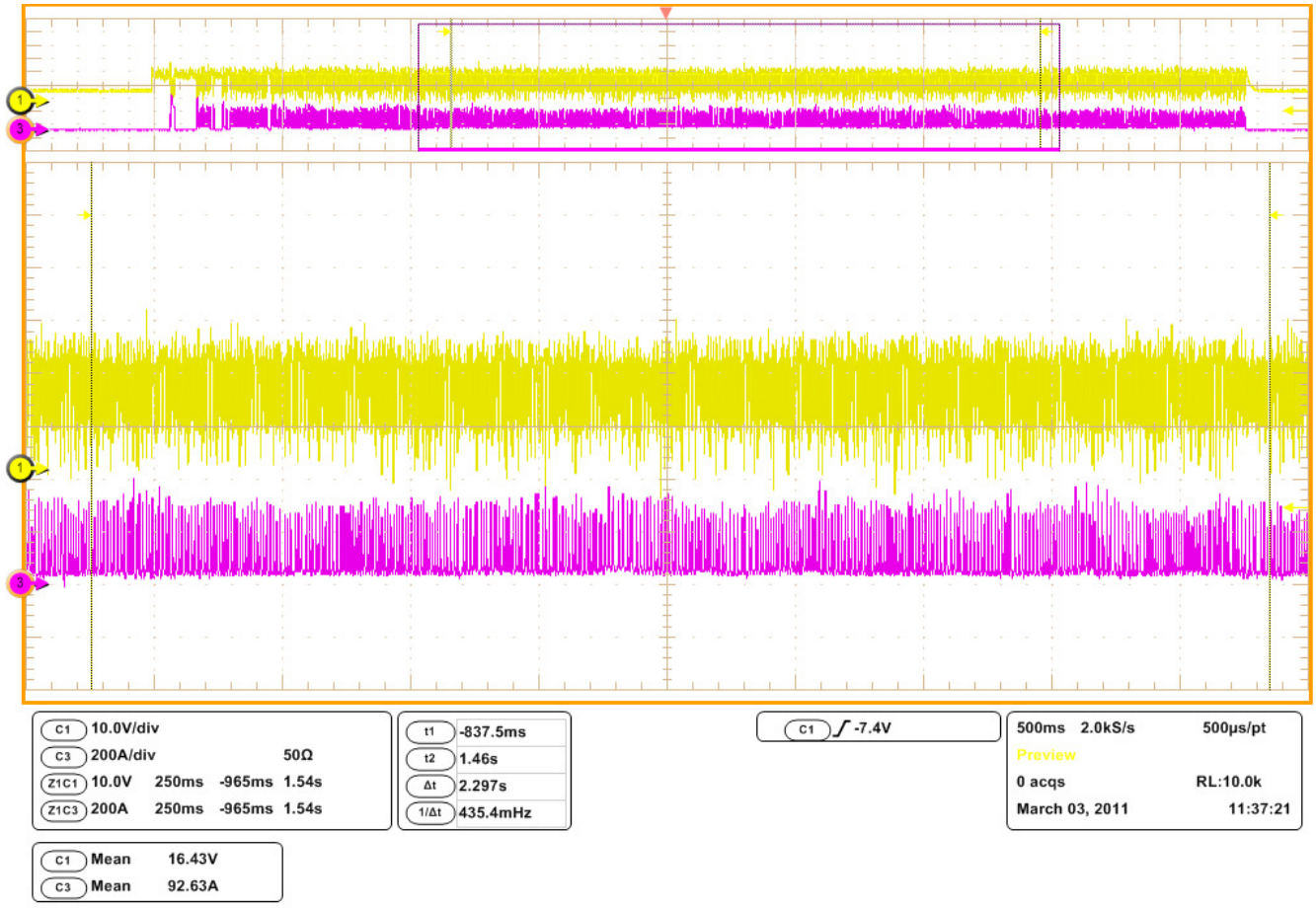

Fig G.14 Welder output average voltage (yellow, top) and average current (purple, bottom) using shielded 0.030” wire on 12 GA (0.109”) steel with 25% CO_2 gas shows 1.52 KW average output power

Appendix H – Switching Frequency Tests of Prototype Welder

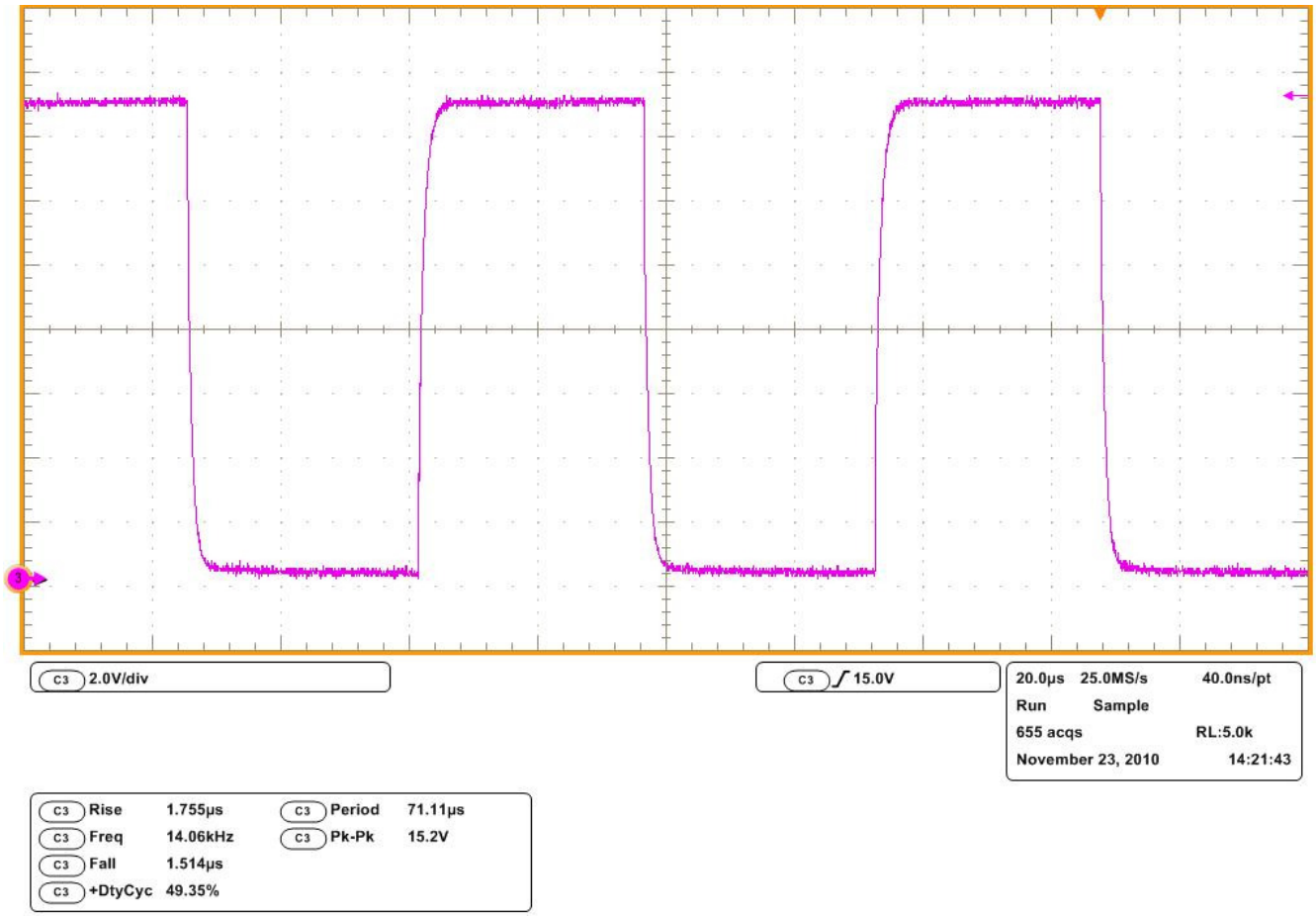

Fig H.1 Switching Signal between MOSFET Driver and High Power MOSFETs Observed in Circuit at 14.1 KHz

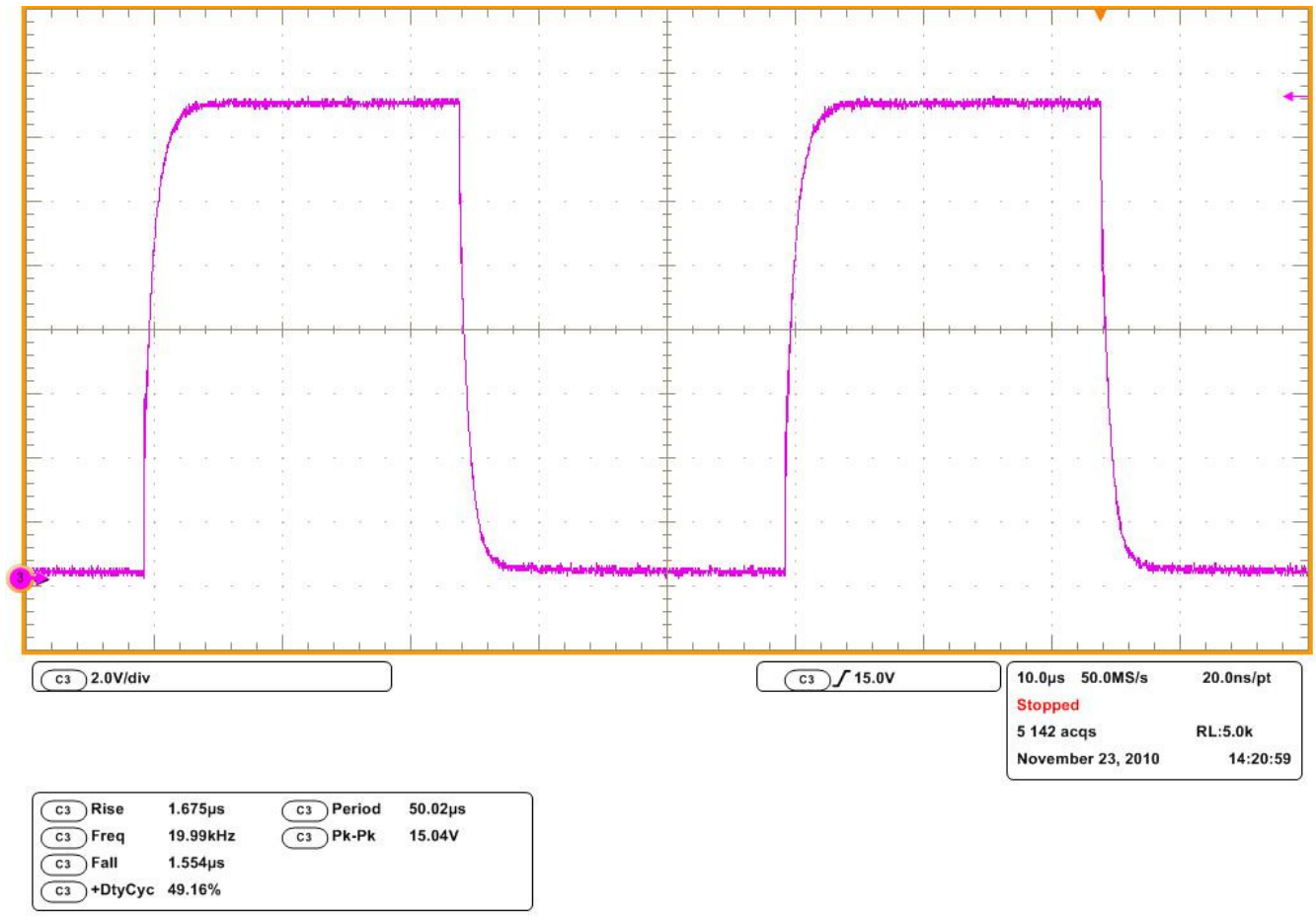

Fig H.2 Switching Signal between MOSFET Driver and High Power MOSFETs Observed in Circuit at 20 KHz

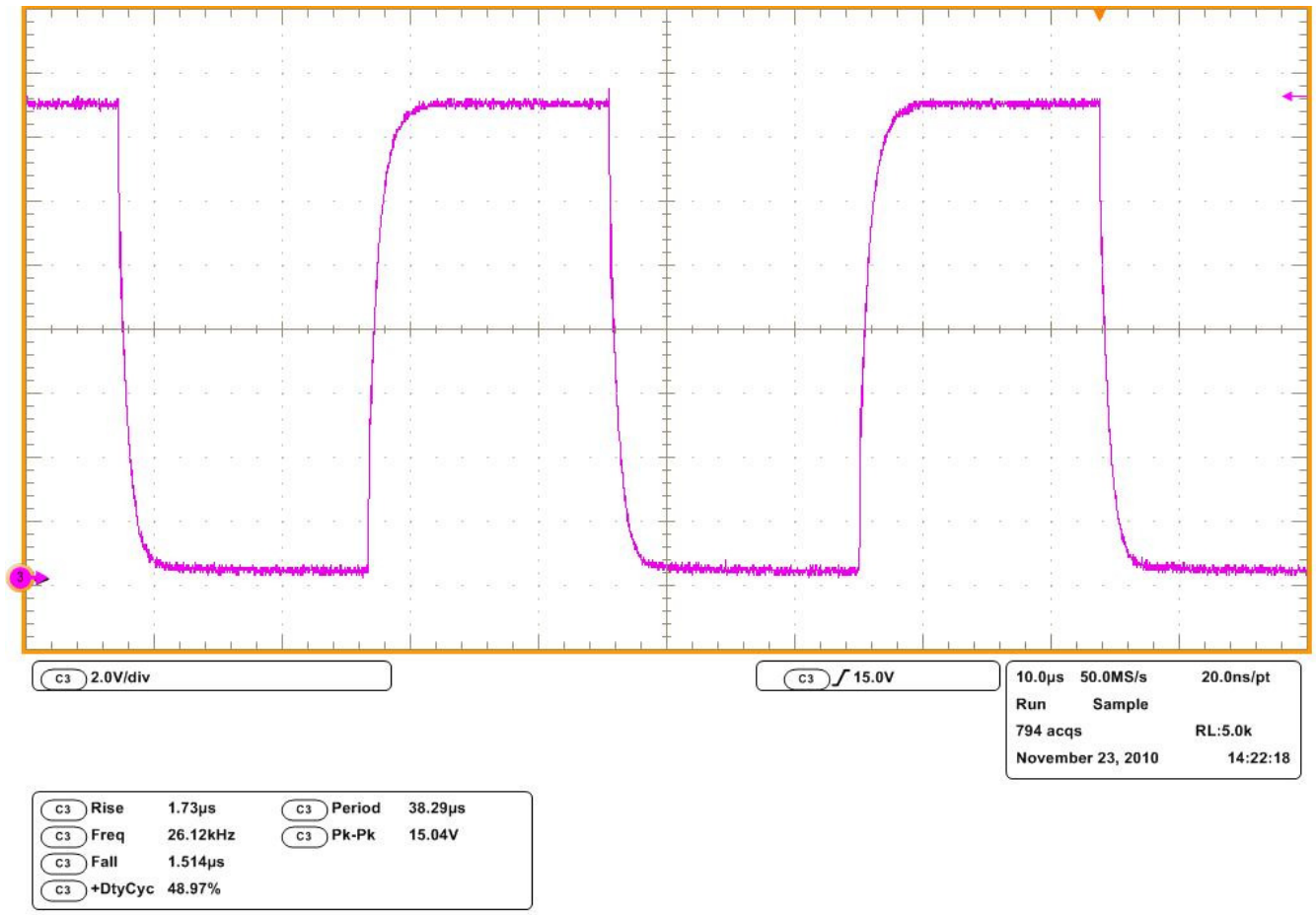

Fig H.3 Switching Signal between MOSFET Driver and High Power MOSFETs Observed in Circuit at 26.1 KHz

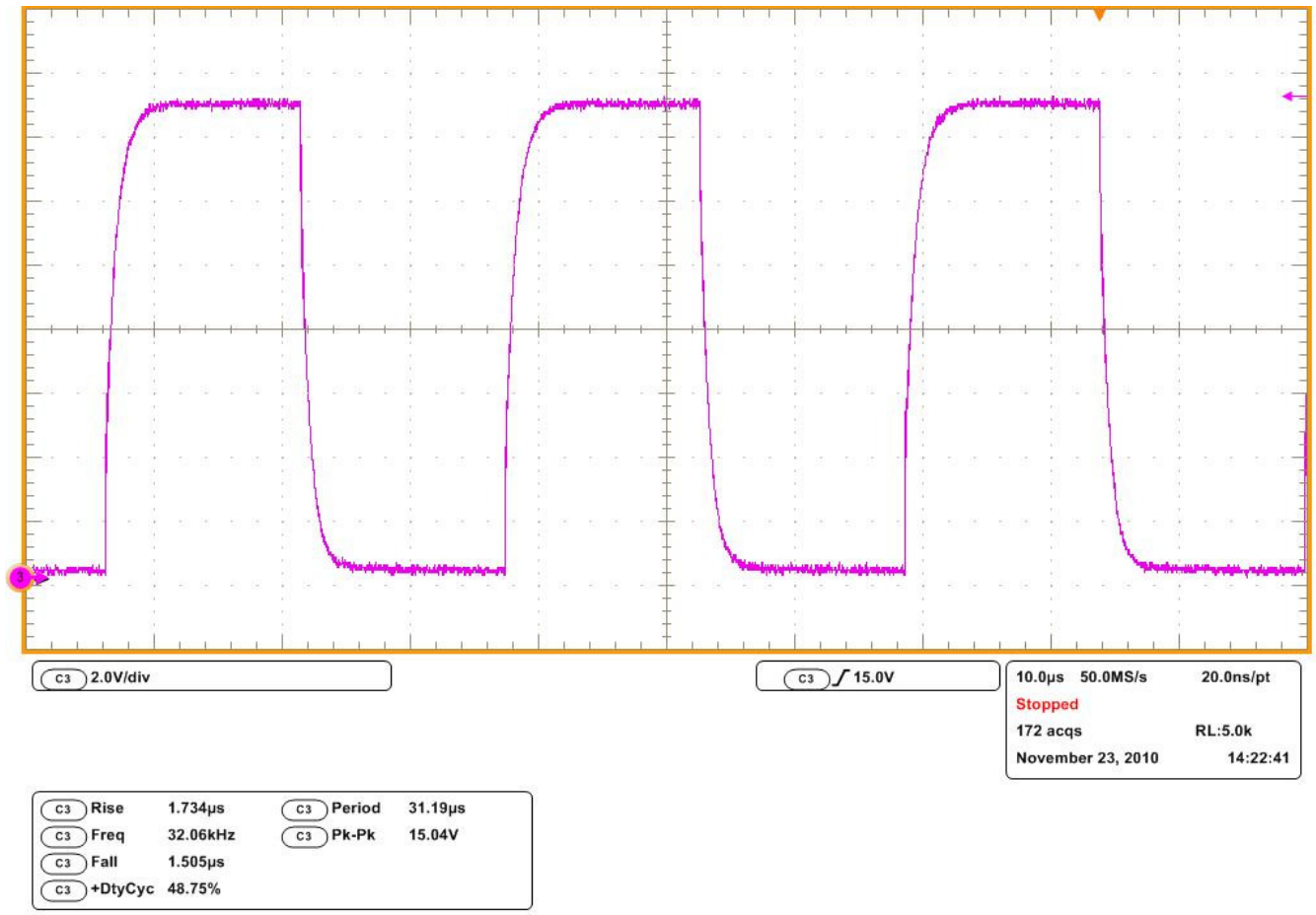

Fig H.4 Switching Signal between MOSFET Driver and High Power MOSFETs Observed in Circuit at 32 KHz

Appendix J – Saber Sketch Simulation Data of Switching Circuit

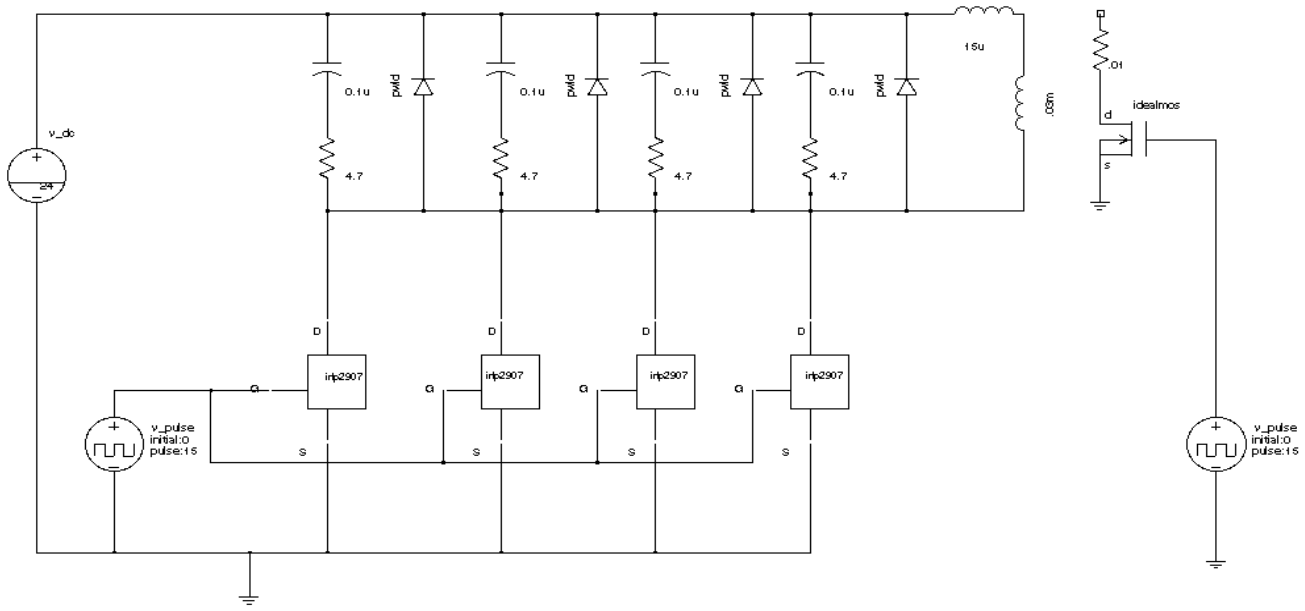

Fig J.1 Simulation switching circuit model using non-ideal switching components, without added parasitic components.

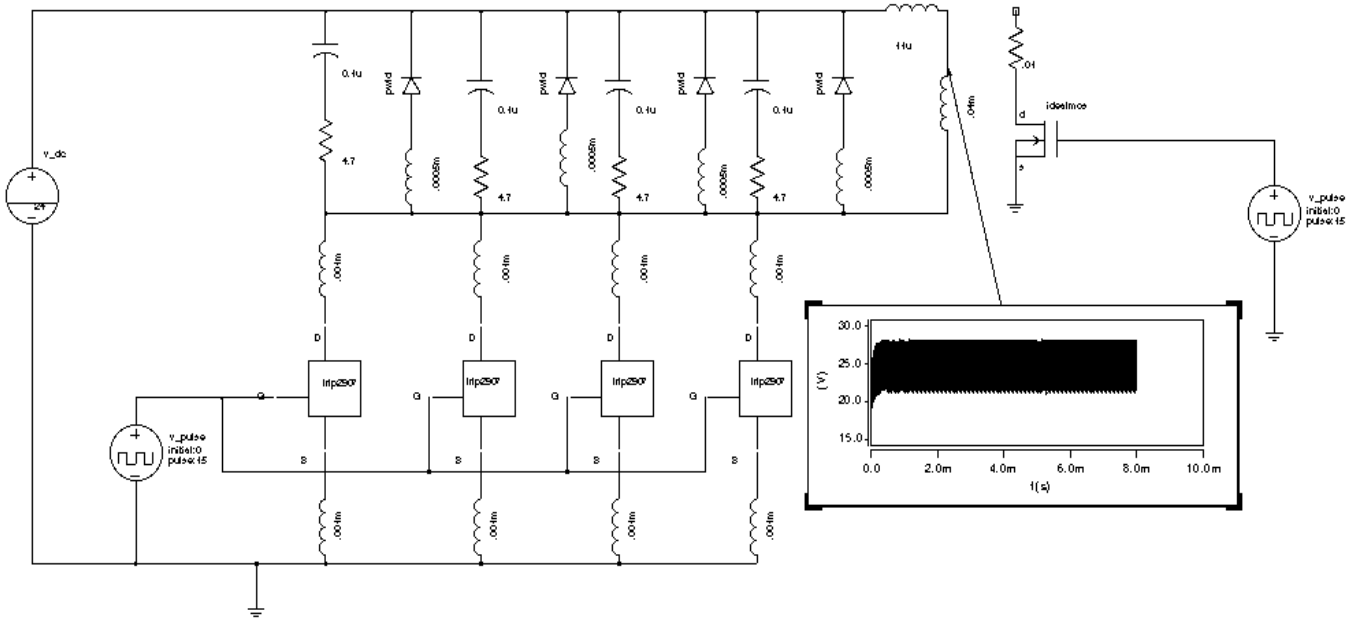

Fig J.2 Simulation switching circuit model using non-ideal switching components, with parasitic inductance added.

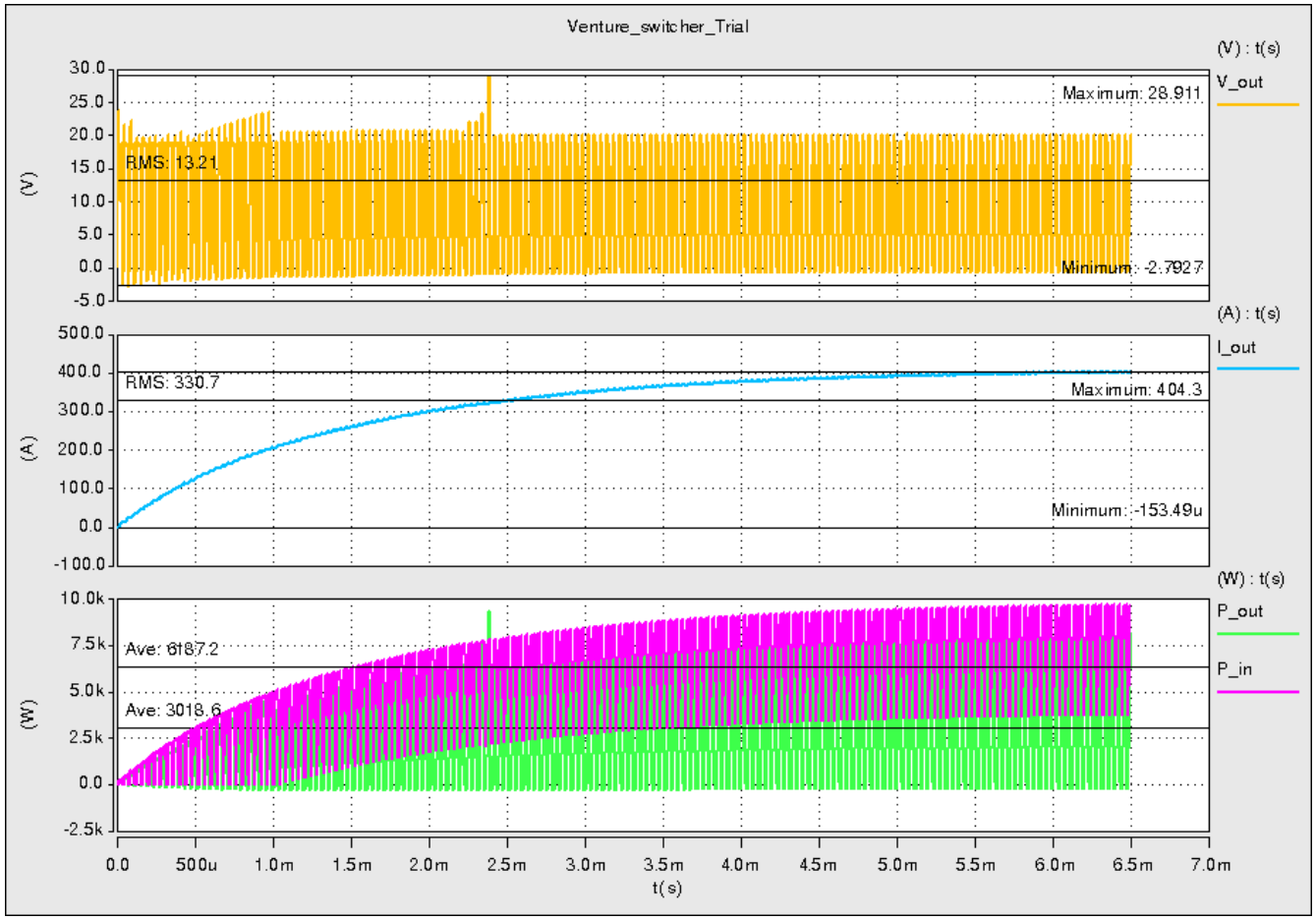

Fig J.3 Simulation 400 A load, maintain 66% duty cycle

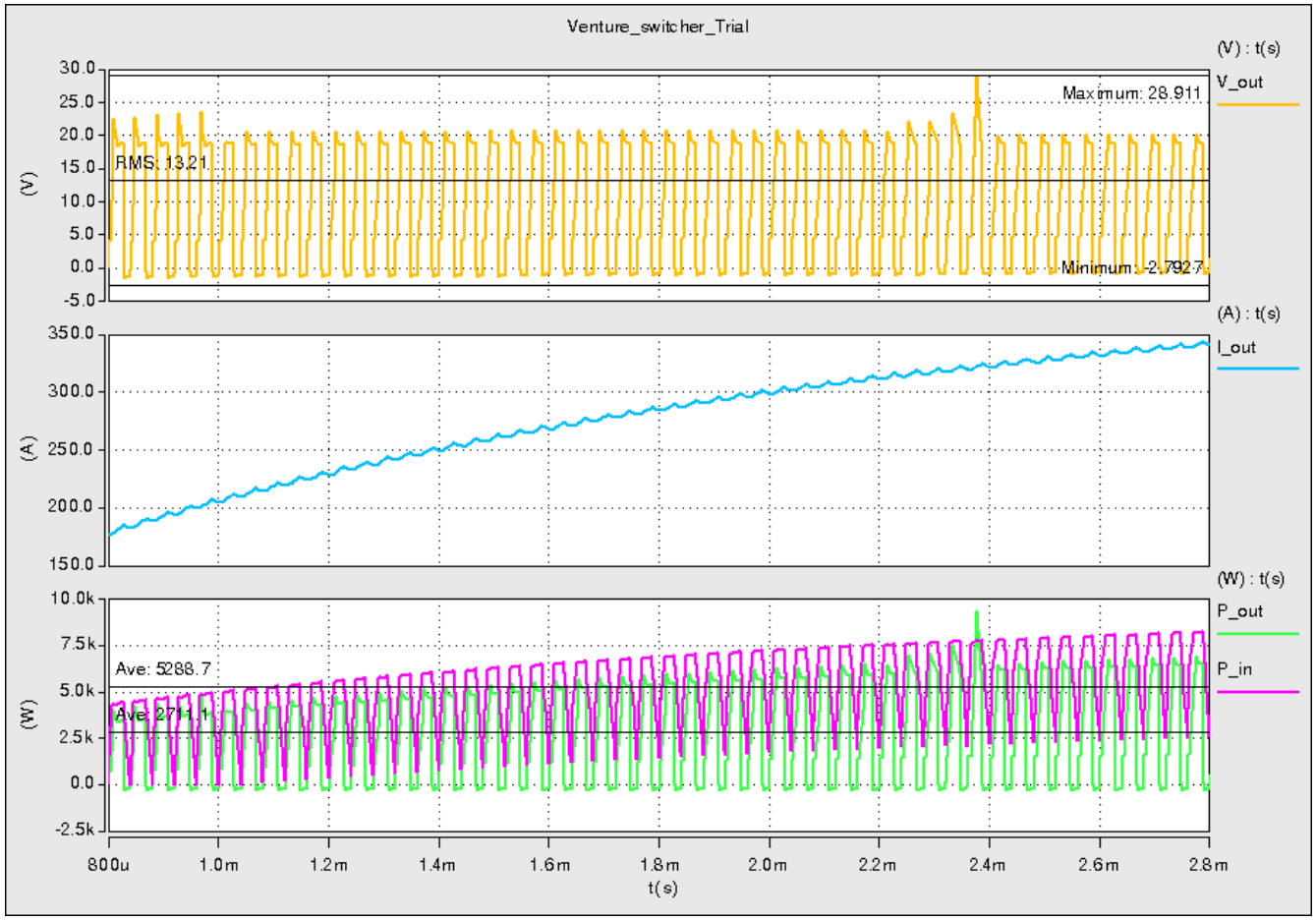

Fig J.4 Simulation 400A load, maintain 66% duty cycle